Bridging the Gap from Continuum Mechanics to Molecular Dynamics for Nanoscale Systems

BY

Qilu He

B.S., Shanghai University, 2006

THESIS

Submitted as partial fulfillment of the requirements

for the degree of Doctor of Philosophy in Mechanical Engineering

in the Graduate College of the

University of Illinois at Chicago, 2015

Chicago, Illinois

Defense Committee:

        Carmen Lilley, Chair and Advisor

        Jeremiah Abiade

        Thomas Royston, Department of Bioengineering

        Laxman Saggere

        Ahmed Shabana

ACKNOWLEDGEMENTS

TABLE OF CONTENTS

TABLE OF CONTENTS (Continued)

LIST OF FIGURES

LIST OF TABLES

LIST OF ABBREVIATIONS

CA   Cantilever

SS   Simply-supported

FF   Fixed-fixed

MD   Molecular Dynamics

NEMS   Nano-Electro-Mechanical Systems

ND   Normalized Difference

FCC   Face-Centered-Cubic

BCC   Body-Centered Cubic

HCP   Hexagonal Close Packed

AFM   Atomic Force Microscopy

AR   Aspect Ratios

A   Analytical

N   Numerical

EAM   Embedded Atom Model

MEAM   Modified Embedded Atom Method

LAMMPS   Large-scale Atomic/Molecular Massively Parallel Simulator

CG   Conjugate Gradient

NVT   Number of Particles, Volume, Temperature

NVE   Number of Particles, Volume, Energy

FFT   Fast Fourier Transform

PDE   Partial Differential Equation

SUMMARY

Bending nanowires and nanoplates are widely used as flexible beams in Nano-Electro-Mechanical Systems (NEMS) for force and mass sensors. Usually, the vertical deflection and resonant frequencies of the nanowires and plates are the most crucial parameters in these systems. Although the nanoscale beam-like structures have been designed and fabricated for various applications, deriving the mechanical theories specifically applicable to nanoscale materials and enhancing the accuracy of the mechanics of these nanoscale structures is still a bottle neck in designing nanotechnology. Typically, there are two different ways to accomplish the mechanical modeling for nanoscale materials, such as modeling with continuum mechanics by adding size effects and modeling from atomic scale theory. However, both of these methods have some fundamental issues or limitations and cannot be directly applied to accurately achieve accurate mechanical modeling for nanoscale materials.

A literature review on continuum mechanics, surface stress and surface elasticity modeling, nonlocal elasticity and molecular dynamics simulation has been introduced in this thesis. Nonlocal elasticity theory is a potential modeling method to study the mechanical properties of nanoscale materials. However, nonlocal elasticity has not been fully developed because the physical meaning of the nonlocal parameter e_0 is unknown. The parameter e_0 was studied to unify surface effects, nonlocal effects, and molecular dynamics simulations. These three methods should be consistent because they are different methods to study the same size effects at the nanoscale. The research goal is to develop mechanical modeling theories for nanoscale structures with critical dimensions of 1-100nm. To achieve this goal, the research aim is to test the hypothesis that Euler-Bernoulli or Timoshenko beam theory with surface effects, Eringen's nonlocal elasticity, and the corresponding nonlocal beam theories, and MD simulation

SUMMARY (Continued)

results can be unified for nanoscale structures with critical dimensions of 1-100nm. Three boundary conditions were considered in this thesis, such as cantilever, simply-supported and fixed-fixed.

First, a more general solution of continuum beam theories with surface effect has been obtained and developed to investigate the surface effect on bending nanowires with the "core-shell" approach. Timoshenko beam theory with surface effects has been applied with consideration of shear effect and rotational inertia effect. Consequently, the limitation of aspect ratio of Euler-Bernoulli beam theory was eliminated. The modeling for the resonant frequencies of the first three vibration modes of nanowires with three boundary conditions was detailed.

Second, the solutions of the resonant frequencies with surface stress effect and nonlocal effect have been compared. A bridging theory by incorporating surface properties with the nonlocal elasticity theory parameter e_0 has been developed to bridge the classical beam theories with nonlocal beam theory at the nanoscale. Two different modeling methods for the resonant frequencies of simply-supported nanowires were introduced. The two methods are Timoshenko beam theory with surface effects and nonlocal Timoshenko beam theory. With the hypothesis that the solutions from the two methods are consistent, the theoretical relation between the surface stress τ and the nonlocal parameter e_0 has been derived. It was found that e_0 for a simply-supported nanowire in flexural vibration is not a fixed number, but depends on the following parameters: the lattice length a, the elastic modulus E, the surface stress τ, the cross-section size w and shape (included in I and H), the length of the beam L and the vibration modes n. The nonlocal parameter e_0 is based on eliminating the nearest neighbor assumption from classical elasticity theory and describes surface effects when the critical length (cross-section size for the

SUMMARY (Continued)

nanowires) is comparable to the atomic structure (defined as a lattice unit length in this thesis). Additionally, by studying the analytical solution for e_0, it was found to be an imaginary number when the surface effects increase the stiffness of the nanowires. This case corresponds to a positive surface stress effect on the simply-supported nanowires in the surface stress modeling. Hence, if the surface elasticity is negligible, the nonlocal parameter e_0 has to be imaginary to match the modeling result of positive surface stress for nanowires with simply-supported boundary conditions.

Finally, molecular dynamics (MD) simulations have also been introduced to verify the above conclusions from the theoretical relation between the surface stress and nonlocal parameter. The MD simulations found the same trends as the theoretical modeling predicts. For example, MD simulations and theoretical modeling both found that e_0 increased with increasing cross-sectional sizes. An imaginary e_0 was also found by calibrating e_0 with the resonant frequencies obtained from the MD simulations. Additionally, the surface stress was solved by the Timoshenko beam theory with surface effects by assuming that the resonant frequency and surface elasticity were known and the surface stress is unknown. The surface stress from the resonance MD simulations is almost a constant, which is more obvious for Ag(100) with 2% variation as compared to Ag(110) with a 20% variation. However, there is a difference between the calculated surface stress in our research and the values from references. The possible reasons for the shift and the future work have been discussed at the end of the thesis.

CHAPTER 1. Introduction

1.1 <u>Background and Motivation</u>

Bending nanowires and nanoplates are widely used as flexible beams in Nano-Electro-Mechanical Systems (NEMS) for force and mass sensors[1] to detect chemical[2] and biological[3] reactions or other parameters such as temperature change[4], liquid viscosity[5] and surface stress[6]. Usually, the vertical deflection and resonant frequencies of the nanowires and plates are the most crucial parameters in these systems. The measured shift of deflection[7, 8] or resonant frequencies can be used to predict the value of the force or mass change.[9, 10]

As shown in Figure 1.1, the most common force sensor design is a cantilever beam made with a nanowire, with a free end or with an applied load [11]. For example, nano- or macroscale cantilever sensors have been proven to be ideal structures for DNA detecting and analysis.[12, 13] A nanocantilever array coated with specific reagents can be used to detect and measure the presence of particular antigens or disordered DNA. The biosensor arrays are designed so that when specific bimolecular interactions occur on one surface of the cantilever, the cantilever bends. The deflection can be measured, and the presence of particular antigens and disordered DNA sequences can be detected in a given serum.[14] Nanocantilevers are also used to detect the change in proteins by measuring the difference of deflection when the protein was absorbed onto a Au surface.[15, 16] It can also be used to sense bioreactions and chemical reactions at the microlevel. The quantity and the speed of the mass changing implies that if the reaction has occurred and the rate of occurrence. Intermolecular forces arising from adsorption of small molecules are known to induce surface stress, directly resulting in the mechanical bending of a

solid surface or a cantilever.[17] Nanocantilever sensors have also been utilized to detect varying hydrogen levels in the environment. Analytic molecules diffuse into the cantilever coating and the coating swells with exposure to the analytical vapor. With mass absorption, an interfacial stress between the coating and cantilever occurs, which leads to bending.[18] Also, the "bending plate" method is a typical experimental method to measure the surface stress with the curvature and deflection of the beam.[6]
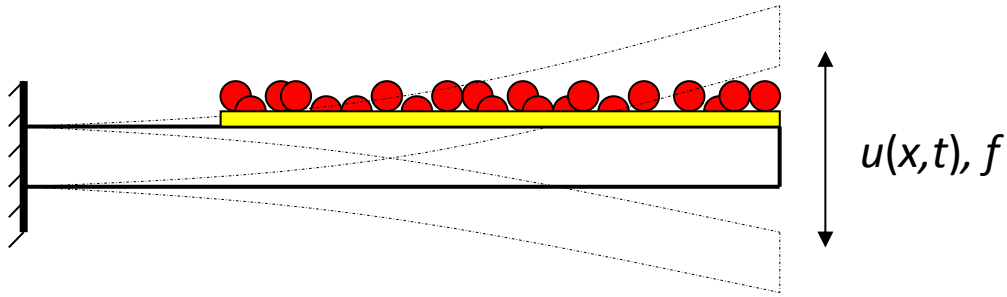
Figure 1.1. A simple model of the cantilever force sensor. The red circles represent the target particles in the research environment and the yellow layer represents the reagent to detect the targets. The letter *u* represents the static deflection and *f* represents the resonant frequencies which are commonly used to sense the target particles.

Although the nanoscale beam-like structures have been designed and fabricated for various applications, deriving the mechanical theories specifically applicable to nanoscale materials and enhancing the accuracy of the mechanics of these nanoscale structures is still a bottle neck in designing nanotechnology.[19] As shown in Figure 1.2, typically, there are two different ways to accomplish the mechanical modeling for nanoscale materials. Similar to the nanoscale

fabrication, these two approaches can be referred to as a top-down approach, which is from the macroscale to nanoscale, and bottom-up, which is from the atomic scale to nanoscale.[20]
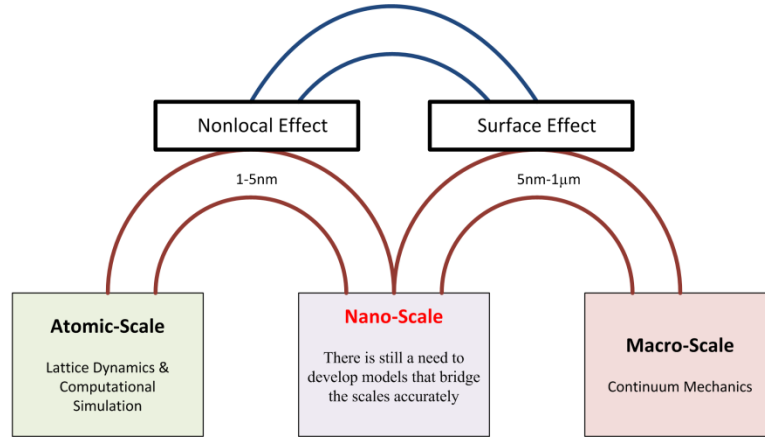
Figure 1.2. Illustration of the size ranges for different modeling methods across scales.

Macroscale (classical) mechanics, such as the Euler-Bernoulli beam theory and the Kirchhoff-Love plate theory are the most common methods to model the mechanical properties of nanoscale materials because of their convenience.[21] Classical continuum mechanics modeling is based on the assumption that the object is completely continuous and ignores the atomic structure. When the length scales are much larger than the dimensions of the particles and the corresponding chemical bond, such models are accurate. However, when the size of the object approaches the nanoscale, this assumption is questionable and the resulting theories based on continuum mechanics need to be validated. In general, atomistic properties such as van der Waals interaction [22, 23], surface effects [24-32], and nonlocal effects [33-44] can significantly

alter material behavior at the nanoscale. For example, as the size shrinks, the surface area to volume ratio becomes much larger than for a bulk material. Therefore, the surface effect, which is negligible in classical continuum mechanics, must be considered at the nanoscale.[24-30, 32] Surface effects, including surface stress and surface elasticity, have been well studied. [45-50] Yet, there are still some remaining questions, such as fully exploring boundary condition effects on the resulting behavior.

Additionally, the nearest neighbor assumption is not valid at the atomic and nanoscale, as the external length (e.g. cross-section size) is close to the internal length (lattice unit length).[51] Thus, nonlocal elasticity theory for nanobeams and nanoplates has been developed from lattice dynamics.[33-44] However, since nonlocal elasticity was not originally derived for nanoscale mechanics, bridging from the atomic scale to the nanoscale still has several unanswered questions. For example, an existing fundamental question is what is the physical meaning of the nonlocal parameter e_0 in nonlocal elasticity? To date, this parameter is not well defined and the spectrum of value(s) for e_0 of nanoscale structures is unknown.

Molecular dynamics (MD) simulation is also a modeling tool to predict the mechanical behaviors of nanoscale materials from the atomic scale to nanoscale.[52, 53] The basic concept incorporated in MD simulations is using Newton's mechanics to describe the relation, for example velocity, force and potential energy, between pairs of particles in the investigated object.[54] MD simulation can be used to accurately depict the properties at the atomic scale, such as the displacement and velocity of particles and the potential and kinetic energy for a system of particles. Compared to the size and the time length needed to capture the mechanical properties of nanoscale structures, such as resonance, the size[55, 56] and time[57, 58] scale of MD is very small and the computational time and power required to bridge between MD

(Ångstrom and femtosecond) and the nanoscale (nanometers and nanoseconds) can be prohibitive. Therefore, MD simulation is typically still an expensive method which requires considerable computational power and simulation time due to the time step in the MD simulation and experimental time scale.[54]

Thus, a fundamental issue in modeling at the nanoscale is that nanoscale structures with critical dimensions from 1-100nm, which are too small for continuum mechanics but too large for MD. Deriving a series of optimized mechanical theories specifically for this size range would address a fundamental knowledge gap in theory development for nanoscale structures.

1.2 **Goal and Objectives**

The research goal is to develop mechanical modeling theories for nanoscale structures with critical dimensions of 1-100nm. To achieve this goal, the research aim is to test the hypothesis that Euler-Bernoulli or Timoshenko beam theory with surface effects, Eringen's nonlocal elasticity and the corresponding nonlocal beam theories, and MD simulations results should all be consistent for nanoscale structures with critical dimensions of 1-100nm. Thus, the approach will unify and further develop these theories and methods so that they describe the mechanical behavior nanostructures within the chosen size scale. The three methods will be studied to unify the three approaches by implementing surface properties with nonlocal elasticity. The resulting model will be tested by comparing with MD simulations.

Each method will be introduced individually in Chapters 3-5. The modeling procedures will be discussed in detail. The comparison among the three methods will be presented in Chapter 6. Briefly, in Chapter 3, the resonance modeling of Timoshenko beam theory with surface effects

will be introduced for cantilever, simply-supported and fixed-fixed boundary conditions. In Chapter 4, the solution of the resonant frequencies from the nonlocal Timoshenko beam theory will be derived. The numerical method for the three boundary conditions is presented. Additionally, the analytical solution of the simply-supported case is derived and the difference between the numerical and analytical solutions is tested. The procedures of MD simulation setup for the tensile and resonance tests of nanowires will be introduced in Chapter 5. In Chapter 6, the comparisons among the results from the three methods are discussed. The nonlocal Timoshenko beam theory is first compared to the surface effects to obtain the analytical relation between e_0 and τ for the simply-supported case. The nonlocal Timoshenko beam theory is also compared to the resonance MD simulations to obtain the e_0 of the simulated structures for all the three boundary conditions.

The first research objective is to obtain and verify a more general solution of continuum beam theories with surface effect to investigate the surface effect on bending nanowires with the "core-shell" approach. In Chapter 3, the theoretical modeling of resonant frequencies and free undamped vibration of nanowires has been identified and analyzed with the dynamic form of Timoshenko beam theory with surface stress. Timoshenko beam theory includes shear effect and inertia of beams. It is a more accurate model for an arbitrary aspect ratio (i.e. <5). Hence, it is a more general theory than Euler-Bernoulli beam theory as used in some publications [29, 30, 32, 45, 59]. Three boundary conditions, cantilever, simply-supported and fixed-fixed, were tested to study boundary condition effects. The Timoshenko model with surface properties will be discussed in detail and a study of boundary condition effects will be presented to compare with existing research on modeling with Euler-Bernoulli beam theory. The validation of the theoretical modeling is also presented in Chapter 3. As examples, the theoretical solution of

resonant frequency obtained from the Timoshenko beam theory with surface effect will be verified by comparing to the MD simulation of Au(100) with dimensions of 4.08x4.08x49nm, 5.71x5.71x68.5nm and 7.34x7.34x88.1nm, as found in Reference [53].

The second objective of this research is to develop a bridging theory by incorporating surface properties with the nonlocal elasticity theory parameter e_0 to bridge the classical beam theories with nonlocal beam theory at the nanoscale. To date, there are still several unanswered questions to the application of nonlocal elasticity at the nanoscale, in particular, an fundamental question that remains is what is the physical meaning of the parameter, e_0? This question has hindered applying nonlocal elasticity to widely model nanoscale structures[39]. Some researchers have focused on answering this question.[60-62] However, the existing published works are still based on the nearest neighbor assumption. When the nearest neighbor assumption is included in the modeling, the outcome of the nonlocal parameter e_0 does not contain nonlocal effects, such as surface properties, but other effects, such as the effect of higher order difference terms in the Taylor series expansion.[60-62] Thus, while there are published works on solving e_0, they do not include nonlocal effects. To the best of our knowledge, there is no existing published research on calibrating e_0 with nonlocal material properties, namely surface properties, although Eringen stated that the surface effect was a main source for nonlocal effects.[63] Therefore, it is hypothesized that by comparing the nonlocal effect to those of surface effect, e_0 can be defined.

In Chapter 4, the numerical solution of nonlocal Timoshenko beam theory for the resonant frequencies of nanowires with the above mentioned three boundary conditions is introduced. The analytical solution of the resonant frequencies for a simply-supported beam is derived and verified by comparing to the numerical solution.

In Chapter 5, the MD simulations to model the elastic modulus and resonant frequencies of nanowires are introduced. The MD simulations were used to obtain the mechanical properties of nanoscale materials, such as the elastic modulus. The results from the MD simulations were used to verify the bridging calculation between the beam modeling with surface effects and nonlocal effect.

In Chapter 6, the analytical solution of e_0 is derived for the simply-supported boundary condition. The analytical solution of e_0 is solved by equaling the resonant frequencies of nanowires from the Timoshenko beam theories with surface effects and with nonlocal effect. The resonant frequencies from the two methods should be equal with the hypothesis of this thesis that the Timoshenko beam theories with surface effects and with nonlocal effect are consistent.

One should also note that the parameter e_0 is used to only describe a negative surface stress if it is restricted to a real value. Wang and *et al.* [39] and numerous other researchers [37, 39, 43, 44] found that a real e_0 always reduces the stiffness of a simply-supported beam or plate, which is identical to the effect of negative surface stress. However, materials can also have a positive surface stress, as commonly found in FCC metals.[64] Additionally, researchers have also found that certain combinations of boundary conditions and dimensions lead to an undetermined e_0[65]. Herein, it is proposed that in these cases, e_0 may be imaginary in value. In Chapter 6, the relation between surface stress τ and e_0 for simply-supported nanowires is studied. The results indicate that including imaginary values of e_0 widen the spectrum of nanostructures that can be modeled with nonlocal elasticity.

The third objective of the research is to validate the hypothesis that Timoshenko beam theory with surface effects, Eringen's nonlocal elasticity and the corresponding nonlocal beam theories, and MD simulations results should be consistent at the nanoscale range of 1-100nm.

The hypothesis was tested by comparing beam theory with surface effect and beam theory with nonlocal effect with molecular dynamic simulations. In Chapter 5, MD simulations of the transverse vibration of Ag(100) and (110) nanowires with cross-section size 2-4nm and aspect ratio 10 is performed to obtain the resonant frequencies with cantilever, simply-supported and fixed-fixed boundary conditions. The nonlocal parameter e_0 was calibrated by comparing the fundamental resonant frequency predicted for Ag(100) and Ag(110) from nonlocal Timoshenko beam theory with that calculated from MD simulations for three boundary conditions. The surface stress of the simulated material is also calibrated with the equations derived in Chapter 3. Therefore, the three methods as mentioned in the hypothesis are fully compared.

It was found that MD simulations support the proposition that e_0 can be either real or imaginary with different combination of lattice orientation and boundary condition from the theoretical comparison between surface effect and nonlocal effect. The simulation data also agree with the e_0 found by the analytical calibration. For example, the absolute value of e_0 is found to increase with an increase in cross-section size from the analytical solution. The simulations also indicate the same trend for values of surface stress τ. However, the quantitative value for the surface stress from the resonance simulation and calibrated with the beam modeling is slightly different from the surface stress value from Ref. [64, 66]. The possible reasons for these differences and potential approaches that may address them will be discussed in the conclusions and the future work found in Chapter 7.

CHAPTER 2. Literature Review

Much research effort has focused on beam or plate modeling of nanoscale materials with surface or nonlocal effects. The fundamental theoretical framework has been extensively developed for both approaches. Yet, there are still critical fundamental knowledge gaps that prevent the two theories from being bridged. In this chapter, we summarize the literature on both theories and identify the fundamental knowledge gaps to bridging the theories.

2.1 Surface Property Effects on the Mechanical Behavior of Nanoscale Structures

It is well known that as size scales approach the nanoscale, the surface area to volume ratio becomes large and the relative percentage of surface atoms increase as compared to bulk atoms. Surface properties different from the bulk material are due to the uncoordinated surface particles.[67, 68] On surfaces, these particles lack adjacent atoms and dangling bonds are present.[69] As a result, the surface has properties that are different from the bulk volume and these properties are commonly described with surface stress, surface elasticity, or surface energy [27, 70]. Researchers have found that the surface effect can have a significant influence on elastic properties[29, 47], fracture and yield strength[27], and melting of nanowires.[71] Typically, the surface effect on the mechanical properties of nanomaterials is studied with surface stress and surface elasticity or with surface energy [27, 70].

Surface stress is defined as the reversible work per unit area needed to elastically stretch a pre-existing surface.[68] Surface elasticity is the characteristic of the surface layer that has a different elastic property from that of the bulk material.[72] Surface energy is defined as the

reversible work per unit area involved in forming a surface.[68] Usually, the surface stress is used to describe a thin surface within continuum mechanics modeling.[29, 32, 47, 71] In addition, surface elasticity will affect mechanical behavior as nanoscale structures decrease in size. Surface energy is usually modeled with the surface Cauchy-Born model [27, 70], which is a quasi-continuum computational method to couple atomistic simulation to continuum simulation to obtain the overall mechanical behavior for discrete systems.[73, 74] This thesis mainly focuses on the first method, which is the surface stress and surface elasticity modeling with continuum mechanics methods to study nanoscale structures with critical dimensions from 1-100 nm.

The effects of surface stress and surface elasticity properties on nanowires have been studied by applying the Young-Laplace equation into the classical beam theory (e.g., the Euler-Bernoulli beam theory). [45-50] He and Lilley[47] applied this method to solve the overall elastic modulus of the nanowires with cantilever, simply-supported and fixed-fixed boundary conditions. It was found by studying the analytical solutions that, when considering a positive surface stress, the cantilever nanowires behaved softer and simply-supported and fixed-fixed nanowires behaved stiffer than the nanowires without surface stress. Thus, the behavior differed than that of nanowires modeled without surface stress and resulted in an apparent softening or stiffening of the nanowire depending on the boundary conditions. It was also found that these solutions agreed with the static bending tests for Ag and Pb nanowires, see Reference [75]. They also used the dynamic form of the Euler-Bernoulli beam theory to solve the resonant frequency of nanowires for the same boundary conditions.[29] The results were compared with the solution from the Surface Cauchy-Born model [27, 70] with surface energy. Their approach and the Surface Cauchy-Born model predict a similar trend in resonant frequency shift of Au nanowires,

where a cantilever has a lower resonant frequency than frequency calculated without surface stress, and the opposite trend occurs for the simply-supported and fixed-fixed nanowires.

Song demonstrated the importance of the effects of initial stresses in the nanowires that are caused by deformation due to surface stresses.[45] They derived a new formulation by incorporating the surface stress, the surface-induced initial stress and surface elasticity into the Euler–Bernoulli beam theory. They found that the surface-induced initial stress is usually neglected in the Young–Laplace model. However, it still has significant influence on the overall mechanical properties of nanowires.

The surface effect on axial buckling behavior of nanowires has also been studied with the governing equations of beam buckling theories. Wang and Feng [49] introduced a method based on the Timoshenko buckling theory to determine the critical compressive load of a nanowire with surface stress. It was found that the shear deformation lowered the critical compression force of buckling. However, a positive residual surface stress increased the critical force of buckling. A simply-supported Ag nanowire with a circular cross-section was used as an example and it was shown that the surface effect becomes more significant as the diameter decreases or when the aspect ratio increases. The shear effect becomes more significant for a nanowire when the aspect ratio is relatively smaller.

Wang and Feng also used a similar procedure to investigate the surface effects on the buckling behavior of piezoelectric nanobeams. [32] Surface elasticity, residual surface stress and surface piezoelectricity were included in modeling the mechanical behavior for the normalized critical electric potential to buckle a cantilever nanobeam. It was found that when the dimension of the cross-section approaches the nanoscale, the surface elasticity increases the critical electric potential of the piezoelectricity slightly. Conversely, as the surface stress increases, the critical

electric potential decreases. Relatively, the surface stress effect is much more significant than the surface elasticity.

Surface properties have also been considered when modeling plates. He *et al.* [46] derived a model based on Gurtin and Murdoch's surface elasticity theory to study thin elastic films with nanoscale thickness. Lu *et al.* [76] referred to He's derivation and derived the governing equation of static bending of thin plates with surface stress and elasticity. Assadi *et al.* [77] incorporated surface elasticity and residual stresses into Kirchhoff plate theory to solve for the resonant frequency of a simply-supported nanoplate. Si(100) with a negative surface stress and a negative surface elasticity was studied as an example. The negative surface stress and elasticity were found to reduce the resonant frequency of the nanoplates.

The vibration behavior of nanoplates with surface stress effects was studied by Ansari and Sahmani.[78] Classical plate theory and first order shear deformation theory are used to develop non-classical continuum plate models for free vibration analysis of the nanoplates including surface stress effects. A closed form analytical solution was derived to obtain the natural frequencies of nanoplates corresponding to various values of the axial half wavenumber, transverse half wavenumber, aspect ratios, and surface elastic constants.

As detailed above, although the surface stress and elasticity with continuum mechanics modeling has been studied widely, there are still two fundamental issues that remain. The first issue in beam modeling with surface effects is an ambiguous size limitation of aspect ratio for the application of surface properties. Park concludes that the aspect ratio is the key parameter that correlates the resonance frequency shift due to the surface energy with the surface Cauchy-Born model.[27, 70] He introduced the method that combined the surface Cauchy-Born model and finite element method to investigate the resonant properties of Si nanowires of both fixed-

fixed and cantilever boundary conditions with surface energy. [27, 70] The research demonstrates how surface effect cause variations in nanowire resonant frequencies from those expected from macroscale beam theory. We propose that the aspect ratio should also be a key parameter for the modeling with surface stress and elasticity. However, due to the assumption of ignoring the shear effects, Euler-Bernoulli beam theory has a limitation that the aspect ratio must be larger than 5, when the shear effect is negligible.[79] By using the Timoshenko beam theory, the shear effect and inertia of the beam is considered and the beam can be any aspect ratio. The model will directly address aspect ratio limitations and thus would be a more general solution.

The second issue in the current research of bending nanowires and nanoplates with a surface effect is that the boundary condition effect has not been fully studied. Due to convenience in obtaining analytical solutions, most researchers only model simply-supported nanostructures using various approaches.[32, 76-78] As found with Stoney's equation, the additional loading due to surface stress is a function of the curvature.[31] Since different boundary conditions lead to different directions and values of curvatures [79], the boundary condition effect is thus important when investigating the influence of the surface effect on the mechanical behavior of nanostructures. Thus, three boundary conditions, such as cantilever, simply-supported and fixed-fixed, will be analyzed with the modified Timoshenko beam theory. The details of the Timoshenko beam modeling with surface properties and the effects of boundary conditions will be presented in Chapter 3.

2.2 <u>Nonlocal Elasticity and Nonlocal Beam Modeling at the Nanoscale</u>

When any dimension of a nanostructure approaches the atomic scale, long range atomic interactions result in nonlocal effects on the mechanical behavior. Thus, there is a breakdown in the assumed conditions for continuum mechanics modeling. In 1983, using lattice dynamics without the nearest neighbor assumption (shown in Figure 2.1), Eringen developed a new elastic stress-strain relationship for small scale materials, defined as having any dimension of the material close to the lattice length, and termed it as nonlocal elasticity.[51, 63] With nonlocal elasticity modeling, the interatomic interactions are considered (i.e. modeled) as nonlocal effects.[44] Nonlocal elasticity assumes that the stresses at a reference point are functions of the strains at all points of the body in the continuum. The stress strain relationship is described below as

$$t_{ij} = \int_V \alpha(|x - x'|, \lambda) C_{ijkl} \varepsilon(x') dV(x') = \int_V \alpha(|x - x'|, \lambda) \sigma_{ij} dV(x') \qquad (2.1)$$

Herein, t_{ij}, σ_{ij}, ε_{ij} and C_{ijkl} are the nonlocal stress, macroscopic (classical) stress, strain, and elasticity tensor, respectively. The variable α is the nonlocal modulus, which indicates the nonlocal effects at the reference point x produced by local strain at the source x'. The variable λ is defined as $\lambda = e_0 a/l$. The parameter e_0 is the nonlocal parameter to bridge the internal and external characteristic lengths. The parameter a is the internal characteristic length (e.g., lattice parameter, granular distance, etc.), l is an external characteristic length (e.g., crack, length, wavelength, etc.), and V is the volume of the object.[39] This theory is based on classical continuum mechanics, while taking into account the discrete particle effect.[80] Since the critical parameter e_0 is not well defined, nonlocal elasticity is still a developing theory and its application for modeling the nanoscale mechanics has significant limitations.
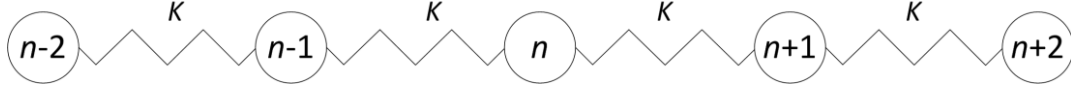
(a)
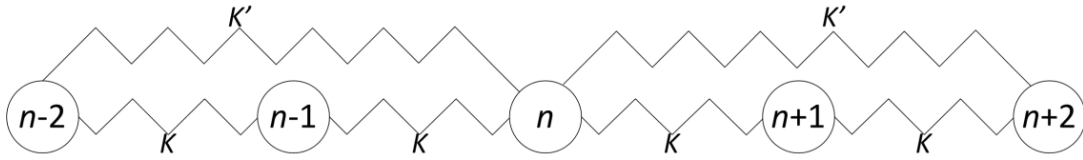
(b)

Figure 2.1. The illustrations of 1D lattice dynamics of 5 atoms for classical and nonlocal elasticity. Figure 2.1(a) Classical elasticity with nearest neighbor assumption. Figure 2.1(b) Nonlocal elasticity without nearest neighbor assumption. K is the stiffness between the nearest atoms and K' is the stiffness between the atoms with one extra atom between them.

The nonlocal elastic modulus, α, must satisfy several conditions as described in Ref [63] and restated below.

(1) α acquires its maximum at $x'=x$ and attenuates with $|x'-x|$.

(2) When $\lambda \to 0$, α must revert to the Dirac delta function so that classical (local) elasticity is included when the internal characteristic length vanishes (e.g. $l \to \infty$ or $a \to 0$ for macroscale materials).

(3) For small internal characteristic lengths (i.e., $\lambda=1$), nonlocal theory should approximate atomic lattice dynamics.

One of the widely accepted functions of α is [63]

$$\alpha\left(|\mathbf{x}|,\lambda\right)=\left[2\pi\left(e_0a\right)^2\right]^{-1}K_0\left(\sqrt{\mathbf{x}\cdot\mathbf{x}}/l\lambda\right) \tag{2.2}$$

Where, the variable K_0 is determined using the modified Bessel function shown below [81]

$$K_0\left(r\right)=\frac{1}{2}\int\limits_{-\infty}^{\infty}\left[\exp\left(-\sqrt{r^2+z^2}\right)\Big/\sqrt{r^2+z^2}\right]dz \tag{2.3}$$

The variable r is the variable of the modified Bessel function and can be either real or imaginary, and z is the variable of integration.

By applying Green's function[81], the integral equation (Eq. 2.1) with α in the form of Eq. (2.2) can be simplified into a partial differential equation with the following relationship[63]

$$\left[1-\left(e_0a\right)^2\nabla^2\right]t_{ij}=\sigma_{ij}=C_{ijkl}\varepsilon_{ij} \tag{2.4}$$

Early research on nonlocal elasticity by Eringen in 1980s and 1990s, was developed to model screw dislocation, surface waves[63] and wave propagation[82] of crystalline structures at the atomic scale. More recently, nonlocal elasticity has been developed to model the mechanical properties of nanoscale structures. To the best of our knowledge, Wang was the first person to extend the governing equation of nonlocal beam theory with the stress-strain relationship defined in Eq. 2.4 to study the wave propagation in carbon nanotubes in 2005.[83] In 2007, Reddy derived the equation of motion of Euler–Bernoulli, Timoshenko, Reddy, and Levinson beam theories with Eringen's stress-strain relation (Eq. 2.4) for nanoscale materials. Analytical solutions of bending, vibration, and buckling for simply-supported nanowires were obtained to study the effect of the nonlocal behavior by using an assumed value for the nonlocal parameter e_0.[33] Recently, by using Reddy's equations and method, static deflection, free vibration,

uniaxial prestressed vibration and resonance of nanobeams and nanoplates have been studied with assumed values of e_0.[33-44]

Papargyri *et al.* considered the surface effect and nonlocal effect by comparing the mechanical behavior of nanobeams in deflection and in buckling as predicted with nonlocal effects and with the surface energy effect.[34] They found that the beam deflection decreases and the buckling load increases with increasing e_0. It was found that the surface energy effect is less significant for bending and buckling as compared to the nonlocal effect. However, herein it is hypothesized that such a difference should not exist since surface and nonlocal effects are two different ways to describe the same size effect. Specifically, Eringen stated that nonlocal effects would be able to model surface effects. Thus, it can be expected that the modeling results from both methods would be similar. It is postulated that the resulting difference found in Papargyri's work between the nonlocal and surface energy effects is due to arbitrarily assuming values for the nonlocal parameter e_0. Papargyri *et al.* also derived and solved the static bending of nonlocal Kirchhoff plates with the aid of the principle of virtual work with the boundary conditions of two opposite sides being clamped and the other simply-supported.[38] In this paper, they still arbitrarily assumed the value of e_0, and the nonlocal effect is not clear because of lack of knowing the physical attributes that affect the value of e_0.

Zhu and Dai solved the general solution for a nonlocal elastic bar in tension analytically and numerically for nanowires.[36] The governing equation of the 1D bar tensile problem was derived with Eq. 1.4. They found that the normal stress is not uniformly distributed in a bar with constant strain and nonlocal effects. This is different from the modeling with traditional elasticity, which has a linear relation between stress and strain (Hooke's law). Conversely, in local elasticity, the stress is constant if the applied strain is constant. In the nonlocal modeling, stress

concentrations were found at the two ends of the bar due to the nonlocal effect, even if the applied strain is uniform.

Murmu and Pradhan derived the nonlocal theory for nanoplates under uniaxial prestressed conditions, with the hypothesis that e_0 should always be real.[37] Their model is a combination of a transverse vibration problem and a buckling problem. They concluded that the nonlocal parameter, aspect ratios, boundary conditions, and initial uniaxial prestress have significant effects on vibration response of the nanoplates. For example, the resonant frequencies of the nanoplates and the critical compressive load are reduced by the nonlocal effect for the simply supported boundary conditions. A similar conclusion has been found by other researchers, where the stiffness of simply-supported beams and plates are always reduced with real e_0 values, i.e., resulted in lower resonant frequencies or larger deflections.[37, 39, 43, 44] However, a surface stress can either increase or decrease the stiffness of the beams and plates due to the boundary condition. In addition, a surface stress can be either positive or negative. The combination of simply-supported boundary condition and positive surface stress can result in an apparent stiffness increase[47]. Therefore, there seems to be a contradiction between the beam modeling with surface stress and nonlocal effect, although they are just different ways to describe the size effect and should be consistent. The ability for nonlocal theory to predict stiffness changes of a nanobeams or nanoplate is limited with a real e_0, since it can only predict a lower stiffness.

A fundamental issue in the nanoscale nonlocal elasticity is that the physical meaning of the material parameter e_0 is not well defined, which hinders its widespread application for nanoscale structures. Although nonlocal elasticity has been applied to nanoscale modeling of static bending[84], dynamic vibration[85-87], buckling[88] and wave propagation[83] of nanoscale materials, the bridging between the atomic scale and nanoscale has not been well studied.

Researchers usually assume a series of values for e_0 when establishing their theories. [33-42] They also restrict e_0 to a real number [33-42] which can only describe a negative surface and ambiguous size ranges.[39] This range is discussed in more detail in Chapter 6. To date, there has been limited research on the origin of e_0, especially at the nanoscale. While some researchers have tried to develop e_0 to enhance the accuracy of their calculations, but some results do not contain the true nonlocal effect with the nearest neighbor assumption. For example, Challamel and *et al.* derived a fixed solution to the nonlocal parameter material parameter e_0 for buckling [60] and flexural vibration[61] models, i.e. $e_0=0.289$ for buckling and $e_0=0.408$ for flexural vibration of a beam without an applied external load (free vibration). Wang *et al.* continued their work and derived e_0 for the situation between pure buckling and free flexural vibration, which is an axially forced vibrating beam.[62] However, their work on parameterizing e_0 does not include nonlocal effects. In actuality, the difference between Wang and Hu's model and classical linear elasticity is that they consider more terms for the finite difference approximation as shown in Eq. (2.5) and reproduced from Ref. [89].

$$\frac{\left(2u_n - u_{n+1} - u_{n-1}\right)}{a^2} = \frac{\partial^2 u_n}{\partial x^2} + \frac{a^2}{12}\frac{\partial^4 u_n}{\partial x^4}$$

(2.5)

In Eq. 2.5, a is the distance between each atom and x is the location of the atoms. The first term at the right hand side of Eq. (2.5) is the finite difference approximation in classical elasticity, which is the second derivate of the displacement with respect to the location. The second additional term is used to calibrate e_0 in Ref. [30-33], but it does not include nonlocal effects. Conversely, Eringen specified that nonlocal theory should account for surface physics, such as surface stresses, when he first developed the nonlocal elasticity theory.[34] Thus, the modeling includes nonlinear effects and not nonlocal properties. Thus, we propose that e_0 can be parameterized by incorporating surface effects (i.e. nonlocal) on the mechanical behavior of

nanobeams as proposed by Eringen, rather than by incorporating local models with additional finite difference terms. The outcomes of this study would be an analytical solution to e_0 that includes surface properties for nanoscale beams that have both positive and negative surface stresses. The approach will be based on solving the fundamental resonant frequency for simply-supported nanowires with Timoshenko beam theory with surface stress and nonlocal Timoshenko beam theory. Furthermore, we will calibrate e_0 with the calculated resonant frequencies of nanowires from molecular dynamics simulations for the other two boundary conditions and verify the analytical solution of e_0 for the simply-supported case obtained from the theoretical comparison.

2.3 <u>The Evaluation and Verification of Classic Continuum Mechanics, Beam Theory with Surface Stress and Molecular Dynamics Simulations</u>

2.3.1 *<u>Classic Continuum Mechanics</u>*

Continuum mechanics is usually used to model the mechanical behavior of nanoscale system if the size effect is assumed to be negligible.[21] Govindjee and Sackman tested the size limitation of the Euler-Bernoulli beam theory with the following model for multi-wall carbon nanotubes as shown in Figure 1.[90] This calculation can also be applied to verify the beam theory on the multi-layer beams with other materials. Figure 1 shows the cross-section and the variable definition of the model. The beam is made up of n layers of atoms with a distance s. The thickness of each layer is t and the distance to the center of sheet j is defined R_j.
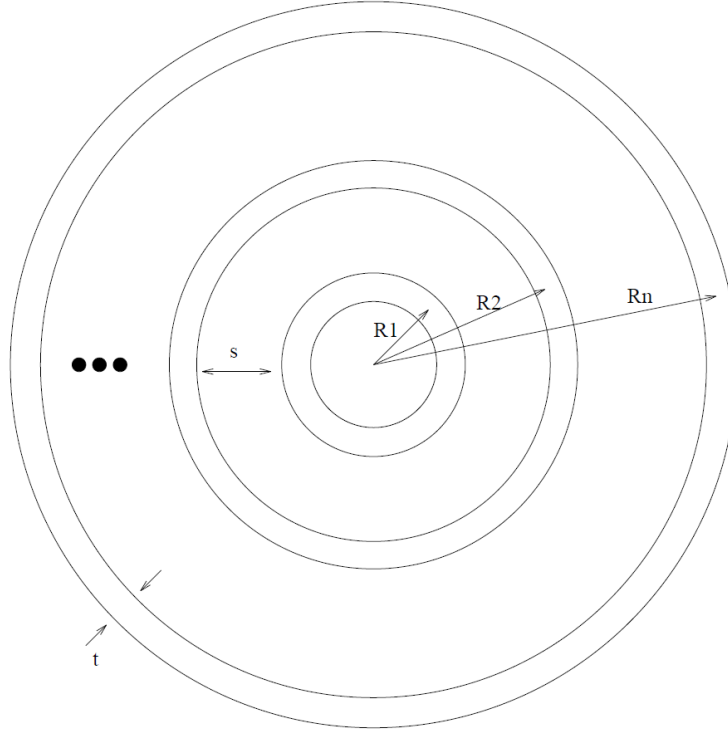
Figure 2.2. Cross-sectional dimensions for a multi-walled beam.

The elastic modulus $\bar{E}$ is the variable to evaluate the validation of the assumption of the continuum materials. The assumption is that a limited number of atom layers can be assumed as a solid continuum media and the mechanics of the material can be described with Euler-Bernoulli beam theory. The surface effect was not considered. It is found that if the moment of inertia is calculated by the polynomial $I = \dfrac{\pi}{4}\left[\left(R_n + t/2\right)^4 - \left(R_n - t/2\right)^4\right]$ and $t \ll s$, n has to be larger than 201 for the validity of the continuum cross-section hypothesis. In this case, $\bar{E}$ is between $0.99E$ to $1.01E$, where E is the bulk scale Young's modulus of the material. When $n=2$, $\bar{E} = 2.15E$ and the beam theory obviously does not work for such a small size. The break down

22

size of continuum mechanics with the polynomial moment of inertia is relatively large. However, the modeling can be improved if $I = \int_{R_n+t/2+s/2}^{R_1-t/2-s/2} r^3 \mathrm{d}r$ and $t << s$. With the new defined I, $n=2$ leads to $\bar{E} = 0.97E$ and the Euler-Bernoulli beam theory is relatively still valid for such a small size.

It can be seen that the break down size scale of continuum mechanics depends on many conditions. For example, with the model of Figure 1, the size limitation depends on n, s, t and R_n. For different materials with different chemical structures (n, s, t and R_n), the size limitations of the continuum mechanics are different. However, by improving the modeling equations (e.g., by changing the method of calculating the moment of inertia or adding surface effects), the amended continuum mechanics theories still work for much smaller size scales. In this thesis, we will apply two different ways to modify the continuum mechanics in order to describe the nanoscale mechanics. Surface effect and nonlocal effect will be added separately on the classical beam theories to describe the surface atoms of the nanowires.

2.3.2 *Beam Theory with Surface Stress Effect Modeling*

Wang and Feng derived the equation to describe the surface stress effect from Young-Laplace Equation.[31] Young-Laplace equation describes that the stress jump across a surface is related to the curvature tensor of the surface as shown in Eq. (2.6).

$$\left\langle \sigma_{ij}^{+} - \sigma_{ij}^{-} \right\rangle n_i n_j = \sigma_{\alpha\beta}^{s} \kappa_{\alpha\beta} \qquad (2.6)$$

Where σ_{ij}^{+} and σ_{ij}^{-} denote the stresses above and below the surface, respectively, n_i is the unit vector normal to the surface, $\sigma_{\alpha\beta}^{s}$ is the surface stresses and $\kappa_{\alpha\beta}$ is the curvature tensor.

If the surface stress effect of a nanowire can be described with the Young-Laplace Equation, the surface stress contributes a transverse load when the beam is in bending. The transverse load is expressed as

$$p(x) = H \frac{d^2 u}{dx^2} \qquad (2.7)$$

where H is a parameter determined by the surface stress along the nanowire longitudinal direction and the nanowire cross-sectional geometry.[29] For a circular or rectangular nanowire, H is expressed as

$$H = \begin{cases} 2\tau D...\text{(circle)} \\ 2\tau w...\text{(rectangle)} \end{cases} \qquad (2.8)$$

where D is the diameter of the circular nanowire, w is the width of the rectangle nanowire and τ is the surface stress.

As defined in Eq. (2.7), by adding the additional distributed load from the surface stress to the continuum mechanics equation, (e.g., beam theories), the surface stress effect has been studied for the nanoscale materials for different types of problems. The surface stress effect on the static deflection [47, 91], resonant frequencies [26, 92-94], buckling[49, 95-99] and quality factor [30] of the nanowires have been studied. One straight forward way to check the validation of the surface stress modeling is the convergence to continuum mechanics for larger sizes. The trend and convergence can evaluate if the theory over-estimates the surface stress effect. All these models find that the surface stress effect vanishes when the cross-section size of the structures grows. For example, as the cross-section reach 100nm or above, the resonant frequency of the nanowires only has less than 1% shift as compared to the classical beam theories for all aspect ratios and boundary conditions. Therefore, this modeling method does not over-estimate the surface stress effect for larger sizes.[26, 29] However, the precision of Eq. (2.7)

for smaller size scale is still unclear and if the equation under-estimates the surface effect is not known. The pre-condition of Eq. (2.7) is that the surface stress can be described with the Young-Lapalce equation, which is more commonly used for liquid and air interaction[100]. In order to verify Eq. (2.7), the comparison between different theoretical methods is not enough. Experimental data is better to verify Eq. (2.7). However, due to the size limitation of the atomic force microscopy for the mechanical test of nanowires, the minimum size for the bending nanowire test is 20nm[101] or 30nm[75, 102]. Figure 2.2 shows the comparison of the overall elastic modulus of Ag(100) nanowires from the static deflections of fixed-fixed nanowires among the Euler-Bernoulli beam theory with surface stress[47], Timoshenko beam theory with surface stress[91] and the experimental data[101]. The lengths of the tested nanowires were fixed as 1μm and the diameters of the cross-section changed as labeled in Figure 2.2. In Figure 2.2, the theoretical modeling methods generally have good agreements with the experimental data. As the cross-section grows, the results based on the Timoshenko beam theory are closer to the experimental data due to the smaller aspect ratio. More experimental data with different boundary conditions, sizes and materials is needed in the future to further and completely test the break down size of Eq. (2.7) and the improved beam equations with surface stress effect.
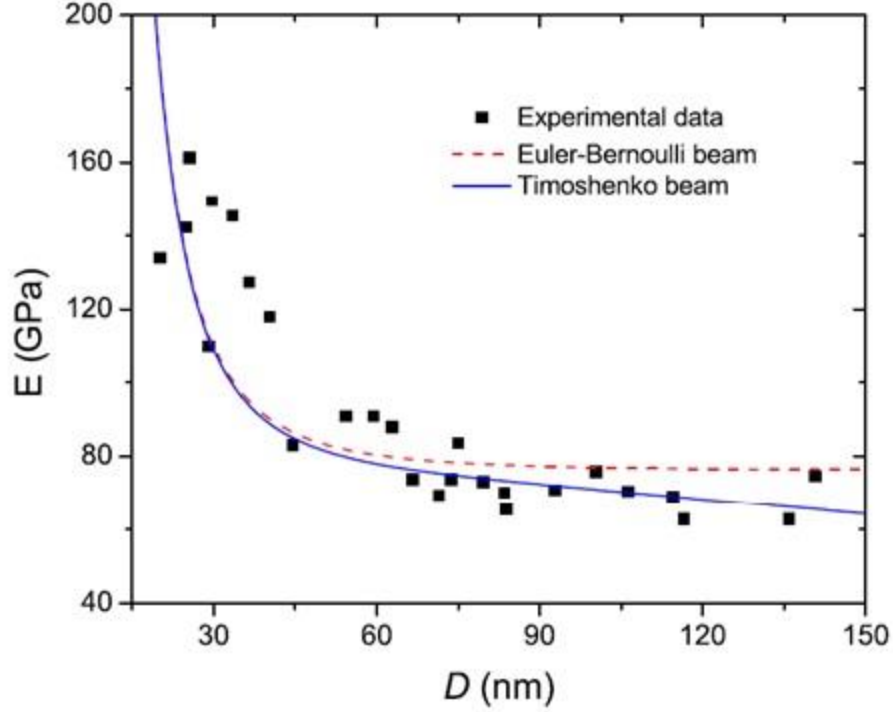
Figure. 2.3. The comparison of the overall elastic modulus of Ag(100) nanowires from the static deflections of fixed-fixed nanowires among the Euler-Bernoulli beam theory with surface stress[47], Timoshenko beam theory with surface stress[91] and the experimental data[101].

In Chapter 3 of the thesis, the resonant frequencies of fixed-fixed Au(100) nanowires are also compared to the molecular dynamics simulation results to verify the theoretical modeling. The aspect ratio is fixed as 12. The largest difference between the simulation and theoretical results is 7% for the smallest tested cross-section size of 4.08nmx4.08nm. Please refer section 3.3 and table 3.I for the details of the comparison and the following section for the validation of MD simulations.

2.3.3 *Molecular Dynamics Simulations*

Computational physics, for example MD simulations, is the study and application of numerical analysis to solve problems for which a quantitative theory already exists.[103] The basic concept in MD simulations is incorporating classical multibody dynamics (Newton's second law) and the potentials (energy) between pairs of particles at the atomic scale/resolution to model the properties, including mechanical behaviors of nanostructures.[54] The validity and accuracy of MD simulations depend on the interatomic potentials used as inputs.[104] The interatomic potentials, which are typically based on the experimental data, can directly depict the properties at the atomic scale, such as the displacement, velocity and the kinetic energy of particles. By imposing a dynamics rule (energy conservation or constant average temperature of the system), macroscale mechanical properties can be obtained from the atomic scale information.[105, 106] The application of MD simulations at the nanoscale includes determining material properties such as a nanostructure's elastic modulus[107-110] and ultimate strength[107, 110] or mechanical behavior such as static deflection[111] and resonant frequencies[53, 112].

In this section, the discussion about the MD simulations will be separated into two parts. The first part of the discussion focuses on the atomic scale potentials, which ensure that the MD simulations are valid at the atomic scale. The elastic constants from the Embedded Atom Model (EAM) potentials are compared. The ability of EAM potentials to describe the surface properties is also discussed. The nanomechanics should be an overall result of the atomic scale properties of all atoms in the body. Therefore, the second part presents the results and verification of the tensile, static bending and resonance tests for nanowires with MD simulations from literatures. Our MD simulation setups and results for these three types of tests will be introduced in Chapter

5 and 6. The MD simulation results will be finally applied to develop the theoretical modeling on nano mechanics.

A potential function (or usually just called potential) describes the force interaction between a pair or group of particles (atoms or molecules). A pairwise potential only considers the energy between two atoms, such as the Lennard-Jones potential. The expression of Lennard-Jones potential is [113]

$$V = 4\varepsilon \left[\left(\frac{\sigma}{r} \right)^{12} - \left(\frac{\sigma}{r} \right)^{6} \right] \tag{2.9}$$

where, V is the intermolecular potential (energy) between the two atoms or molecules. ε is the well depth. σ is the distance at which the intermolecular potential between the two particles is zero. r is the distance of separation between both particles.

The $\left(\frac{\sigma}{r} \right)^{12}$ term of the Lennard-Jones potential describes the short rage interaction of the chemical bonds, which is the major effect of the atoms. The $\left(\frac{\sigma}{r} \right)^{6}$ term in the Lennard-Jones potential describes the long range effect of the atom interactions, mainly the van der Waals force. Therefore, the van der Walls force effect can be included in the MD simulations with the right choice of potentials. The verification of Lennard-Jones potentials was achieved by comparing the curves from Eq. (2.9) to the experimental data and can be found in Ref. [113, 114].

The simulations introduced in this thesis were based on the EAM potentials. In addition to the pairwise potential, EAM considers the electron cloud contribution, as the first term in Eq. (2.10). In EAM models, an atom is assumed to locate in electron cloud which is uniform and thus spherical in shape. The embedding energy represents the energy required to place an atom into the electron cloud.[115] Therefore, EAM can be more accurate than the pairwise potentials if the

electron effect is significant. EAM is found to be particularly appropriate for the metallic systems studied in this thesis.[115, 116]. For the EAM model, the total energy of atom i can be expressed as the following: [117]

$$E_i = F_i(\bar{\rho}_i) + \frac{1}{2}\sum_{j \neq i}\Phi_{ij}(r_{ij})$$

(2.10)

Where, F_i is the embedding term, which is the energy to embed atom i into the background electron density; $\bar{\rho}_i$ is the host electron density at atom i due to the remaining atoms of the system. The term Φ_{ij} is the pair-wise addition of the interaction and r_{ij} is the distance between atoms i and j. Similar to Lennard-Jones potentials, Φ_{ij} can contain the van der Walls force effect if the long range effect of the atoms are considered. These parameters are generally obtained by fitting cohesive energy, equilibrium lattice constant, elastic constants, unrelaxed vacancy formation energy, bond length, and diatomic bond strength.[104]

Elastic constants of cubic crystals (C_{11}, C_{12}, C_{44}) can be calculated with the derived EAM functions.[115, 118, 119] The bulk mechanical properties, for example the elastic modulus, shear modulus and Poisson's ratio, depend on the elastic constants of the crystals.[120] These three elastic constants are usually compared to the experimental data to verify the EAM potentials. Daw and Baskes derived and studied the F_i and Φ_{ij} function for Ni and Pb (both are FCC crystals).[115] The elastic constants of Ni were C_{11}=2.438dyn/cm^2, C_{12}=1.506dyn/cm^2 and C_{44}=1.278dyn/cm^2 compared to C_{11}=2.465dyn/cm^2, C_{12}=1.473dyn/cm^2, and C_{44}=1.247dyn/cm^2 from experiment. The elastic constants of Pb were C_{11}=2.305dyn/cm^2, C_{12}=1.803dyn/cm^2 and C_{44}=0.755dyn/cm^2 compared to C_{11}=2.341dyn/cm^2, C_{12}=1.761dyn/cm^2, and C_{44}=0.712dyn/cm^2 from experiment. Baskes *et al.* derived the EAM potential for Ni$_3$Al. The elastic constants of Ni$_3$Al were C_{11}=2.516dyn/cm^2, C_{12}=1.370dyn/cm^2 and C_{44}=1.262dyn/cm^2 compared to

C_{11}=2.302dyn/cm^2, C_{12}=1.493dyn/cm^2, and C_{44}=1.316dyn/cm^2 from experiment.[118] Leach reported the comparison of the cubic elastic constants for Ag crystals. The values from the EAM calculation were C_{11}=1.24dyn/cm^2, C_{12}=0.93dyn/cm^2 and C_{44}=0.46dyn/cm^2, compared to C_{11}=1.24dyn/cm^2, C_{12}=0.934dyn/cm^2, and C_{44}=0.461dyn/cm^2 from experiment.[119]

From the above presented data of the cubic elastic constants, we can see that the EAM potential is an efficient way to model the elastic properties of the referenced crystals. The cubic elastic constants calculated with the published EAM potentials were close to the experimental data which supports that the EAM potentials can depict the elastic properties of the nanoscale materials.

Additionally, EAM potential can describe the surface properties of the materials. EAM potentials can be used to calculate the total energy for both bulk atoms and surface atoms using Eq. (2.10). Due to uncoordinated chemical bonds for surface atoms, the surface atoms are usually more active and have higher kinetic energy than the bulk atoms. Daw and Baskes also applied EAM potentials to calculate the surface energy and surface relaxation for Ni. It is found that the surface energy for Ni (100), (110) and (111) were 1550, 1740 and 1310 erg/cm^2 compared to the measured 1725 erg/cm^2.[115]

The surface stress can be calculated from the surface energy. The relation between surface energy and surface stress is

$$\tau_{\alpha\beta} = A^{-1}\partial(\gamma A)\partial\varepsilon_{\alpha\beta} \tag{2.11}$$

where A is the area of the surface unit cell, γ is the surface energy, $\varepsilon_{\alpha\beta}$ is the strain tensor.

With Eqs. (2.10) and (2.11), Wan *et al.* calculated the value and direction of surface stress and surface energy for FCC metals, e.g. Cu, Ag, Au, Ni, Pd, Pt, Al and Pb with different crystalline orientations.[64] Their results calculated with EAM were compared to the effective-

crystal theory and experimental data and found in good agreement. The comparison data can be found in Ref. [64]. The calculation in Refs. [115] and [64] support that the EAM is an effective way to model the surface property of FCC metals. The MD simulations for the mechanical properties of nanomaterials with the EAM potential will incorporate surface properties. EAM is able to describe the nanomechanics for both bulk and surface atoms. The simulation results based on EAM potentials can be treated as a standard method to model mechanical properties of nanoscale materials. [104, 111, 121, 122]

With the rapid development of computational power, MD simulations are commonly used to predict the mechanical properties of nanoscale materials. However, due to the gap in size scales and time steps between the MD simulations and experiments, it is still difficult to compare experimental with theoretical results. Typically, as listed in Table 1, the cross-section sizes in MD simulations are less than 10nm, but the typical minimum experimental size for the nanoscale mechanical test is ~100nm, for example 80-300nm in Ref.[123]. Guenole discussed three reasons of the difficulties in comparing the simulation and experimental results. First, the mechanical properties, such as the elastic modulus or resonant frequencies of nanowires, strongly depend on the geometry and size as shown with the MD simulations. However, it is hard to precisely control the geometry and size in an experiment. Second, the experimental stress field inside a nanowire is much more complex than that applied in simulations. Finally, a real nanowire is rarely free of defects, which are commonly introduced during the fabrication process.[124] These three reasons lead the comparison between MD simulations and experiments difficult. Guenole *et al.* simulated the yield strain and stress for Si nanowires (with cross-section size between 2.72x2.72nm and 43.45x43.45nm) along the [001] direction at 300K (room temperature).[124] They found a 20.2% yield strain and 14.3 GPa yield stress, as compared to 6% and 12 GPa

measured from experiment using 100x100nm cross-section[125] Si nanowires. The differences are caused by the size difference and the three abovementioned reasons.

The following table shows the validation of MD simulations for predicting the macroscale mechanical properties of nanoscale materials. EAM potential and FCC metals are emphasized. Both tensile test and bending (deflection and resonant frequency) test are included to show the different ways to verify the simulation result.

Table 2.I shows that the results of the mechanical properties for nanomaterials from MD simulations are close to the classical continuum theory prediction. However, there are some variations that need to be explained further. One fundamental issue of the existing MD simulations is that the simulation results are not compared with the theoretical modeling that includes nanoscale size effects. For example, the MD simulations and beam theory with size effects are usually studied independently, even if the MD simulation is a good way to support the theoretical modeling of the size effects, such as the surface stress effect or nonlocal effect. Ref. [111] mentioned that the difference between the MD simulation results and classical beam theory results is probably caused by the surface effect. But they did not calculate the surface effect and perform the comparison quantitatively. Since the EAM potential can model the surface effect, the MD simulation results with EAM should also contain the surface effect. The MD simulation results therefore can be applied to study nanomechanics, especially for surface properties. Herein, we will include surface effects in the beam modeling to study MD simulation results.

Table 2.I. The verification of MD simulations for predicting the mechanical properties of nanoscale materials.

Model	Material(s)	Potential	Verification method	Verification result	Reference
Tensile Test (12x12x32 lattice units at 10, 300 and 800K)	Al	Morse Potential (Pairwise Potential)	Yield Stress from MD vs. Ab initio calculation	2.30 GPa at a strain of 0.035 vs. 1.57 GPa at a strain of 0.040	[107]
Tensile Test (cross-section size=1.83x1.83nm at 0K)	Au	EAM	Elastic modulus from MD vs. Bulk values	<100> 42.3GPa vs. 42.3GPa <110> 80.8GPa vs. 80.8GPa <111> 116.5GPa vs. 116.2GPa	[108]
Tensile Test (cross-sction size=3x3nm-6x6nm at 300K)	Au(100)	EAM	Elastic modulus from MD vs. Bulk values	33.2GPa vs. 46.49Gpa	[109]
Resonant Frequency (120x20x1 lattice lengths at 300K)	Ni	EAM	FFT of the Displacement from MD vs. Euler-Bernoulli Beam Theory	Poor agreement 2.4166GHz vs. 25.244GHz for simply-supported 2.3271GHz vs. 57.22GHz for fixed-fixed	[112]
Tensile and Static Bending Tests (cross-section of 2-8nm at unspecified temperature)	Ag(100) and (110)	EAM	Elastic modulus from MD Tensile Test vs. MD vs. Bulk Values	Normalized elastic moduli with respect to the bulk values were calculated. Ag(100) 0.95-1.05 for tensile test, 0.65-1.03 for cantilever bending test. Ag(110) 1.2-2.1 for tensile test and 1.4-2.3 for cantilever bending test.	[111]
Resonant Frequency Tests (10x10, 14x14, and 18x18 lattice lengths for the cross-section and aspect ratios are 8-17 at 4.2 and 300K)	Au(100)	EAM	Resonant frequencies for first three vibration modes MD vs. Euler-Bernoulli and Timoshenko theories	Timoshenko beam theory's result is closer to the simulation result due to the shear effect. Shear effect is more significant for small aspect ratio and higher vibration mode. The difference between the simulation and theoretical results due to the size effects were not discussed.	[53]

2.4 <u>Summary of Literature Review</u>

As discussed above, a fundamental knowledge gap for nonlocal beam theory is that the nonlocal parameter e_0, which bridges the atomic scale and nanoscale, is not well defined or clearly understood. The hypothesis of this research is that Timoshenko beam theory with surface effects, Eringen's nonlocal elasticity and the corresponding nonlocal beam theories, and MD simulations results should be consistent at the nanoscale for structures with critical dimensions from 1-100nm. To the best of our knowledge, no researchers have incorporated surface effects with nonlocal effects within a beam theory to study the nonlocal parameter e_0. Since analytical solutions of the resonant frequency of simply-supported nanowires from both Timoshenko beam theory with surface effect or nonlocal effect exist, we propose to study the parameters of e_0 by defining an analytical solution. Additionally, MD simulations will be performed to calculate the resonant frequencies of nanowires with cross-section 2-4nm from the free vibration. The simulation results can be used to verify the theoretical and analytical calibration for simply-supported and investigate e_0 for the cantilever and fixed-fixed boundary conditions.

CHAPTER 3. Modeling and Analysis of Nanowires with Timoshenko Beam Theory Incorporated with Surface Stress for Three Boundary Conditions

3.1 <u>Introduction</u>

In this chapter, Timoshenko beam theory incorporated with surface stress was studied to model the resonant frequencies of nanowires. The procedure to develop the Timoshenko beam theory with surface stress is similar to previously found in Ref.[29], by incorporating the Young-Laplace Equation with the Euler-Bernoulli beam theory. However, Timoshenko beam theory was applied in this thesis to eliminate the limitation of aspect ratio with Euler-Bernoulli beam theory. In addition, since it is known that the surface effect depends on the boundary conditions, cantilever, simply-supported and fixed-fixed nanowires will be studied to verify the modeling results. Finally, Face-Centered-Cubic (FCC) metal nanowires, Au(100) and Ag(100) with different cross-sectional sizes and aspect ratios, were studied. The resonant frequencies from nonlocal Timoshenko beam theory will be compared to the resonant frequencies derived from this chapter to solve for e_0.

Euler-Bernoulli beam theory with surface stress effects to model static bending and transvers vibration of nanowires has been widely studied.[25, 28, 29, 32, 47] However, the Euler-Bernoulli beam theory is based on the assumption that the normal planes are always perpendicular to the neutral planes (Figure 3.1 (a)), but this is only true when the beam is slender (a length to diameter ratio, i.e. aspect ratio, greater than 10). However, the nanowire structures integrated into Nanoelectromechanical Systems (NEMS) sometimes have aspect ratios less than 5 [49] and the shear force may become significant to the elastic behavior of these systems.[79]

Since the research objective is to study the size effect of the nanoscale materials with wider applicability, for example eliminating the aspect ratio limitation of Euler-Bernoulli beam theory, a more general beam theory is desired to include a larger range of parameters that may affect the nonlocal parameter e_0.

Timoshenko beam theory considers shear deformation and is suitable for analyzing the elastic behaviors of either short or long beams. Contrary to the Euler-Bernoulli beam theory, the angular rotation of a beam, as shown in Figure 3.1(b), is not equal to du/dx due to the shear effect. Also, the shear force, V, is not equal to EId^3u/dx^3, where E is elastic modulus and I is the second moment of area. Instead, the shear force is equal the following expression

$$V = AkG(\varphi - du/dx) \tag{3.1}$$

where, A is the cross-sectional area, k is the Timoshenko shear coefficient which depends on the geometry, G is the shear modulus, φ is the angular displacement, u is the vertical displacement of the neutral axis and x is the axial position. For a circular and rectangular cross-section beam, the shear coefficients are:

$$k = \begin{cases} (6+12\upsilon+6\upsilon^2)/(7+12\upsilon+4\upsilon^2)...\text{(circle)} \\ (5+5\upsilon)/(6+5\upsilon)........................\text{(rectangle)} \end{cases} \tag{3.2}$$

where υ is Poisson's ratio.[15]

du/dx=φ

(a)

du/dx

φ

(b)
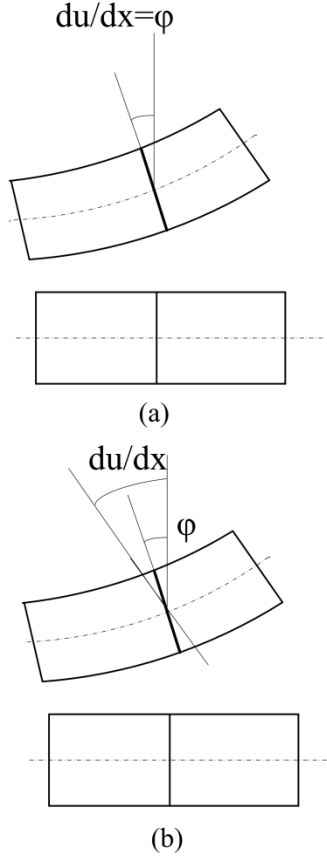
Figure 3.1. Illustration of the difference between the assumptions of the Euler-Bernoulli and Timoshenko beam theory. (a) In the Euler-Bernoulli theory, the angular displacement is equal to the derivate of the deflection with respect to the axial position x. (b) In the Timoshenko theory, the angular displacement has an additional term due to the shear effect.

By applying Eq. (3.1) and Newton's second law, the dynamic form of the Timoshenko beam theory can be expressed with the following two partial differential equations (PDEs) [126]:

$$\frac{\rho A \partial^2 u}{\partial t^2} - p(x,t) = \frac{\partial}{\partial x}[AkG(\frac{\partial u}{\partial x} - \varphi)] \tag{3.3}$$

and $\quad \frac{\rho I \partial^2 \varphi}{\partial t^2} = AkG(\frac{\partial u}{\partial x} - \varphi) + EI \frac{\partial^2 \varphi}{\partial x^2}$. $\tag{3.4}$

For Eqs. (3.3) and (3.4), ρ is the density of the nanowire material, t represents time, and p is the distributed load on the beam.

In addition to the shear effect for nanowires with aspect ratios less than five, the surface effect also has to be considered at the nanoscale. The surface effect is due to the uncoordinated surface atoms, where surface atoms lack adjacent atoms and dangling bonds are present.[28] As a result, the surface has properties that are different from the bulk volume and are commonly described with such parameters as surface stress, surface elasticity, or surface energy.[17] Researchers have found that surface effect can have a significant influence on elastic properties [29, 47], fracture and yield strength [27], and melting of nanowires.[71]

Previous research by He and Lilley incorporated surface stress and elasticity into the Euler Bernoulli beam theory to obtain an overall elastic modulus.[47] They showed that surface stress has different effects for different boundary conditions. For example, for a positive surface stress and cantilever beam boundary conditions, the nanowires appear stiffer as compared to nanowires without surface stress. The opposite occurred for simply-supported and fixed-fixed beams with positive surface stress.[47] In addition, Cuenot *et al.* utilized an atomic force microscopy (AFM) to observe the surface tension effect on the mechanical properties of Ag and Pb nanowires and polypyrrole nanotubes.[75] Wang and Feng introduced a thin surface layer to investigate both surface elasticity and residual surface stress on the natural frequency of microbeams.[32] They also applied the Timoshenko's beam theory to investigate both the static and dynamic behavior of buckling nanowires.[49] In addition, Zhang *et al.* modeled nanowires with rectangle cross-sections for three different boundary conditions and applied pure bending moment at the end to study the stiffening effect of tensile surface stress.[25] Finally, Miller and Shenoy applied a continuum mechanics model with surface stress and elasticity to describe the size dependence of

the stiffness of plates and bars in either uniaxial tension or bending. [71] However, the modeling of surface effects coupled with shear effects and boundary condition effects have not been widely studied. Thus, this chapter will include a detailed study on the combined effects of surface properties and shear effects on the resonant behavior of nanowires.

3.2 <u>Theoretical Modeling of the Timoshenko Beam Theory with Surface Stress</u>

As seen in Figure 3.2, the surface effect is modeled with the "core-shell" approach where the surface is assumed as a thin layer. This thin layer has mechanical properties that differ from the bulk material and are typically characterized with the parameters surface energy or surface stress and surface elasticity. Surface elasticity has been found to have a negligible effect on the mechanical behavior for critical dimensions larger than 10 nm.[24] Thus, only surface stress will be considered in this discussion.
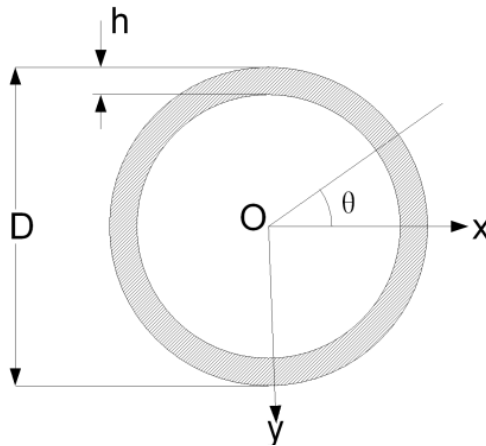
Figure 3.2. Cross-sectional view of a circular nanowire modeled with the core-shell approach.

By applying the Young-Laplace equation [31], the surface stress contributes a transverse load when the beam is in bending, as seen in Figure 3.3. The transverse load is expressed as [47]

$$p(x) = H \frac{d^2 u}{dx^2} \tag{3.5}$$

where H is a parameter determined by the surface stress along the nanowire longitudinal direction and the nanowire cross-sectional geometry.[47] For a circular or rectangular nanowire, H is expressed as

$$H = \begin{cases} 2\tau D ... \text{(circle)} \\ 2\tau w ... \text{(rectangle)} \end{cases} \tag{3.6}$$

where D is the diameter of the circular nanowire, w is the width of the rectangle nanowire and τ is the surface stress.
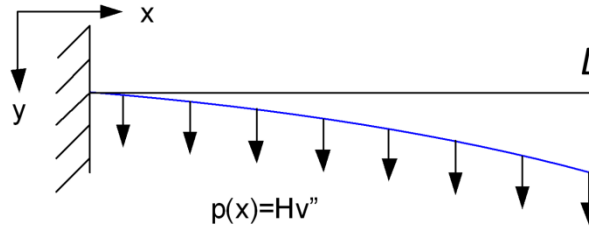
Figure 3.3. A cantilever beam with a transverse load caused by surface stress.

From Eqs. (3.4) and (3.5), the Timoshenko beam theory can be expressed as two PDEs for both the deflection and angular displacement.[127]

$$(1+\frac{H}{AkG})EI\frac{\partial^4 u}{\partial x^4}+\rho A\frac{\partial^2 u}{\partial t^2}-H\frac{\partial^2 u}{\partial x^2}-(\rho I+\frac{EI\rho}{kG}+\frac{\rho IH}{AkG})\frac{\partial^4 u}{\partial x^2\partial t^2}+\frac{\rho^2 I}{kG}\frac{\partial^4 u}{\partial t^4}=0 \qquad (3.7)$$

$$(1+\frac{H}{AkG})EI\frac{\partial^4 \varphi}{\partial x^4}+\rho A\frac{\partial^2 \varphi}{\partial t^2}-H\frac{\partial^2 \varphi}{\partial x^2}-(\rho I+\frac{EI\rho}{kG}+\frac{\rho IH}{AkG})\frac{\partial^4 \varphi}{\partial x^2\partial t^2}+\frac{\rho^2 I}{kG}\frac{\partial^4 \varphi}{\partial t^4}=0 \qquad (3.8)$$

By using separation of variables and defining $u(x,t)=\sum_{n=1}^{\infty}X_n(x)e^{i\omega_n t}$ and

$\phi(x,t)=\sum_{n=1}^{\infty}\Phi_n(x)e^{i\omega_n t}$, Eqs. (3.7) and (3.8) can be reduced to:

$$P\frac{\partial^4 X}{\partial x^4}+Q\frac{\partial^4 X}{\partial x^2}-R=0 \qquad (3.9)$$

$$P\frac{\partial^4 \Phi}{\partial x^4}+Q\frac{\partial^4 \Phi}{\partial x^2}-R=0 \qquad (3.10)$$

where the variables P, Q and R are defined as $P=(1+\frac{H}{AkG})EI$, $Q=\rho(I+\frac{EI}{kG}+\frac{IH}{AkG})\omega_n^2-H$ and

$R=\rho A\omega_n^2$. The variable ω_n is the nth mode circular resonant frequency.

The variables X and Φ are the spatial (time-independent) solutions of the vertical deflection

and the angular displacement. Neglecting $\frac{\partial^4 u}{\partial t^4}$ [126], the solutions for X and Φ are

$$X_n(x)=C_{1n}\cosh(S_{1n}x)+C_{2n}\sinh(S_{1n}x)+C_{3n}\cos(S_{2n}x)+C_{4n}\sin(S_{2n}x) \qquad (3.11)$$

$$\Phi_n(x)=D_{1n}\cosh(S_{1n}x)+D_{2n}\sinh(S_{1n}x)+D_{3n}\cos(S_{2n}x)+D_{4n}\sin(S_{2n}x) \qquad (3.12)$$

where, the index n=1, 2, 3...,

$$S_{1n}=\sqrt{\frac{\sqrt{Q^2+4PR}-Q}{2P}} \quad \text{and} \quad S_{2n}=\sqrt{\frac{\sqrt{Q^2+4PR}+Q}{2P}}.$$

Three different boundary conditions were studied, as shown schematically in Figure 3.4.

They are cantilever (CA), simply supported (SS) and fixed-fixed (FF) and the corresponding

boundary conditions are described as follows [79]:

$u(0)=\varphi\,(0)=M(L)=V(L)=0$ \qquad (CA)

41

$u(0)=u(L)= M(0)=M(L)=0$ (SS)

$u(0)=u(L)=\varphi(0)= \varphi(L)=0$ (FF)

where M is the bending moment.
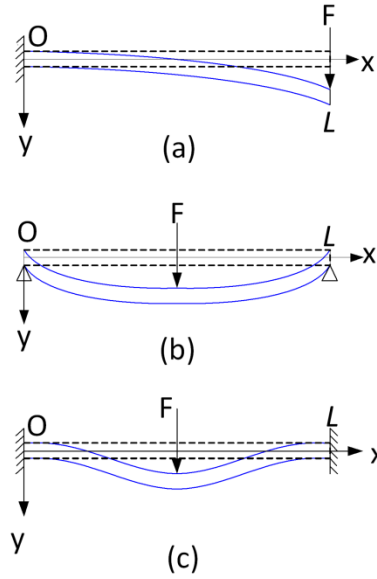
Figure 3.4. Illustration of the three boundary conditions studied. (a) CA, (b) SS and (c) FF.

3.2.1 *Resonant Frequency Modeling*

Applying the boundary conditions to Eqs. (3.11) and (3.12) above, the resonant frequency of a simply-supported nanowire can be obtained analytically as shown below in Eq. (3.13). [49]

$$\omega_n = \sqrt{[\frac{(1+\frac{H}{AkG})EIn^4\pi^4}{L^4}+\frac{Hn^2\pi^2}{L^2}]/[\rho A+\frac{\rho n^2\pi^2(\frac{EI}{kG}+I+\frac{HI}{AkG})}{L^2}]}$$ (3.13)

The resonant frequencies for a cantilever and fixed-fixed nanowire can be obtained numerically by solving Eqs. (3.14) and (3.15) respectively.

$$\begin{vmatrix} 0 & \delta_{1n} & 0 & -\delta_{2n} \\ 1 & 0 & 1 & 0 \\ S_{1n}\sinh(S_{1n}L) & S_{1n}\cosh(S_{1n}L) & -S_{2n}\sin(S_{2n}L) & S_{2n}\cos(S_{2n}L) \\ S_{1n}^2\cosh(S_{1n}L) & S_{1n}^2\sinh(S_{1n}L) & -S_{2n}^2\cos(S_{2n}L) & -S_{2n}^2\sin(S_{2n}L) \end{vmatrix} = 0 \qquad (3.14)$$

$$\begin{vmatrix} 0 & \delta_{1n} & 0 & -\delta_{2n} \\ 1 & 0 & 1 & 0 \\ \delta_{1n}\sinh(S_{1n}L) & \delta_{1n}\cosh(S_{1n}L) & \delta_{2n}\sin(S_{2n}L) & -\delta_{2n}\cos(S_{2n}L) \\ \cosh(S_{1n}L) & \sinh(S_{1n}L) & \cos(S_{2n}L) & \sin(S_{2n}L) \end{vmatrix} = 0 \qquad (3.15)$$

Herein, δ_{1n} and δ_{2n} are defined as,

$$\delta_{1n} = \frac{AkG - \rho I \omega_n^2 - EIS_{1n}^2}{AkGS_{1n}} \quad \text{and} \quad \delta_{2n} = \frac{AkG - \rho I \omega_n^2 + EIS_{2n}^2}{AkGS_{2n}}.$$

Figure 3.5 is the plot of the determinant (3.15) with respect to resonant frequencies for Ag(100) with D=10nm, AR=2.5, a density of ρ=10500kg/m^3, an elastic modulus of E=76GPa, a surface stress of τ=0.89N/m, and a Poisson's ratio of υ=0.3.[5] The intersection points of the determinant curve and the horizontal axis are the solutions of the resonant frequencies of each mode (n=1, 2, 3…). The solution can be found in Table 3.V with D=10nm and AR=2.5.
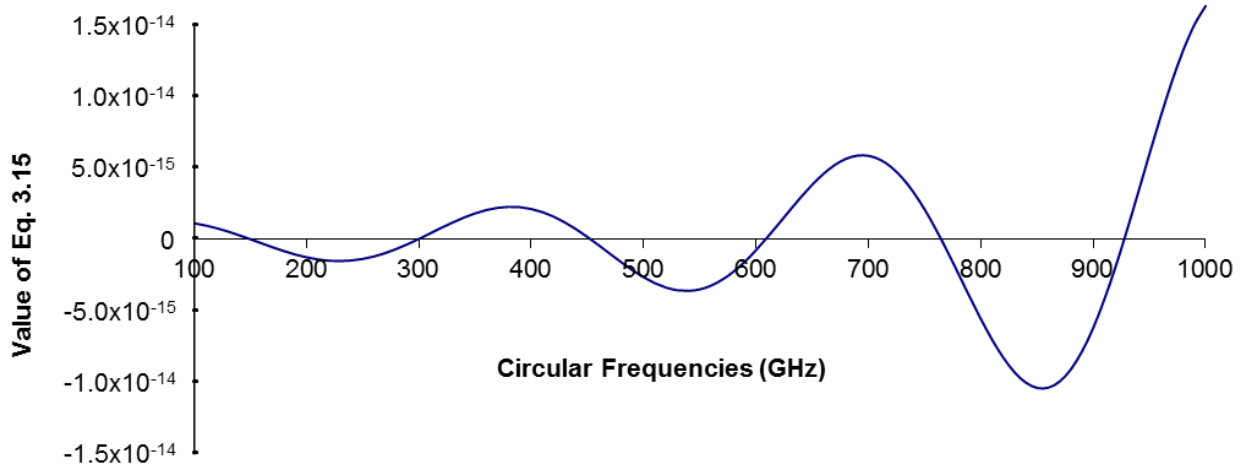
Figure 3.5. Illustration of the values of determinant versus circular frequencies for fixed-fixed Ag nanowire with *D*=10nm and *AR*=2.5.

3.2.2. *Free Vibration Modeling*

In the free vibration models, an initial concentrated static force *F* is applied at the free end of the cantilever, and at the midpoint of simply-supported and fixed-fixed nanowires. Thereafter, a complete solution of the nanowires' vibration after removing the exciting point force *F* can be obtained. The vibration of the nanowires is a function of the displacement with respect to location and time. The vibration solution is achieved with the initial conditions and the resonant frequencies.

The initial condition of the vibration of the nanowires is the static deflection solution and zero velocity. The static bending solutions for the Timoshenko beam theory with surface stress and three boundary conditions are shown in Eq. (3.16) [91].

$$v(x,t=0) = \begin{cases} \dfrac{F}{H\eta}\sinh[\eta(L-x)] + xF\cosh(\eta L)(\dfrac{1}{H}+\dfrac{1}{AkG}) - \dfrac{F}{H\eta}\sinh(\eta L), x\in[0,L] & \text{Cantilever} \\[3mm] -\dfrac{F\sinh(\eta x)}{2H\eta\cosh(\eta L/2)} + \dfrac{Fx}{2H} + \dfrac{Fx}{2AkG}, x\in[0,L/2] & \text{Simply-supported} \\[3mm] \dfrac{-F\cosh(\eta x)+F\cosh[\eta(x-L/2)]+F-F\cosh(\eta L/2)}{2\eta H\sinh(\eta L/2)} + \dfrac{Fx}{2H} + \dfrac{Fx}{2AkG}, x\in[0,L/2] & \text{Fixed-fixed} \end{cases}$$ (3.16)

where, $\eta = \sqrt{\dfrac{AkGH}{EI(AkG+H)}}$, (3.17)

and F is the applied force in the static bending to stimulate the initial condition.

From Eq. (3.11) and the determinants (3.14) and (3.15) for the cantilever and fixed-fixed nanowires respectively, the spatial solution is

$$X_n(x) = C_n\left[\cosh(S_{1n}x) + \frac{1}{\alpha_n}\sinh(S_{1n}x) - \cos(S_{2n}x) - \frac{\delta_{2n}}{\delta_{1n}\alpha_n}\sin(S_{2n}x)\right]$$ (3.18)

and for the simply-supported nanowires, the spatial solution is

$$X_n(x) = C_n\sin(S_{2n}x),$$ (3.19)

where n indicates nth mode of the vibration.

C_n are the unknown constants that need to be solved with respect to Eq. (3.16). For a cantilever boundary condition,

$$\alpha_n = \left[-S_{1n}\sinh(S_{1n}L) - S_{2n}\sin(S_{2n}L)\right] / \left[S_{1n}\cosh(S_{1n}L) + \frac{\delta_{1n}}{\delta_{2n}}S_{2n}\cos(S_{2n}L)\right]$$ (3.20)

and for fixed-fixed boundary condition,

$$\alpha_n = \left[\sinh(S_{1n}L) - \frac{\delta_{2n}}{\delta_{1n}}\sin(S_{2n}L)\right] / \left[\cos(S_{2n}L) - \cosh(S_{1n}L)\right]$$ (3.21)

If we consider a cantilever boundary condition, after applying the initial conditions, Eq. (3.22) can be obtained as stated below.

$$u(x,t=0) = \frac{F}{H\eta}\sinh[\eta(L-x)] + xF\cosh(\eta L)(\frac{1}{H}+\frac{1}{AkG}) - \frac{F}{H\eta}\sinh(\eta L), x\in[0,L]$$ (3.22)

The initial conditions can be expanded into a series of sine functions as shown in Eq. (3.23), where m indicates positive integers, such as 1, 2, 3…

$$u(x,t=0)=\sum_{m=1}^{\infty}B_m\sin(\frac{m\pi x}{L}) \tag{3.23}$$

The spatial term can also be expanded into a series of sine functions, as shown in Eq. 3.24.

$$C_n\left[\cosh(S_{1n}x)+\frac{1}{\alpha_n}\sinh(S_{1n}x)-\cos(S_{2n}x)-\frac{\delta_{2n}}{\delta_{1n}\alpha_n}\sin(S_{2n}x)\right]=\sum_{n=1}^{\infty}\sum_{m=1}^{\infty}C_nb_{nm}\sin(\frac{m\pi x}{L}) \tag{3.24}$$

Finally, the initial condition can be applied to obtain C_n in Eq. (3.25).

$$\sum_{m=1}^{\infty}B_m\sin(\frac{m\pi x}{L})=\sum_{n=1}^{\infty}C_n\sum_{m=1}^{\infty}b_{nm}\sin(\frac{m\pi x}{L})=\sum_{n=1}^{\infty}\sum_{m=1}^{\infty}C_nb_{nm}\sin(\frac{m\pi x}{L}) \tag{3.25}$$

Then the following linear relationship can be used to solve for C_n.

$$\begin{bmatrix} b_{11} & b_{12} & \cdots & b_{1n} & \cdots & b_{1\infty} \\ b_{21} & b_{22} & \cdots & b_{2n} & \cdots & b_{2\infty} \\ \vdots & \vdots & \ddots & & & \vdots \\ b_{m1} & b_{m2} & & b_{mn} & & b_{m\infty} \\ \vdots & \vdots & & & \ddots & \vdots \\ b_{\infty 1} & b_{\infty 2} & \cdots & b_{\infty n} & \cdots & b_{\infty\infty} \end{bmatrix}\begin{bmatrix} C_1 \\ C_2 \\ \vdots \\ C_n \\ \vdots \\ C_\infty \end{bmatrix}=\begin{bmatrix} B_1 \\ B_2 \\ \vdots \\ B_m \\ \vdots \\ B_\infty \end{bmatrix} \tag{3.26}$$

The coefficients C_n for each resonant frequency can be calculated by this set of linear equations. Theoretically, a ∞ by ∞ matrix is needed to calculate the coefficient; thus, by limiting the number of frequencies, there are numerical errors that need to be tested to validate the results. The discussion of the error is discussed in section 3.4.

3.3. A Comparison of the Resonant Frequencies Calculated with Timoshenko Beam Theory with Surface Stress to those Calculated with MD Simulations

Table 3.I presents the comparison of the first three resonant frequencies for Au(100) nanowires calculated with MD simulations and Timoshenko beam theory with a tensile surface stress of 1.03N/m[128]. The boundary condition for the nanowires is fixed-fixed. The elastic modulus (E) were obtained from Reference [52] from tensile simulations with the indicated temperatures and geometries shown in Table 3.1. As can be seen, there is good agreement between the results from MD simulation and those calculated with Timoshenko beam theory with surface stress. The results of calculation are slightly larger than from the MD simulation particularly when the dimension is small. The maximum error for the calculated fundamental frequency is 7% for the 4.08x4.08x49 (nm) nanowire at 300K. As the dimension grows, the fundamental frequencies approach the values from the MD calculations. In contrast, the resonant frequencies of the higher modes show smaller values than the values calculated with MD simulations.

Table 3.I. The first three resonant frequencies for fixed-fixed Au nanowires with different geometry (density ρ=19,300kg/m^3 and Poisson's ratio of v=0.44). The geometry, temperature, elastic modulus and MD results are from Ref. [53]. The surface stress value of Au(100) is from Ref. [128].

Dimension(nm)	T(K)	E(Pa)	From MD			From the Timoshenko theory with surface stress (1.03N/m)		
			f_1(GHz)	f_2(GHz)	f_3(GHz)	f_1(GHz)	f_2(GHz)	f_3(GHz)
4.08x4.08x49	4.2	39	2.71-2.78	7.28-7.33	13.8-13.9	2.96	7.06	12.39
	300	33.8	2.56-2.63	6.87-6.95	12.9-13.2	2.82	6.69	11.67
5.71x5.71x68.5	4.2	41.6	1.95-1.97	5.24-5.25	9.92-9.94	2.05	5.02	8.92
	300	39.1	1.99	5.19-5.20	9.62-9.87	2.01	4.89	8.68
7.34x7.34x88.1	4.2	42.9	1.53	4.09	7.74	1.56	3.88	6.95
	300	41.8	1.54-1.55	4.05-4.19	7.5	1.55	3.83	6.87

3.4 <u>The Free Vibration Solution</u>

Ag was used to study the free vibration of nanowire beam. The material parameters for Ag are a density of $\rho=10500\text{kg/m}^3$, an elastic modulus of $E=76GPa$, a surface stress of $\tau=0.89\text{N/m}$ [47], and a Poisson's ratio of $\upsilon=0.3$. Table 3.II below lists the values of C_1 corresponding to the fundamental resonant frequency calculated with n number of resonant frequencies and the relative error for a free vibrating Ag cantilever nanowire. From Table 3.II, it can be seen that if 30 frequencies and vibration modes are used to calculate the displacement, the error is 0.00007% and can be considered as negligible. Therefore, thirty vibration modes were used for the remaining calculations.

Table 3.II. C_1 Based on n frequencies and the associated calculation error (Cantilever Ag nanowire with $D=20$ nm, $L=20D$) for $F=1\text{nN}$ (nano Newtons). $C_{1,n}$ is calculated by using Eq. (3.26), with a nxn matrix.

Number of ω_n N	$C_{1,n}$	$C_{1,n}-C_{1,n-1}$	$(C_{1,n}-C_{1,n-1})/C_{1,n}$
2	3.647319×10^{-8}	4.09×10^{-10}	1.12142%
5	3.650733×10^{-8}	-5.76×10^{-12}	-0.01579%
10	3.651363×10^{-8}	1.55×10^{-12}	0.00424%
20	3.651324×10^{-8}	1.20×10^{-13}	0.00033%
30	3.651322×10^{-8}	2.54×10^{-14}	0.00007%

The free vibration solution of a cantilever, simply-supported and fixed-fixed Ag nanowires with a 20 nm diameter cross-section and aspect ratio (*AR*) of 20 are presented in Figure 3.6-3.8. The initial applied force was 1nN. As can be seen, the surface stress expands the amplitude of

deflection for a cantilever but reduces the amplitude of simply-supported and fixed-fixed nanowires, similar to the static deflection solution. As can also be expected, the vibration of a cantilever is slower when surface stress is included but simply-supported and fixed-fixed are faster as compared to the solution with bulk material properties due to the change in resonant frequency from the surface stress.

The normal stress and velocity of each point on the nanowire with respect to different time and position can be calculated and the kinetic and elastic potential energy can be derived with the vibration solution.
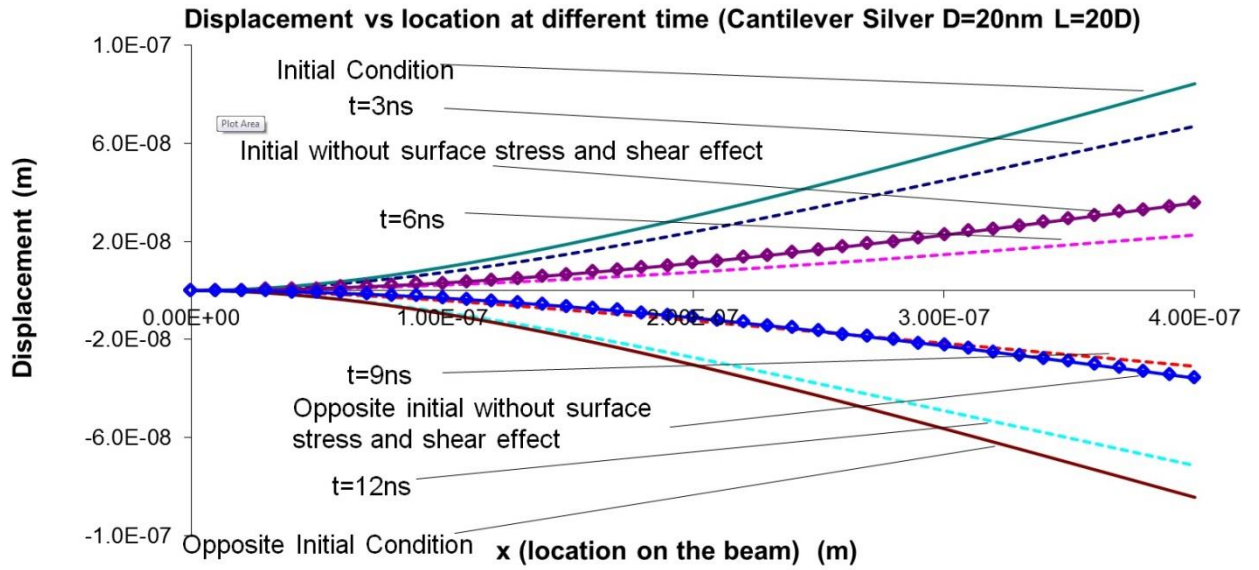
Figure 3.6. The vibration displacement of a cantilever Ag nanowire (*D*=20nm, *AR*=20).
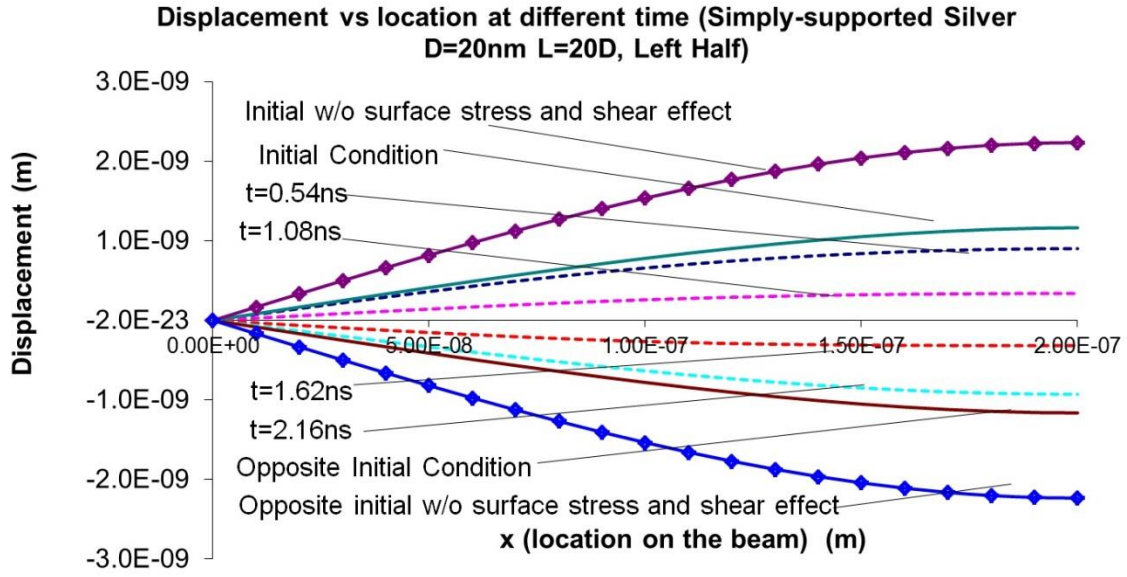
Figure 3.7. The vibration displacement for half (x∈[0, *L*/2]) of a simply-supported Ag nanowire (*D*=20*nm*, *AR*=20).
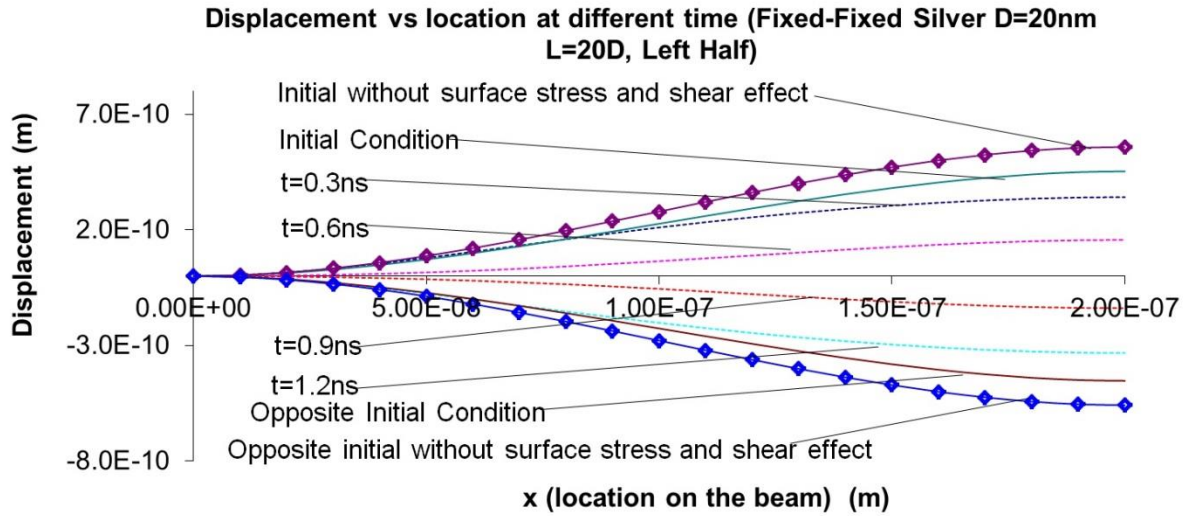
Figure 3.8. The vibration displacement for half (x∈[0, *L*/2])) of a fixed-fixed Ag nanowire (*D*=20*nm*, *AR*=20).

3.5 <u>Analysis of Shear and Surface Effects</u>

3.5.1 *<u>Influence of Shear and Surface Effects on the Fundamental Frequency</u>*

In order to compare the surface and shear effects, ten aspect ratios (*AR*) were studied, *AR*= 2.5, 5, 7.5, 10, 12.5, 15, 17.5 and 20, for nanowires with diameters of 10 nm, 20 nm, 100 nm, and 500 nm. A normalized resonant frequency ratio was used to study the effects of surface stress. This ratio is defined as $F_{i1}=\omega_{i1}/\omega_1$ where the fundamental resonant frequency, ω_i. The subscript *i* is the theory used in the calculations and denoted as (1) for Timoshenko beam theory with surface stress, (2) for Timoshenko beam theory without surface stress, and (3) for Euler-Bernoulli beam theory with surface stress. The fundamental frequency ω_1 is calculated with the classical Euler-Bernoulli beam theory.

The numerical calculations were validated by studying the case of Timoshenko beam theory when $\tau=0$, see Figure 3.9, for the three different boundary conditions. As can be seen, the normalized fundamental resonant frequencies approach the frequencies as those calculated with the Euler-Bernoulli beam theory without surface stress when the aspect ratios become large. By including the shear deformation, the Timoshenko beam theory predicts a larger bending deformation as compared to the Euler-Bernoulli beam theory. Therefore, in general, Timoshenko beams behave as more flexible beams and have lower fundamental resonant frequencies than those predicted with the Euler-Bernoulli beam theory. As can also be seen in Figure 3.9, the shift in resonant fundamental frequency due to the shear effect is independent of size (i.e. diameter independent) and depends only on the aspect ratios, where the shear effect becomes more pronounced for small aspect ratios. In addition, the change in the fundamental resonant
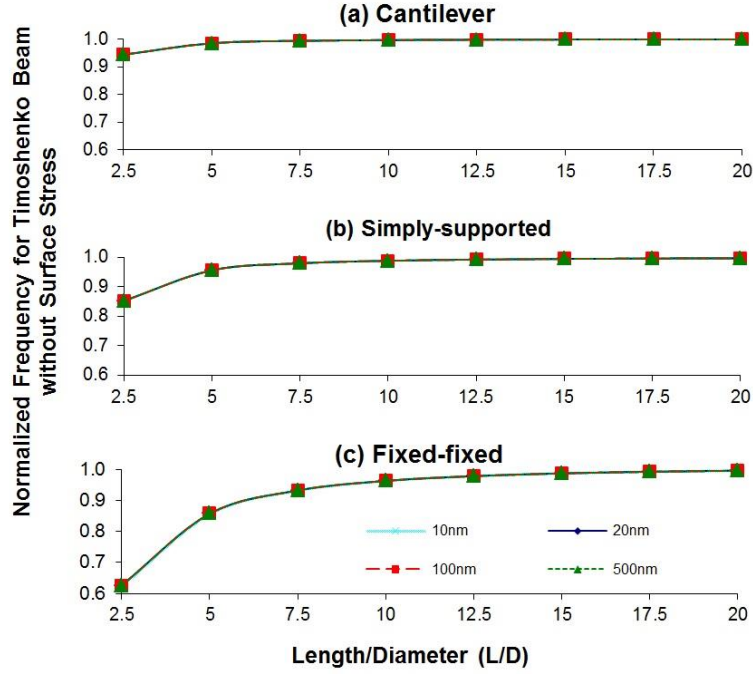
Figure 3.9. The normalized fundamental frequencies versus aspect ratio for Ag nanowires from the Timoshenko beam theory for $\tau=0$ and the three different boundary conditions: (a) cantilever, (b) simply-supported and (c) fixed-fixed.

Boundary condition effects were considered by comparing the normalized fundamental resonant frequencies, F_{i1}. The normalized fundamental resonant frequencies are calculated with (1) Timoshenko beam theory with surface stress (see Figures 3.10(a), 3.11(a), 3.12(a)) and (2) Euler-Bernoulli beam theory with surface stress (see Figures 3.10(b), 3.11(b), 3.12(b)) for the three different boundary conditions. Figure 3.10 illustrates the change in fundamental resonant frequency of a cantilever nanowire. The fundamental resonant frequency decreases as the diameter decreases for all three diameter nanowires due to surface stress for both the Timoshenko and Euler-Bernoulli beam theory with surface stress. It can also be seen that the

surface stress effect decreases with decreasing aspect ratios. The Timoshenko and Euler-Bernoulli beam theory with surface stress predict similar resonant frequencies until the *AR*<5.
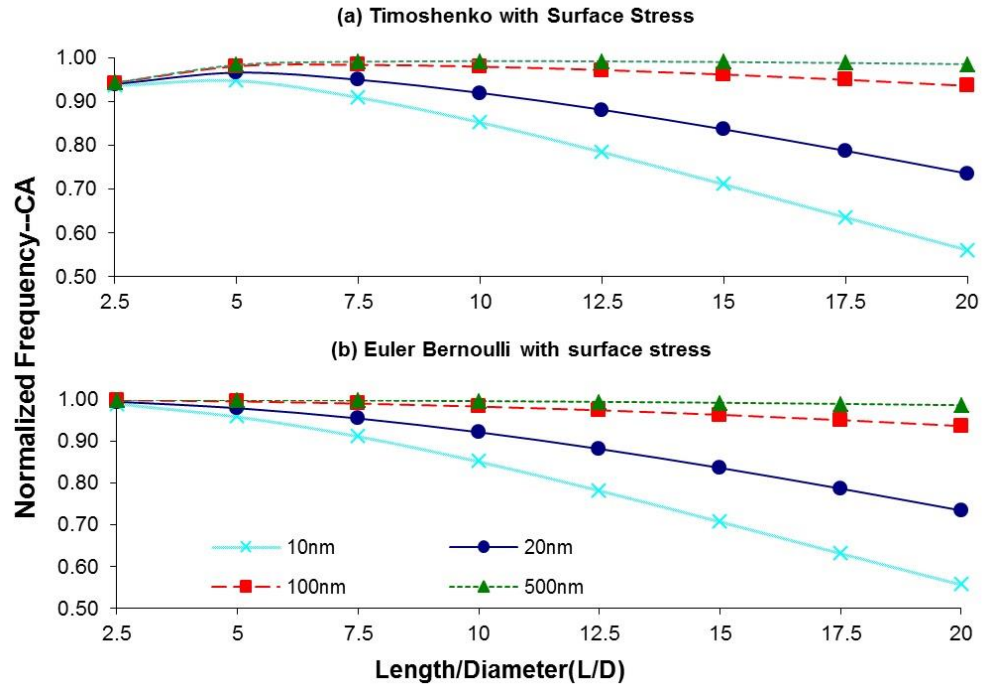
Figure 3.10. The normalized fundamental frequency versus aspect ratio for cantilever Ag nanowires calculated with (a) Timoshenko and (b) Euler-Bernoulli beam theory with surface stress.

When the *AR*=2.5, the Timoshenko beam theory with surface stress predicts a lower resonant fundamental frequency (approximately 5.6% decrease) than the Euler-Bernoulli beam theory with surface stress. In this case, for small aspect ratios, the shear effect is greater than surface effects even for the smallest diameter nanowire (*d*=10 nm).

Figures 3.11 and 3.12 illustrate the change in fundamental resonant frequency of a simply-supported and fixed-fixed nanowire respectively. The fundamental resonant frequency increases for all three diameter nanowires due to surface stress for both the Timoshenko and Euler-Bernoulli beam theory with surface stress. The increase in fundamental resonant frequency is greater for a simply-supported nanowire because it has only a negative curvature while the fixed-fixed nanowire has both a positive and negative curvature. Also, the surface stress effect is more significant as the diameter decreases and the surface stress effect decreases with decreasing aspect ratios. The Timoshenko and Euler-Bernoulli beam theory with surface stress predict similar resonant frequencies until the *AR*<5. When the *AR*=2.5, the Timoshenko beam theory with surface stress predicts a lower fundamental resonant frequency, approximately 14.7% and 37.8% decrease for a simply-supported and fixed-fixed nanowire respectively, than the Euler-Bernoulli beam theory with surface stress. As the aspect ratio decreases, the shear effect increases and can be dominant as compared to the surface effects even for the smallest diameter nanowire.
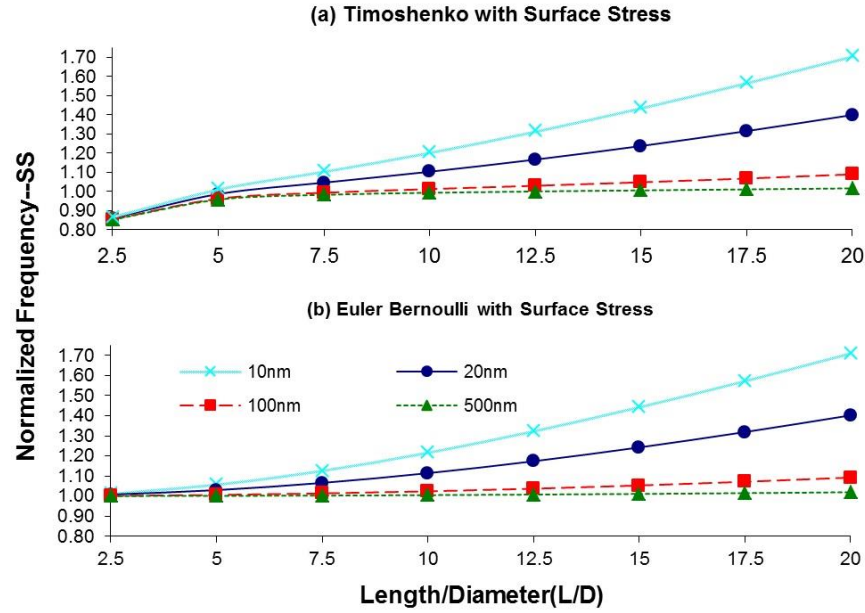
Figure 3.11. The normalized fundamental frequency versus aspect ratio for simply-supported Ag nanowires from (a) Timoshenko and (b) Euler-Bernoulli beam theory with surface stress.
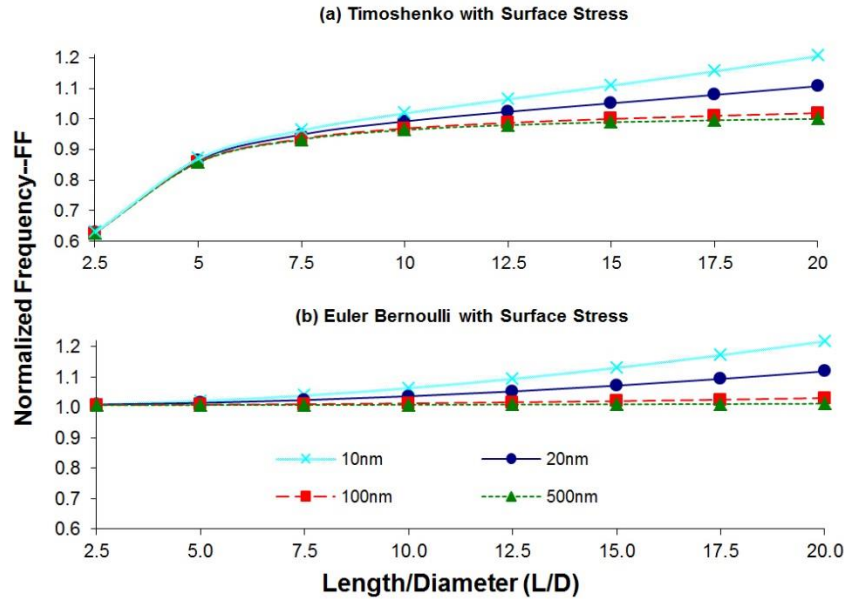
Figure 3.12. The normalized fundamental frequency versus aspect ratio for fixed-fixed Ag nanowires from (a) Timoshenko and (b) Euler-Bernoulli beam theory with surface stress.

3.5.2 *Analysis of higher order resonant frequencies*

Tables 3.II-IV list the three lowest frequencies and corresponding frequency ratios for Ag nanowires with diameters D=10 nm and 500 nm, AR=2.5, 10 and 20, and with different boundary conditions. The values predicted with the Euler-Bernoulli theory without surface stress are also given. The classical Euler-Bernoulli beam theory shows that the frequency ratios depend on the boundary conditions. Thus, the frequency ratios between each modes are constants for bulk cantilever, simply supported, and fixed-fixed beams as listed in the last rows of Tables 3.III-3.V. However, if shear effects and surface stress are included in modeling the resonant behavior, the frequency ratios will change. Comparing a large nanowire, (D=500nm and AR=20) for the three boundary conditions, the frequency ratios are similar to the constants from the Euler Bernoulli beam theory because the influence of both shear and surface effects are limited. However, there is a shift with either small dimensions or small aspect ratios.

For a small aspect ratio (AR=2.5), the shear effect is dominant. The ratios ω_2/ω_1 and ω_3/ω_1 are smaller than the constants obtained with the classical Euler Bernoulli beam theory. Thus, the shear effect not only reduces the fundamental resonant frequencies of the nanowires for the different boundary conditions, but also reduces the higher order frequencies. Furthermore, the influence on the higher order frequencies is more significant than on the fundamental frequency.

For a large aspect ratio (AR=20), the surface effect is dominant. For cantilever nanowires with small dimensions, ω_2/ω_1 is much larger than the bulk ratio. However, ω_3/ω_2 is slightly smaller than the bulk ratio given in Table 3.III. Figure 3.13 illustrates the shapes of the first three vibrating cantilever beam modes. As the number of modes increases, the beam contains more waves but the overall shape tends to a straight line with less influence from surface stress. The first cantilever mode exhibits a single curvature while the remaining modes contain mixed

curvatures (similar to the fixed-fixed beam in Figure 3.4). The mixed curvatures for the higher resonant frequencies are believed to cause the lower surface stress influence on other frequencies, e.g. ω_2 and ω_3. Thus, the higher resonant frequencies are expected to be closer to the bulk. Finally, as listed in Tables 3.IV and 3.V, the frequency ratios for simply-supported and fixed-fixed nanowires are smaller than the bulk values. Since the positive surface stress increases the fundamental frequencies of simply-supported and fixed-fixed nanowires, higher order frequencies are also predicted to be closer to the bulk values by the decreased ratios. The tendency of the ratios for the fixed-fixed nanowires agrees with the MD simulations [53], where ω_2/ω_1 and ω_3/ω_1 are also smaller than the bulk values.
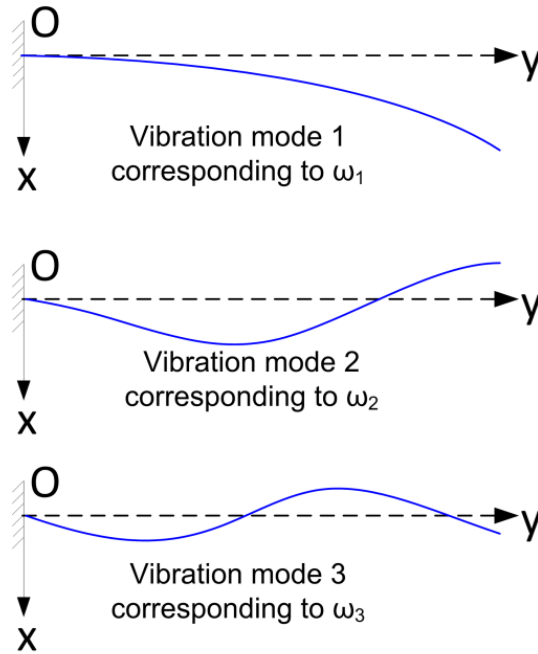
Figure 3.13. The shape of the vibration modes of a cantilever beam corresponding to different frequencies.[126]

Table 3.III. The three lowest frequencies and the corresponding ratio for the cantilever Ag nanowires calculated from the Timoshenko beam theory with surface stress. The ratios from the Euler-Bernoulli beam theory without surface stress are presented for comparison.

D(nm)	AR	ω_1(GHz)	ω_2(GHz)	ω_3(GHz)	ω_2/ω_1	ω_3/ω_1	ω_3/ω_2
10	2.5	35.460	165.328	396.949	4.662	11.194	2.401
	10	2.018	15.312	39.695	7.589	19.673	2.592
	20	0.332	4.512	11.311	13.598	34.086	2.507
500	2.5	0.714	3.280	6.851	4.594	9.595	2.089
	10	0.047	0.288	0.770	6.123	16.386	2.676
	20	0.012	0.074	0.204	6.338	17.483	2.758
Bulk slender beam (From the Euler-Bernoulli theory without surface stress)					6.276	17.578	2.801

Table 3.IV. The three lowest frequencies and the corresponding ratio for the fixed-fixed Ag nanowires calculated from the Timoshenko beam theory with surface stress. The ratios from the Euler-Bernoulli beam theory without surface stress are presented for comparison.

D(nm)	AR	ω_1(GHz)	ω_2(GHz)	ω_3(GHz)	ω_2/ω_1	ω_3/ω_1	ω_3/ω_2
10	2.5	92.246	270.421	458.796	2.932	4.974	1.697
	10	8.014	26.974	55.927	3.366	6.979	2.073
	20	2.838	8.014	16.098	2.824	5.672	2.009
500	2.5	1.812	5.370	9.131	2.964	5.041	1.700
	10	0.132	0.508	1.086	3.855	8.237	2.137
	20	0.034	0.132	0.292	3.910	8.650	2.212
Bulk slender beam (From the Euler-Bernoulli theory without surface stress)					4.000	9.000	2.250

Table 3.V. The three lowest frequencies and the corresponding ratio for the fixed-fixed Ag nanowires calculated from the Timoshenko beam theory with surface stress. The ratios from the Euler-Bernoulli beam theory without surface stress are presented for comparison.

D(nm)	AR	ω_1(GHz)	ω_2(GHz)	ω_3(GHz)	ω_2/ω_1	ω_3/ω_1	ω_3/ω_2
10	2.5	150.871	298.852	453.139	1.981	3.003	1.516
	10	15.244	38.752	70.284	2.542	4.611	1.814
	20	4.508	11.233	20.692	2.492	4.590	1.842
500	2.5	2.997	5.946	9.026	1.984	3.012	1.518
	10	0.288	0.751	1.379	2.608	4.787	1.835
	20	0.075	0.202	0.389	2.709	5.201	1.920
Bulk slender beam (From the Euler-Bernoulli theory without surface stress)					2.756	5.405	1.961

3.6 <u>Conclusions</u>

In summary, a theoretical study of the effects of surface stress and shear force on the resonant behavior and amplitude of the vibration of nanowires has been presented. The resonant frequencies for square cross-section Au(100) nanowires were compared to values calculated with MD simulations with good agreement. A continuum mechanics based approach results in accurate results with a high efficiency for resonant frequency calculations. It was shown that the nanowires modeled with the Timoshenko beam theory with surface effects had decreasing fundamental resonant frequencies due to the shear effect as the aspect ratios decreased. Also, it was found that the surface effect becomes negligible as compared to the shear effect for all nanowires diameters when the aspect ratio is small (i.e. <5). This is in comparison to nanowires modeled with the Euler-Bernoulli beam theory with surface effects. In the case of the Euler-

Bernoulli beam theory, the surface effect is significant for all aspect ratios when the diameters are small (e.g. 10 nm and 20 nm) and decreases with increasing diameter. Finally, the ratios between the higher order frequencies and the fundamental frequencies demonstrate that the shear effect has larger influence on the higher order frequencies. Conversely, the surface effect has smaller influence on the higher order frequencies.

In summary, the resonant frequencies and vibration of nanowires have been modeled with Timoshenko beam theory with surface stress for different boundary conditions. The solutions from this chapter will be compared to the nonlocal Timoshenko beam theory in order to study and parameterize the nonlocal effect in the following chapters.

CHAPTER 4. The Modeling of Resonant Frequencies for the Transverse Vibration of Nanowires with Nonlocal Elasticity and Timoshenko Beam Theory

4.1 <u>Introduction</u>

In this chapter, the resonant frequencies of the transverse vibration of nanowires are solved with nonlocal Timoshenko beam theory integrated with nonlocal elasticity by using the material parameter e_0. The purpose of the calculation is to compare the nonlocal effect with the surface stress effect and MD simulations. The comparison can be used to determine e_0 and further develop the nonlocal beam theory for nanoscale materials, based on the hypothesis that a surface effect is a nonlocal effect and thus both modeling approaches should give consistent results. The resonant frequencies for all the three boundary conditions, such as cantilever, simply-supported and fixed-fixed are solved numerically. The analytical solution of a simply-supported nanowire is obtained by neglecting higher order terms. The analytical solution is then compared to the numerical solution with higher order terms to test the accuracy of the analytical solution. The analytical solution can clearly show the relation between surface stress τ and nonlocal parameter e_0 for the simply supported boundary condition.

4.2 Numerical Solution of the Resonant Frequencies of Nanowires Using Nonlocal Elasticity with Timoshenko Beam Theory for Three Different Boundary Conditions

Nonlocal elasticity states that the stresses at a reference point are functions of the strains at all points of the body in the continuum. This theory is based on the classic continuum mechanics, but adds discrete particle effects.[44, 63] With nonlocal elasticity, interatomic interactions are considered as nonlocal effects. The stress-strain relationship is described as

$$t_{ij} = \int_V \alpha(|x-x'|, \lambda) C_{ijkl} \varepsilon(x') dV(x') = \int_V \alpha(|x-x'|, \lambda) \sigma_{ij} dV(x').$$

(4.1)

The variables t_{ij}, σ_{ij}, ε_{ij} and C_{ijkl} are the nonlocal stress, macroscopic (classical) stress, strain, and elasticity tensor, respectively. The variable α is the nonlocal modulus which indicates the nonlocal effects at the reference point x produced by local strain at the source x'. The variable λ is defined as $\lambda = e_0 a/l$, where e_0 is the nonlocal material parameter. The variable a is an internal characteristic length, and herein is assumed to equal the lattice length of the material. The variable l is an external characteristic length, herein defined as the cross-sectional size. Finally, V is the volume of the material.[63]

By applying Green's function[81], the integral equation (Eq. 4.1) can be simplified into a partial differential equation with the following relationship[63], which is the basic stress-strain relationship in nonlocal elasticity,

$$(1 - \lambda^2 l^2 \nabla^2) t_{ij} = \sigma_{ij} = C_{ijkl} \varepsilon_{ij}.$$

(4.2)

Using Eq. (4.2), the dynamic form of the governing equation of nonlocal Timoshenko beam can be expressed as the following[33]:

$$EI \frac{d^2\varphi}{dx^2} - AkG(\frac{du}{dx} + \varphi) = \rho I \frac{d^2\varphi}{dt^2} - (e_0 a)^2 \rho I \frac{d^4\varphi}{dx^2 dt^2}$$

(4.3)

and

$$AkG\left(\frac{d\varphi}{dx}+\frac{d^2u}{dx^2}\right)=\rho A\left[\frac{d^2u}{dt^2}-(e_0a)^2\frac{d^4u}{dx^2dt^2}\right].$$ (4.4)

The variables E, I, A, G, φ, u and x represent elastic modulus, the second moment of area, cross-sectional area, shear modulus, angular displacement, vertical displacement of the neutral axis, and the axial position of the beam, respectively. The variable ρ is the density of the material and t represents time. Here, k is the Timoshenko shear coefficient and depends on the geometry.[33] The definition of k is Eq. (3.2) in Chapter 3.

Eqs. (4.3) and (4.4) can be converted into two partial differential equations that contain either φ or u as shown below.

$$\frac{(e_0a)^4\rho^2I}{kG}\frac{\partial^8\varphi}{\partial x^4\partial t^4}+\left[(e_0a)^2\rho I+\frac{(e_0a)^2EI\rho}{kG}\right]\frac{\partial^6\varphi}{\partial x^4\partial t^2}-\frac{2(e_0a)^2\rho^2I}{kG}\frac{\partial^6\varphi}{\partial x^2\partial t^4}$$

$$-\left[\rho I+\frac{\rho EI}{kG}+\rho A(e_0a)^2\right]\frac{\partial^4\varphi}{\partial x^2\partial t^2}+\frac{\rho^2I}{kG}\frac{\partial^4\varphi}{\partial t^4}+EI\frac{\partial^4\varphi}{\partial x^4}+\rho A\frac{\partial^2\varphi}{\partial t^2}=0$$ (4.5)

$$(e_0a)^4\frac{\rho^2I}{kG}\frac{\partial^8u}{\partial x^4\partial t^4}+\left[(e_0a)^2\rho I+\frac{(e_0a)^2EI\rho}{kG}\right]\frac{\partial^6u}{\partial x^4\partial t^2}-\frac{2(e_0a)^2\rho^2I}{kG}\frac{\partial^6u}{\partial x^2\partial t^4}$$

$$-\left[\rho I+\frac{\rho EI}{kG}+\rho A(e_0a)^2\right]\frac{\partial^4u}{\partial x^2dt^2}+\frac{\rho^2I}{kG}\frac{\partial^4u}{\partial t^4}+EI\frac{\partial^4u}{\partial x^4}+\rho A\frac{\partial^2u}{\partial t^2}=0$$ (4.6)

From Eq. (4.3), the normal stress-strain relation of nonlocal elasticity, can be expressed as

$$\sigma_{xx}-(e_0a)^2\frac{d^2\sigma_{xx}}{dx^2}=E\varepsilon_{xx}.$$ (4.7)

Similarly, for the shear stress and strain, the relation is defined as

$$\sigma_{xz}-(e_0a)^2\frac{d^2\sigma_{xz}}{dx^2}=2G\varepsilon_{xz}.$$ (4.8)

With these stress-strain relationships, the external loads have the following relationship with

the deformation [33]. For bending moment $M(x,t)$

$$M(x,t) = EI\frac{\partial \phi}{\partial x} + (e_0 a)^2 \left[\rho A \frac{\partial^2 u}{\partial t^2} + \rho I \frac{\partial^3 \phi}{\partial x \partial t^2} \right].$$

(4.9)

For the shear force, $V(x,t)$, the equation is

$$V(x,t) = AkG(\frac{\partial u}{\partial x} + \phi) + (e_0 a)^2 \rho A \frac{\partial^3 u}{\partial x \partial t^2}.$$

(4.10)

Eqs. (4.5) and (4.6) have the same coefficients attached to variables u and ϕ. Thus, the

general solution to Eqs. (4.5) and (4.6) has the same form. Using separation of variables, the

solutions for u and ϕ are assumed to have the following form spatial and temporal definition as

defined below

$$u(x,t) = \sum_{n=1}^{\infty} X_n(x)e^{i\omega_n t}$$

(4.11)

and

$$\phi(x,t) = \sum_{n=1}^{\infty} \Phi_n(x)e^{i\omega_n t}.$$

(4.12)

The variables X_n and Φ_n are the spatial (time-independent) solutions for the vertical

deflection and angular displacement. The variable ω_n is the nth mode circular resonant frequency.

The index has values $n=1, 2, 3\ldots$

Consequently, the spatial equations with ω_n are

$$\left\{ (e_0 a)^4 \frac{\rho^2 I}{kG} \omega_n{}^4 + EI - \left[\frac{EI\rho}{kG}(e_0 a)^2 + (e_0 a)^2 \rho I \right] \omega_n{}^2 \right\} \frac{\partial^4 u}{\partial x^4}$$

$$- \left\{ \frac{2(e_0 a)^2 \rho^2 I}{kG} \omega_n{}^4 - \left[\rho I + \frac{EI\rho}{kG} + (e_0 a)^2 A\rho \right] \omega_n{}^2 \right\} \frac{\partial^2 u}{\partial x^2} + \frac{\rho^2 I}{kG} \omega_n{}^4 - A\rho\omega_n{}^2 = 0$$

,

(4.13)

and

$$\left\{ (e_0 a)^4 \frac{\rho^2 I}{kG} \omega_n^4 + EI - \left[\frac{EI\rho}{kG} (e_0 a)^2 + (e_0 a)^2 \rho I \right] \omega_n^2 \right\} \frac{\partial^4 \phi}{\partial x^4}$$

$$-\left\{ \frac{2(e_0 a)^2 \rho^2 I}{kG} \omega_n^4 - \left[\rho I + \frac{EI\rho}{kG} + (e_0 a)^2 A\rho \right] \omega_n^2 \right\} \frac{\partial^2 \phi}{\partial x^2} + \frac{\rho^2 I}{kG} \omega_n^4 - A\rho\omega_n^2 = 0$$

(4.14)

If we rename the coefficients as the following,

$$P = (e_0 a)^4 \frac{\rho^2 I}{kG} \omega_n^4 + EI - \left[\frac{EI\rho}{kG} (e_0 a)^2 + (e_0 a)^2 \rho I \right] \omega_n^2 ,$$

(4.15)

$$Q = -\left\{ \frac{2(e_0 a)^2 \rho^2 I}{kG} \omega_n^4 - \left[\rho I + \frac{EI\rho}{kG} + (e_0 a)^2 A\rho \right] \omega_n^2 \right\},$$

(4.16)

$$R = A\rho\omega_n^2 - \frac{\rho^2 I}{kG} \omega_n^4 ,$$

(4.17)

The above equations can be expressed as

$$P \frac{d^4 X_n}{dx^4} + Q \frac{d^2 X_n}{dx^2} - R = 0 \quad \text{and} \quad P \frac{d^4 \Phi_n}{dx^4} + Q \frac{d^2 \Phi_n}{dx^2} - R = 0 .$$

(4.18, 4.19)

The solution for X_n and Φ_n have the following forms

$$X_n(x) = C_{1n} \cosh(S_{1n} x) + C_{2n} \sinh(S_{1n} x) + C_{3n} \cos(S_{2n} x) + C_{4n} \sin(S_{2n} x) ,$$

(4.20)

and $\Phi_n(x) = D_{1n} \cosh(S_{1n} x) + D_{2n} \sinh(S_{1n} x) + D_{3n} \cos(S_{2n} x) + D_{4n} \sin(S_{2n} x)$.

(4.21)

Where, S_{1n} and S_{2n} are the eigenvalues of Eq. 4.13 and 4.14 and are expressed as

$$S_{1n} = \sqrt{\frac{\sqrt{Q^2 + 4PR} - Q}{2P}} \quad \text{and} \quad S_{2n} = \sqrt{\frac{\sqrt{Q^2 + 4PR} + Q}{2P}} .$$

(4.22, 4.23)

The constants C and D are related by Eq. (4.4). If we assume

$$C_{1n} = \delta_{1n} D_{2n}, \text{ and } C_{2n} = \delta_{1n} D_{1n} ,$$

(4.24, 4.25)

65

from Eq. (4.4),

$$\delta_{1n} = \frac{-AkG + \rho I \omega_n^2 + EIS_{1n}^2 - (e_0 a)^2 \rho I \omega_n^2 S_{1n}^2}{AkGS_{1n}} \; .$$

(4.26)

Similarly, If

$$C_{4n} = \delta_{2n} D_{3n} \text{ and } C_{3n} = -\delta_{2n} D_{4n}$$

(4.27, 4.28)

from Eq. (4.4),

$$\delta_{2n} = \frac{-AkG + \rho I \omega_n^2 - EIS_{2n}^2 + (e_0 a)^2 \rho I \omega_n^2 S_{2n}^2}{AkGS_{2n}} \; .$$

(4.29)

Now we can apply the boundary conditions to solve for the resonant frequencies for each case. For a fixed end, both deflection and angular displacement are zero, such that

$X=0$, $\Phi=0$.

(4.30, 4.31)

By applying separation of variables on Eq. (4.9), the spatial equation for the bending moment $\overline{M}$ with the resonant frequencies is

$$\overline{M}(x) = EI \frac{\partial \Phi_n}{\partial x} - (e_0 a)^2 \omega_n^2 \left[\rho A X_n + \rho I \frac{\partial \Phi_n}{\partial x} \right] \; .$$

(4.32)

Integrating Eqs. (4.20) and (4.21) with Eq. (4.32), we have the equation for the bending moment

$$\overline{M}(x) = \left[EI - (e_0 a)^2 \omega_n^2 \rho I \right] \left[D_{2n} S_{1n} \cosh(S_{1n}x) + D_{1n} S_{1n} \sinh(S_{1n}x) + D_{4n} S_{2n} \cos(S_{2n}x) - D_{3n} S_{2n} \sin(S_{2n}x) \right]$$
$$-(e_0 a)^2 \omega_n^2 \rho A \left[C_{1n} \cosh(S_{1n}x) + C_{2n} \sinh(S_{1n}x) + C_{3n} \cos(S_{2n}x) + C_{4n} \sin(S_{2n}x) \right]$$

(4.33)

By using Eqs. (4.24)-(4.29), we can remove the coefficients C_{1n}-C_{4n}. Therefore, the remaining unknown constants *are* D_{1n}-D_{4n} as shown in Eq. (4.34).

$$\overline{M}(x) = \left[EI - (e_0 a)^2 \omega_n^2 \rho I \right]\left[D_{2n} S_{1n} \cosh(S_{1n} x) + D_{1n} S_{1n} \sinh(S_{1n} x) + D_{4n} S_{2n} \cos(S_{2n} x) - D_{3n} S_{2n} \sin(S_{2n} x) \right]$$
$$-(e_0 a)^2 \omega_n^2 \rho A \left[\delta_{1n} D_{2n} \cosh(S_{1n} x) + \delta_{1n} D_{1n} \sinh(S_{1n} x) - \delta_{2n} D_{4n} \cos(S_{2n} x) + \delta_{2n} D_{3n} \sin(S_{2n} x) \right]$$

(4.34)

The coefficients for D_{1n}, D_{2n}, D_{3n} and D_{4n} from the bending moment equation are presented

in Eqs. (4.36-4.39), respectively. The coefficients are needed to further solve for the resonant

frequencies for the simply-supported and cantilever boundary conditions.

$$\left[EI - (e_0 a)^2 \omega_n^2 \rho I \right] S_{1n} \sinh(S_{1n} x) - (e_0 a)^2 \omega_n^2 \rho A \delta_{1n} \sinh(S_{1n} x)$$
$$\left[EI - (e_0 a)^2 \omega_n^2 \rho I \right] S_{1n} \cosh(S_{1n} x) - (e_0 a)^2 \omega_n^2 \rho A \delta_{1n} \cosh(S_{1n} x)$$
$$-\left[EI - (e_0 a)^2 \omega_n^2 \rho I \right] S_{2n} \sin(S_{2n} x) - (e_0 a)^2 \omega_n^2 \rho A \delta_{2n} \sin(S_{2n} x)$$
$$\left[EI - (e_0 a)^2 \omega_n^2 \rho I \right] S_{2n} \cos(S_{2n} x) + (e_0 a)^2 \omega_n^2 \rho A \delta_{2n} \cos(S_{2n} x)$$

(4.35-4.38)

By applying separation of variables on Eq. (4.10), the spatial equation for shear force is

$$\overline{V}(x) = AkG(\frac{dX_n}{dx} + \Phi_n) - (e_0 a)^2 \omega_n^2 \rho A \frac{dX_n}{dx}$$

(4.39)

Substituting Eqs. (4.20) and (4.21) into (4.39) gives

$$\overline{V}(x) = \left[AkG - (e_0 a)^2 \omega_n^2 \rho A \right]\left[C_{2n} S_{1n} \cosh(S_{1n} x) + C_{1n} S_{1n} \sinh(S_{1n} x) + C_{4n} S_{2n} \cos(S_{2n} x) - C_{3n} S_{2n} \sin(S_{2n} x) \right]$$
$$+ AkG \left[D_{1n} \cosh(S_{1n} x) + D_{2n} \sinh(S_{1n} x) + D_{3n} \cos(S_{2n} x) + D_{4n} \sin(S_{2n} x) \right]$$

(4.40)

Substituting Eqs. (4.24)-(4.29), into (4.40), we have the following equation for shear force

with unknown constants with D_{1n}-D_{4n}

$$\overline{V}(x) = \left[AkG - (e_0 a)^2 \omega_n^2 \rho A \right]\left[\delta_{1n} D_{1n} S_{1n} \cosh(S_{1n} x) + \delta_{1n} D_{2n} S_{1n} \sinh(S_{1n} x) + \delta_{2n} D_{3n} S_{2n} \cos(S_{2n} x) + \delta_{2n} D_{4n} S_{2n} \sin(S_{2n} x) \right]$$
$$+ AkG \left[D_{1n} \cosh(S_{1n} x) + D_{2n} \sinh(S_{1n} x) + D_{3n} \cos(S_{2n} x) + D_{4n} \sin(S_{2n} x) \right]$$

(4.41)

From the shear force equation, the coefficients of D_{1n}, D_{2n}, D_{3n} and D_{4n} from Eqs. (4.42)-

(4.45) are shown below, respectively.

$$\left[AkG-(e_0a)^2\omega_n^2\rho A\right]\delta_{1n}S_{1n}\cosh(S_{1n}x)+AkG\cosh(S_{1n}x)$$

$$\left[AkG-(e_0a)^2\omega_n^2\rho A\right]\delta_{1n}S_{1n}\sinh(S_{1n}x)+AkG\sinh(S_{1n}x)$$

$$\left[AkG-(e_0a)^2\omega_n^2\rho A\right]\delta_{2n}S_{2n}\cos(S_{2n}x)+AkG\cos(S_{2n}x)$$

$$\left[AkG-(e_0a)^2\omega_n^2\rho A\right]\delta_{2n}S_{2n}\sin(S_{2n}x)+AkG\sin(S_{2n}x)$$

(4.42-4.45)

Four unknown constants D_{1n}-D_{4n} are needed to be determined for the solution of the vibration of the beam. Similar to the discussion found in Chapter 3 and Figure 3.4, the boundary conditions for the cantilever, simply-supported and fixed-fixed nanowires are: [79]

Cantilever: $X(0)=\Phi(0)=\overline{M}(L)=\overline{V}(L)=0$ (4.46)

Simply-supported: $X(0)=\overline{M}(0)=X(L)=\overline{M}(L)=0$ (4.47)

Fixed-fixed: $X(0)=\Phi(0)=X(L)=\Phi(L)=0$. (4.48)

For example, according to Eqs. (4.20) and (4.21) with (4.48), for fixed-fixed beams, in order to obtain nontrivial solutions for D_{1n}-D_{4n}, the determinant of the coefficient matrix for D_{1n}-D_{4n} must be equal to zero, see Eq. 4.49 below. The resonant frequencies can be derived numerically by solving the equation of the determinant.

$$\begin{vmatrix} 0 & \delta_{1n} & 0 & -\delta_{2n} \\ 1 & 0 & 1 & 0 \\ \delta_{1n}\sinh(S_{1n}L) & \delta_{1n}\cosh(S_{1n}L) & \delta_{2n}\sin(S_{2n}L) & -\delta_{2n}\cos(S_{2n}L) \\ \cosh(S_{1n}L) & \sinh(S_{1n}L) & \cos(S_{2n}L) & \sin(S_{2n}L) \end{vmatrix}=0$$

(4.49)

For cantilever beams, the first two lines of the determinant are the same as fixed-fixed beams, because of the zero deflection and angular displacement at the fixed end (i.e. $x=0$). At the free end where $x=L$, both the bending moment and shear force are zero. Therefore, the determinant for the cantilever boundary condition is

$$\begin{vmatrix} 0 & \delta_{1n} & 0 & -\delta_{2n} \\ 1 & 0 & 1 & 0 \\ CA_{31} & CA_{32} & CA_{33} & CA_{34} \\ CA_{41} & CA_{42} & CA_{43} & CA_{44} \end{vmatrix} = 0 \tag{4.50}$$

Where,

$$CA_{31} = \left[EI - (e_0 a)^2 \omega_n^2 \rho I \right] S_{1n} \sinh(S_{1n}L) - (e_0 a)^2 \omega_n^2 \rho A \delta_{1n} \sinh(S_{1n}L)$$

$$CA_{32} = \left[EI - (e_0 a)^2 \omega_n^2 \rho I \right] S_{1n} \cosh(S_{1n}L) - (e_0 a)^2 \omega_n^2 \rho A \delta_{1n} \cosh(S_{1n}L)$$

$$CA_{33} = -\left[EI - (e_0 a)^2 \omega_n^2 \rho I \right] S_{2n} \sin(S_{2n}L) - (e_0 a)^2 \omega_n^2 \rho A \delta_{2n} \sin(S_{2n}L) \tag{4.51-4.54}$$

$$CA_{34} = \left[EI - (e_0 a)^2 \omega_n^2 \rho I \right] S_{2n} \cos(S_{2n}L) + (e_0 a)^2 \omega_n^2 \rho A \delta_{2n} \cos(S_{2n}L)$$

and

$$CA_{41} = \left[AkG - (e_0 a)^2 \omega_n^2 \rho A \right] \delta_{1n} S_{1n} \cosh(S_{1n}L) + AkG \cosh(S_{1n}L)$$

$$CA_{42} = \left[AkG - (e_0 a)^2 \omega_n^2 \rho A \right] \delta_{1n} S_{1n} \sinh(S_{1n}L) + AkG \sinh(S_{1n}L)$$

$$CA_{43} = \left[AkG - (e_0 a)^2 \omega_n^2 \rho A \right] \delta_{2n} S_{2n} \cos(S_{2n}L) + AkG \cos(S_{2n}L) \tag{4.55-4.58}$$

$$CA_{44} = \left[AkG - (e_0 a)^2 \omega_n^2 \rho A \right] \delta_{2n} S_{2n} \sin(S_{2n}L) + AkG \sin(S_{2n}L)$$

For simply-supported beams, the displacement and bending moment are zero at both two ends (i.e. $x=0$ and $x=L$), thus, the corresponding determinant is

$$\begin{vmatrix} 0 & \delta_{1n} & 0 & -\delta_{2n} \\ 0 & \left[EI - (e_0 a)^2 \omega_n^2 \rho I \right] S_{1n} - (e_0 a)^2 \omega_n^2 \rho A \delta_{1n} & 0 & \left[EI - (e_0 a)^2 \omega_n^2 \rho I \right] S_{2n} + (e_0 a)^2 \omega_n^2 \rho A \delta_{2n} \\ \delta_{1n} \sinh(S_{1n}L) & \delta_{1n} \cosh(S_{1n}L) & \delta_{2n} \sin(S_{2n}L) & -\delta_{2n} \cos(S_{2n}L) \\ SS_{41} & SS_{42} & SS_{43} & SS_{44} \end{vmatrix} = 0$$

$$\tag{4.59}$$

Where

$$SS_{41} = \left[EI - (e_0 a)^2 \omega_n^2 \rho I \right] S_{1n} \sinh(S_{1n}L) - (e_0 a)^2 \omega_n^2 \rho A \delta_{1n} \sinh(S_{1n}L)$$

$$SS_{42} = \left[EI - (e_0 a)^2 \omega_n^2 \rho I \right] S_{1n} \cosh(S_{1n}L) - (e_0 a)^2 \omega_n^2 \rho A \delta_{1n} \cosh(S_{1n}L)$$

$$SS_{43} = -\left[EI - (e_0 a)^2 \omega_n^2 \rho I \right] S_{2n} \sin(S_{2n}L) - (e_0 a)^2 \omega_n^2 \rho A \delta_{2n} \sin(S_{2n}L) \tag{4.60-4.63}$$

$$SS_{44} = \left[EI - (e_0 a)^2 \omega_n^2 \rho I \right] S_{2n} \cos(S_{2n}L) + (e_0 a)^2 \omega_n^2 \rho A \delta_{2n} \cos(S_{2n}L)$$

4.3 Analytical Solution of the Resonant Frequencies of Nonlocal Timoshenko Beam Theory for the Simply-Supported Boundary Condition and the Comparison between the Analytical Solution and Numerical Solution

The solution of the vertical displacement for simply-supported boundary condition is assumed to have the form

$$u(x,t) = \sum_{n=1}^{\infty} C_n \sin\left(n\pi x/L\right)\cos(\omega_n t). \tag{4.64}$$

Where, C_n are unknown constants depending on the initial conditions for vibration. The variable ω_n is the nth mode of vibration frequency.

Similar to Ref. [129], if we assume that the terms $\dfrac{\partial^8 u}{\partial x^4 \partial t^4}$ and $\dfrac{\partial^6 u}{\partial x^4 \partial t^2}$ in Eqs. (4.5) and (4.6) are negligible, the analytical solution of the resonant frequencies of simply-supported nanowires can thus be obtained as

$$\omega_{n(\text{Analytical})} = \sqrt{\dfrac{EI\left(\dfrac{n\pi}{L}\right)^4}{\left[\dfrac{EI\rho}{kG}(e_0 a)^2 + (e_0 a)^2 \rho I\right]\left(\dfrac{n\pi}{L}\right)^4 + \left[\rho I + \dfrac{EI\rho}{kG} + (e_0 a)^2 A\rho\right]\left(\dfrac{n\pi}{L}\right)^2 + A\rho}}. \tag{4.65}$$

In order to test the accuracy of Eq. (4.65) when neglecting $\dfrac{\partial^8 u}{\partial x^4 \partial t^4}$ and $\dfrac{\partial^6 u}{\partial x^4 \partial t^2}$ terms, the analytical solution Eq. (4.65) is compared to the numerical solution Eq. (4.59) of the resonant frequencies of the vibrating nanowires at the transverse direction.

Table 4.I. lists the frequency parameter, $\eta_{\omega_{n(\text{Analytical or Numerical})}} = \sqrt{\omega_{n(\text{Analytical or Numerical})}\sqrt{\left(\dfrac{\rho A L^4}{EI}\right)}}$. The term $\sqrt{\left(\dfrac{\rho A L^4}{EI}\right)}$ is introduced to normalize the resonant frequency as discussed in Ref. [130]. The

error is defined as $\delta = \left[\dfrac{\eta_{\omega_{n(Analytical)}}}{\eta_{\omega_{n(Numerical)}}} - 1 \right] \times 100\%$. As can be seen, the analytical solution is valid for

the first 5 vibration modes, with an error of 1% or less, especially for the lower modes. Therefore,

the accuracy of the analytical solution stated in Eq. (4.65), using the abovementioned

assumptions, is acceptable.

Table 4.I. The comparison of the analytical (A) and numerical (N) solutions for the frequency parameter η. e_0 is chosen to be 0, 10 and 30. Other parameters are $l=10a$, $L=100a$, $E=63$GPa, $a=0.409$nm, $\rho=10500$kg/m^3 and $v=0.3$ as found for Ag<111>.[26, 131, 132]

Vibration Modes	$e_0=0$			$e_0=10$			$e_0=30$		
	$\eta_{\omega n(A)}$	$\eta_{\omega n(N)}$	$\delta(\%)$	$\eta_{\omega n(A)}$	$\eta_{\omega n(N)}$	$\delta(\%)$	$\eta_{\omega n(A)}$	$\eta_{\omega n(N)}$	$\delta(\%)$
1	3.1163	3.1164	-0.0048	3.0438	3.0439	-0.0048	2.6584	2.6585	-0.0048
2	6.0920	6.0958	-0.0636	5.6057	5.6093	-0.0636	4.1704	4.1731	-0.0636
3	8.8331	8.8550	-0.2480	7.5352	7.5540	-0.2480	5.1006	5.1133	-0.2480
4	11.3056	11.3710	-0.5754	8.9212	8.9729	-0.5754	5.7246	5.7577	-0.5754
5	13.5193	13.6572	-1.0094	9.9073	10.0083	-1.0094	6.1596	6.2224	-1.0094

4.4 Conclusion

The resonant frequencies of Timoshenko beam theory are derived numerically with

unknown nonlocal parameter e_0 for three boundary conditions, such as cantilever, simply-

supported and fixed-fixed. The analytical solution for the simply-supported boundary conditions

is also solved with dropping some higher order differential terms. These terms are demonstrated

to have negligible influence (e.g. less than 1% difference) on the resonance of nanowires by comparing the analytical solution to the numerical solution. With the numerical and analytical solution of the resonant frequencies from nonlocal Timoshenko beam theory from in chapter, the comparison among the beam theory with surface effect, the beam theory with nonlocal effect and the MD simulation results will be used to test the hypothesis that these three methods model the same nonlocal effects and thus should be consistent.

CHAPTER 5. Molecular Dynamics Simulation Modeling

5.1 Introduction to Molecular Dynamics Simulations

Molecular dynamics (MD) simulations are used to predict the mechanical behavior of structures from the atomic scale to the nanoscale.[52, 53] The basic concept incorporated in MD simulations is using Newton's mechanics to describe the potential between pairs of particles in the investigated object.[54] MD simulations can be used to accurately depict the properties at the atomic scale, such as the displacement and velocity of particles and the potential and kinetic energy of particle systems. Compared to the size and the time length needed to capture the mechanical properties of nanoscale structures, such as resonance of nanobeams, the size[55, 56] and time[57, 58] scale of MD simulations is very small and the computational time and power required to bridge between MD (Ångstrom and femtosecond) and the nanoscale (nanometers and nanoseconds) can be prohibitive. Therefore, MD simulations are typically still an expensive method, which requires considerable computational power and simulation time due to the time steps required in MD simulations and the experimental time scale.[54] Thus, simulation sizes cannot be too large and to the best ability of the workstation in our laboratory, a nanowire with cross-section size of 10 lattice units with an aspect ratio of 10 is the largest structure that can be practically simulated.

Both tensile simulations for the elastic modulus and vibration simulations for the resonant frequencies of nanowires will be presented in this chapter. The surface effect is found to be associated with the bending curvature, as discussed in Chapter 3. Since there is no bending curvature in the tensile test, the elastic modulus from the tensile test should not include the

surface effects for the beam modeling. Thus, the elastic moduli used in the calculations of the resonant frequencies with surface effects or nonlocal effect in Chapters 3 and 4 will be obtained from the tensile simulations. Other researchers agree with this reasoning and have also applied the elastic moduli from tensile test simulations in their beam modeling. [52, 53, 112]

A potential function (or usually just called potential) describes the force interaction between a pair or group of particles (atoms or molecules) as shown in Eqs. (5.1) and (5.2).[133] For example, a pairwise potential only considers the interactions between two atoms. A pairwise potential only considers the energy between two atoms, such as Lennard-Jones and Morse potentials. The solution of the classical equations of motion (From Newton's second law) can be obtained with the potential energy between the particles. [133] The expression of Lennard-Jones potential is [113]

$$V = 4\varepsilon \left[\left(\frac{\sigma}{r} \right)^{12} - \left(\frac{\sigma}{r} \right)^{6} \right] \tag{5.1}$$

where, V is the intermolecular potential (energy) between the two atoms or molecules. ε is the well depth. σ is the distance at which the intermolecular potential between the two particles is zero. r is the distance of separation between both particles.

The tensile test and the corresponding elastic modulus, yield strength, and strain rate effect of crystalline metals has been studied with MD simulations with pairwise potentials. Yuan *et al.* applied the stress-strain relationship for Al(111) nanowires with the Morse potential.[107] For the strain rate effect, they found that the lower strain rate will result in a lower yield stress, but does not affect the elastic modulus significantly from the linear fitting calculation. Conversely, for the temperature effect, they found that the elastic modulus decreases at higher temperature with the chosen Morse potential. Komanduri *et al.* applied the Morse potential to model the stress-strain relationship for both Face-Centered Cubic (FCC) and Body-Centered Cubic (BCC)

metals.[134] The FCC metals showed more obvious linear stress-strain relationship than the BCC metals. The hypothesis of their research is that that FCC and BCC metals should both behave linearly. Therefore, they concluded that the Morse potential cannot describe the BCC metals as well as FCC metals. Chang and Fang performed MD tensile and fatigue tests of nanoscale copper with the Lennard-Jones potential.[135] They found that the Lennard-Jones potential predicts larger elastic modulus than the Morse potential. Similar to Morse potential, the Lennard-Jones potential also predicts that the modulus decreases with increasing temperature.

Compared to the above mentioned pairwise potentials, the Embedded Atom Model (EAM) is more widely used to model the mechanical behavior of metals. EAM not only considers the nuclei's pairwise effects, but also considers the contribution of energy from electrons to the nuclei. Therefore, EAM can be more accurate than the pairwise potentials unless the electron effect is negligible. EAM is found to be particularly appropriate for the metallic systems studied in this thesis.[115, 116] For the EAM model, the system's total energy can be expressed as the following: [117]

$$E_i = F_i(\bar{\rho}_i) + \frac{1}{2}\sum_{j \neq i} \Phi_{ij}(r_{ij})$$ (5.2)

Where, F_i is the embedding term, which is the energy to embed atom i into the background electron density; $\bar{\rho}_i$ is the host electron density at atom i due to the remaining atoms of the system. The term Φ_{ij} is the pair-wise addition of the interaction and r_{ij} is the distance between atoms i and j.

Diao et $al.$ used EAM to simulate the tensile deformation of Au nanowires with square cross-sections. An external tensile force was applied along the axial directions, which were in the <100> and <111> axial orientations.[108] The elastic moduli were obtained with the energy

method and the virtual stress method. Elastic moduli were found to increase with a decrease in cross-sectional area of the nanowires. Similar to Diao *et al.*'s work, Wang *et al.* performed MD tensile simulations with EAM for Au(100) nanowires with circular cross-section sizes from 2.85-6nm [109] and a strain rate of 1.4×10^9 1/s. The elastic moduli were found to decrease with decreasing cross-sectional size. Additionally, Wang *et al.* found that for the smaller cross-section sizes, for example 2.85nm and 2.97 nm, the nanowires experienced two elastic periods and two plastic periods, which are not common in most of the tensile simulations or experiments. However, the explanation of the two stages was not discussed. Mohan and Liang performed MD simulations of the tensile deformation of Ni nanowires using EAM potentials for different cross-sectional sizes and strain rates at the temperature of 300K-900K.[112] The length of Ni nanowires was a fixed value of 60 lattice lengths (60x3.52 Å) in the <001> direction. The cross-sectional sizes ranged from 5 to 20 lattice lengths. The strain rate applied ranged from 1.67×10^7 1/s to 1.67×10^{10} 1/s. The authors found that the elastic modulus almost remained constant for the chosen cross-sectional sizes and strain rates. But the maximum yield stress increases as the cross-section increases.

MD simulations are also applied to model the bending behavior, such as deflection and resonant frequencies of nanomaterials. In Ref. [112], in addition to presenting results for tensile tests, Mohan and Liang also obtained the flexural deformation of Ni nanowires.[112] Single crystal Ni in the <001> (longitudinal direction) and with a dimension of 120×10×1 lattice units were simulated. Simply-supported and fixed-fixed boundary conditions were applied to obtain the resonant frequencies. The resonant frequencies were calculated and compared to the Euler-Bernoulli beam theory with the elastic modulus obtained through the tensile test. They found that

the resonant frequencies from the simulations are at least one order lower than the theoretical results, but they did explain the reason for this difference.

McDowell *et al.* modeled the cantilever bending and tensile deformation of Ag(100) and Ag(110) nanowires using EAM potentials.[111] Euler-Bernoulli beam theory with a concentrated load at the free end of the cantilever was used to obtain the elastic modulus from the static bending test. The energy method was used to calculate the elastic moduli of the nanowires from the tensile test and Euler-Bernoulli beam theory with the cantilever boundary condition was used to calculate the elastic moduli from the bending simulations. They found a slight difference between the moduli calculated from tensile and bending tests. The authors discussed the possible reasons for the difference, such as a size effect, qualitatively. However, they did not apply any theory to explain the difference quantitatively. The same lattice orientations and energy method used by McDowell *et al.* will be referred to in order to calculate the elastic moduli for Ag in this thesis. The elastic moduli will be applied for the resonant frequency modeling with nonlocal effect to derive the true value of the nonlocal parameter e_0. The details and discussion of the elastic modulus E and nonlocal parameter e_0 from the MD simulations will be given in Chapter 6.

Bulk shear and rotary inertia effects on the resonant Au nanowires were also studied with molecular dynamics simulations using EAM potential by Olsson[53]. Timoshenko beam theory with the elastic modulus from the tensile simulations of Ref. [52] was applied to explain the simulation results. The resonant frequencies from the simulations were found to be lower than calculated by the Euler-Bernoulli beam theory. The author considered that the lower resonant frequencies were caused by the bulk effect such as the shear and inertia effects. However, we believe that the shear and inertia effects are not the only source of the shift. Nonlocal or surface

effects should also be considered to explain the shift for the size scale gap between nanoscale and the bulk scale for continuum mechanics.

It should be noted that in a survey of MD simulations for tensile and bending tests of nanowires, most researchers apply Euler-Bernoulli/Timoshenko beam theories, which are macroscale models, to analyze their simulation results. As such, many researchers can only predict trends with approximate agreements to the macroscale continuum theoretical modeling [53, 108, 109, 111, 112]. In addition, some researchers' simulation results have little agreement with the theoretical modeling[109, 112]. As a result, the difference between the continuum mechanics modeling and MD simulation results for the elastic modulus and resonant frequencies is usually ignored and is not discussed. On the contrary, for the nanoscale materials, the difference between the MD simulation results and continuum mechanics modeling should be emphasized, because this difference is the unique behavior for nanomaterials and caused by the small size scale.

In the research presented in this thesis, Large-scale Atomic/Molecular Massively Parallel Simulator (LAMMPS) from Sandia National Laboratories[90] was employed to investigate the bending and tensile nanowires with cross-section sizes between 2 nm and 4 nm. The beam theories with surface effects and the nonlocal effect are compared to the resonance simulation results in order to derive the nonlocal parameter e_0 in nonlocal elasticity.

5.2 Initialization and Key Procedures in Molecular Dynamics Simulations

As seen in Figure 5.1, the FCC lattice single crystals of Ag nanowires are shown. The first nanowire is oriented with a <001> longitudinal direction along the *z*-axis, and a transverse

direction of <100> and <010> along the *x*- and *y*-axis, respectively. The second nanowire is oriented with a <110> longitudinal direction along the *z*-axis), and a transverse direction of <$\bar{1}$10> and <001> along the *x*- and *y*-axis, respectively. Figure 5.2 shows the configuration of the tensile test, simply-supported and fixed-fixed nanowires with rectangular cross-sections. For simply-supported and fixed-fixed boundary conditions, nanowires were divided into three sections to apply the appropriate boundary conditions. Specifically, at both ends, atoms in one lattice unit were grouped and the corresponding boundary conditions were applied to the atoms in this unit. The third section was the remaining atoms in the body of the nanowire. Cantilevers were divided into two sections, atoms in one lattice unit were grouped at one end to apply the fixed boundary condition, and the remaining atoms were grouped for the second section. The atoms for applying the boundary conditions were not included in defining the length for the theoretical modeling. For example, a nanowire with 7x7x72 lattice units (4.09Å) for fixed-fixed nanowires is considered as 7x7x70 in the theoretical modeling because one lattice unit at each end were fixed and did not contribute to the inertia of the vibration. It should be noted that the <110> and <$\bar{1}$10> unit is $\sqrt{2}$ times as long as a <100> unit. Therefore the 7x7x70 Ag(100) is almost the same size as a 5x7x50 Ag(110) nanowire with a 1% difference in length (7 VS. $5\sqrt{2}$). In the following simulations, the *z* direction is assumed to be the longitudinal direction and the transverse displacement of the vibration is obtained from the *x* direction, which is the direction of excitation for the applied loading. The details of the boundary condition setup and verification can be seen in section 5.4 with Eq. (5.6) and Figure (5.5)
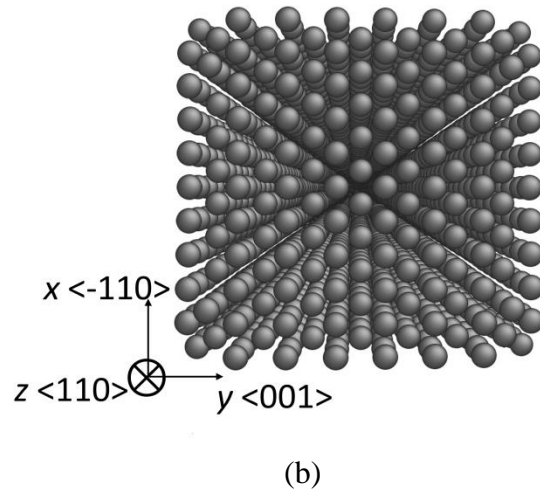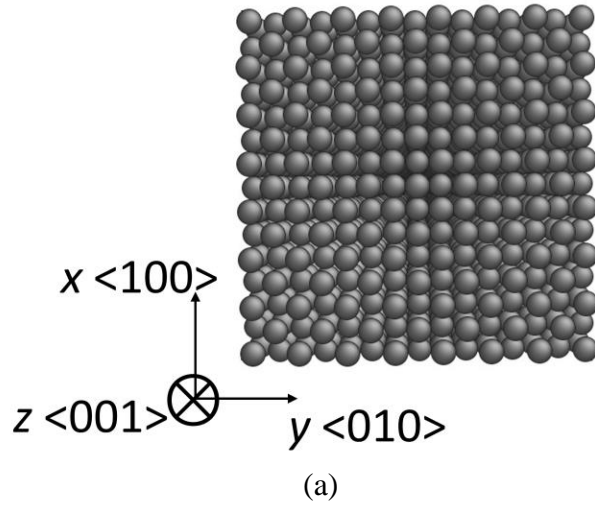
Figure 5.1. The configuration of the lattice orientations (a) Ag(100) for 7x7x70 lattice units and

(b) Ag(110) for 5x7x50 lattice units
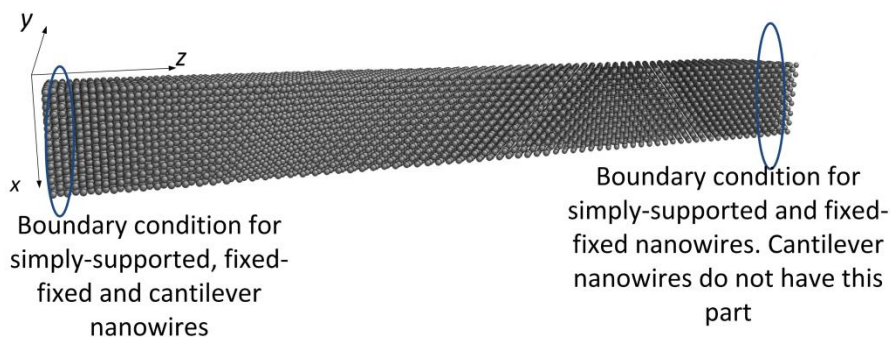
Figure. 5.2. Illustration of the boundary condition set-up

After the step of setting the material and geometry of modeling, the Polak-Ribiere conjugate gradient (CG) algorithm was applied to achieve energy minimization.[136] According to the chemical bonding, crystalline structure, and temperature, energy minimization finds the positions and velocities of atoms, so the summation force on each atom is acceptably close to zero and the global potential energy of the system is close to the minimum. However, an absolute zero force in the simulation is not possible; instead, stopping criteria for the energy minimization is established. With the stopping criteria, the chemical structure of the model is assumed to be stable.[137] For the simulations presented in this thesis, the initial velocity of the atoms at temperature of 1K were first randomly set before the energy minimization. During the procedure of energy minimization, the atom coordinates were adjusted according to the CG algorithm for the minimum local potential energy at the target temperature (1K). Energy minimization is

terminated when one of the stopping criteria is satisfied. In our simulation, the stopping tolerance for energy was set at 1.0×10^{-9} (dimensionless units) and the stopping tolerance for force was 1.0×10^{-16} (eV/Å) [136]. The details and numerical method of the Polak-Ribiere algorithm can be found in Ref. [138].

A thermostat is a crucial step in MD simulations to ensure that the a group of atoms in the defined region follow predetermined physical laws through the time integration step and update the position and velocity for atoms after each time-step.[139] These physical laws include thermal dynamics equations to adjust the system from one temperature to another (or maintain the system at a constant temperature) and total energy conservation.[140-142] NVT and NVE are the most common thermostat methods in MD simulations, where N, V, T and E are defined as the number of the atoms, the volume, average temperature and energy of the defined group.[141, 142]

The numerical method in LAMMPS to control temperature through velocity rescaling and achieve NVT thermostat is called Nose-Hoover algorithm. The NVT thermostat is also called a canonical ensemble.[143] By applying the NVT thermostat, the velocities and positions of the atoms are adjusted according to thermal dynamics equations. There are endothermic and exothermic processes of energy in NVT to adjust the average temperature of this group of atoms. It should be noted that, in MD simulations, the average temperature is a statistical quantity for the entire group of atoms and is calculated with the following equation from the kinetic energy or velocity of the atoms,[144]

$$K = \frac{n k_B T}{2}.$$ (5.3)

Where T is the average temperature of the system; n is the number of degree of freedom in the system, k_B is the Boltzmann constant and K is the kinetic energy of the system.

The relation between the average velocity $\bar{v}$, number of atoms in a group N and the mass m of the atoms and the kinetic energy is[144]

$$K = \frac{Nm\bar{v}^2}{2} \tag{5.4}$$

Usually, the constant temperature is considered to be close to the real experiment environment. If the simulated model needs to be maintained at a constant temperature, a NVT simulation is required.[145] The numerical method of Nose-Hoover style to achieve the velocity and position of the atoms at a given temperature can be seen in Ref. [139].

The NVE thermostat, which is also called a microcanonical ensemble, is applied to ensure that the total energy of the group of atoms is constant. Therefore, the system is considered to be heat insulated and there is no thermal exchange between the defined group of atoms and the external environment or other atoms not in this group. However, the energy exchange between kinetic energy and potential energy exist in the NVE thermostat, and there is temperature change in the NVE thermostat.[141, 142] The numerical integration for NVE thermostat to update the atoms' velocity and position at each time-step can be found in Refs.[146, 147].

The time-step in the simulations was set to 1 femtosecond (fs). Before applying the tensile load or initial deformation for the resonance, the NVT thermostat was applied to set the average temperature of the system at 1K for 10,000 time-steps. After removing NVT, the NVE thermostat was applied for another 10,000 time-steps to output the temperature with the constant total energy of the system. If the output of the average temperature is at the range of 1±0.1K, the atoms are considered well initialized, because the system does not need an energy exchange to adjust the system's average temperature. These initial relaxation procedures are found from the LAMMPS manual and reference [53].

After creating the atomic assembly with prescribed boundaries, the system was deformed. The NVT thermostat was enforced during the procedure of applying loads for both tensile and vibration tests. The reason to choose the NVT thermostat during the load application procedure is as follows. When there are external loads on the system, the energy of the system increases due to increasing elastic potential energy of the system from deformation. If the load is applied slowly, there should be no change in the average system temperature. Thus, a constant average temperature is enforced by applying the NVT thermostat. However, during the period of free vibration, the system should obey energy conservation since there should be no energy loss in the system (i.e. no damping, heat exchange, or external load is added to the system). The nanowires should vibrate freely. Therefore, the NVE thermostat was applied for the free vibration to enforce constant energy, and thus, there is a variable average temperature.

5.3 <u>Tensile Test and Boundary Condition Procedures for Molecular Dynamics Simulations</u>

Two different types of simulations were performed and discussed in this thesis. Firstly, a tensile test was performed to obtain the elastic moduli of the nanowires to be used in the analysis of the vibration modeling. Similar to Ref. [148], a constant velocity was applied at the two ends of the nanowires to achieve a 10^7 (1/s) strain rate for the tensile test. During the tensile test, the positions and velocities of the atoms at the middle were adjusted by the Nose-Hoover integration for a constant temperature of 1K. The relation between the constant strain rate and applied external velocity at the two ends of the nanowires is $\dot{\varepsilon} = 2v_0/L$, where $\dot{\varepsilon}$ is the targeted strain rate, v_0 is the applied constant velocity at each end of the nanowire, and L is the total length of the nanowire. We applied a strain rate of 10^7 (1/s) since strain rates from 1.67×10^7 to 1.67×10^{10}

(1/s) in Ref. [112, 134, 149, 150] were found not to cause variations in elastic moduli values. In these papers, the strain rate does not affect the elastic modulus significantly, although a smaller strain rate is closer to a realistic experimental set-up. The 10^7 (1/s) strain rate was applied until the nanowires fractured and necking was visible. Figure 5.3 shows the necking effect of the nanowire from tensile loading. The elastic modulus was calculated from the change of potential energy with a chosen strain ε using Eq. (5.5) below [111].

$$\frac{\Delta U}{V_0} = E\left(\frac{1}{2}\varepsilon^2 + \frac{1}{3}\varsigma\varepsilon^3\right) \tag{5.5}$$

In the above equation, ΔU is the change in potential energy in the nanowires during the loading, E is the elastic modulus at the strain $\varepsilon=0$, V_0 is the initial volume of the nanowire, and ς is a constant from the third order polynomial fitting. The derivation of this equation can be found in Reference [108]. In this research, the elastic modulus was solved using Eq. (5.5) and applying a strain of $\varepsilon=1\%$. The results of the elastic modulus from the tensile test will be presented in Chapter 6.
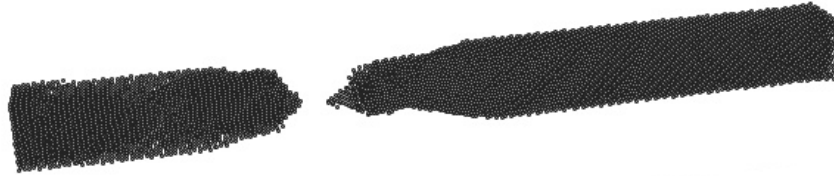
Figure 5.3. The necking effect of the tensile test

The boundary conditions for the resonance simulations are as follows. A fixed end is achieved by setting the initial velocity of the boundary atoms to zero, and then the force on these atoms is set to be zero at all times during the vibration. By checking the velocity of the fixed boundary atoms, we find that the velocity of the boundary atoms is always zero for the period of the vibration, so these atoms are fully fixed. To our best knowledge, we cannot find any references to explain how the simply-supported boundary condition is achieved in MD simulations. In our setup, a simply-supported end is obtained by setting the initial velocity of the boundary atoms to be zero, and then the linear momentum is set to be zero during the bending and vibration. Therefore, these atoms can only have rotational motion but do not move vertically.

5.4 <u>Boundary Condition Verification and Resonance Simulations</u>

The three boundary condition set-ups were verified. The static bending simulations were compared to the fitting curves of the neutral axis from the Euler-Bernoulli beam theory. The size of 2.86x2.86x28.63nm (7x7x70 lattice units) was applied in the verification. The boundary condition set-ups should not be affected by the sizes. As seen in Figure 3.4 and Figure 5.4 (a-c), we added a gradually increasing vertical displacement to a horizontal row of atoms at the center of the free plane of a cantilever or to the mid-plane of a simply-supported and fixed-fixed nanowire. The location of the applied displacement is shown in Figure 5.5. The row of atoms is located at the intersection between the neutral plane in a beam in bending and the free end of a cantilever or mid-plane of a simply-supported and fixed-fixed nanowire. To the author's best knowledge, this was the best method to apply the deformation because the load did not lock the free rotation of the free end of a cantilever and the load was distributed evenly at the depth (y)

direction for the simply-supported and fixed-fixed nanowire. After the angular displacement reaches 1%, we output the vertical displacement of the central atoms. The fitting functions for cantilever, simply-supported and fixed-fixed beams are polynomials described in Eq. 5.3, from Euler-Bernoulli beam theory. L and v are the length of the nanowires and the vertical deflection along the neutral axis, respectively. C_{CA}, C_{SS} and C_{FF}, which are the constant amplitudes of the bending shape, are determined by the elastic modulus, size and boundary conditions. In the fitting test, C_{CA}, C_{SS} and C_{FF} are calibrated by two points, such as ($v=0$, $x=0$) and ($v=v_{max}$, $x=L$) for the cantilever and ($v=v_{max}$, $x=L/2$) for simply-supported and fixed-fixed nanowires. According to Euler-Bernoulli beam theory, the shapes of the bending curves should be third order polynomials, which are associated with the boundary condition and the length of the nanowires, shown in the following expressions.

$$
\begin{aligned}
v &= C_{CA}(3L-x)x^2 & x &= [0,L] & &\text{(Cantilever)} \\
v &= C_{SS}(3L^2 - 4x^2)x & x &= [0, L/2] & &\text{(Simply-supported)} \qquad (5.6) \\
v &= C_{FF}(3L - 4x)x^2 & x &= [0, L/2] & &\text{(Fixed-fixed)}
\end{aligned}
$$
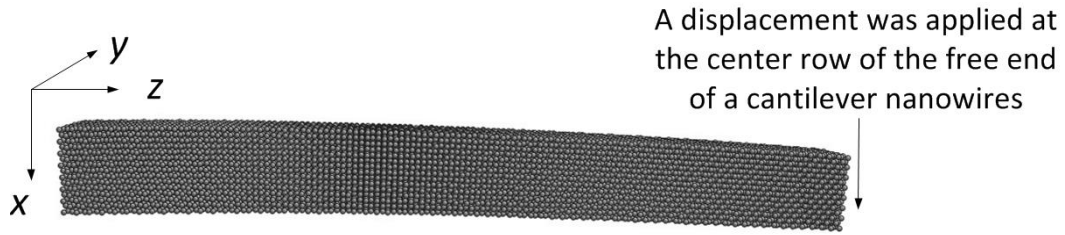
(a)
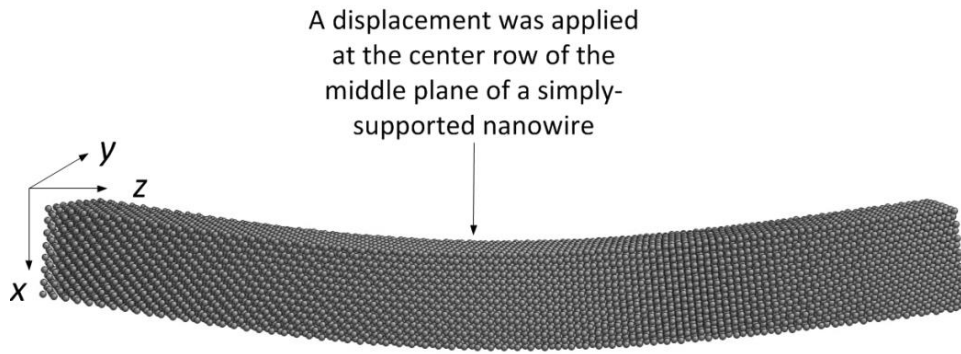
(b)
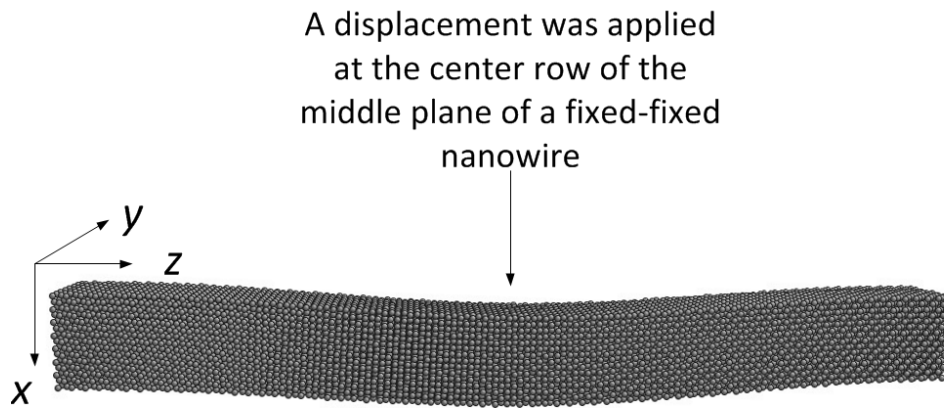
(c)

 Figure 5.4. Nanowires with a point force applied with (a) Cantilever (b) Simply-supported and (c) fixed-fixed boundary conditions.
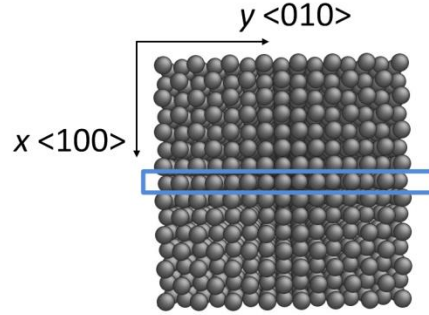
A row of atoms (at the free end of
cantilevers and at the middle of
simply-supported and fixed-fixed)
were applied a displacement to
achieve the initial load for bending.

Figure 5.5. Illustration the position of the applied load to achieve the bending displacement and the three different boundary conditions in MD simulations

Figs. 5.6 (a-c) show the fitting curves and boundary condition verification. Since the deformation of simply-supported and fixed-fixed nanowires are symmetric with respect to the midpoint, only half of the curves for these two boundary conditions are presented. The displacement curves from the simulations for the all three boundary conditions are presented in Eq.(5.4) with a coefficient of determination (R value) very close to 1. The proposed boundary condition set-ups are therefore considered as valid. The negligible differences between the simulations and fitting curves may be caused by the shear effect and size effect of the bending nanowires, which are ignored by the assumptions of Euler-Bernoulli beam theory.
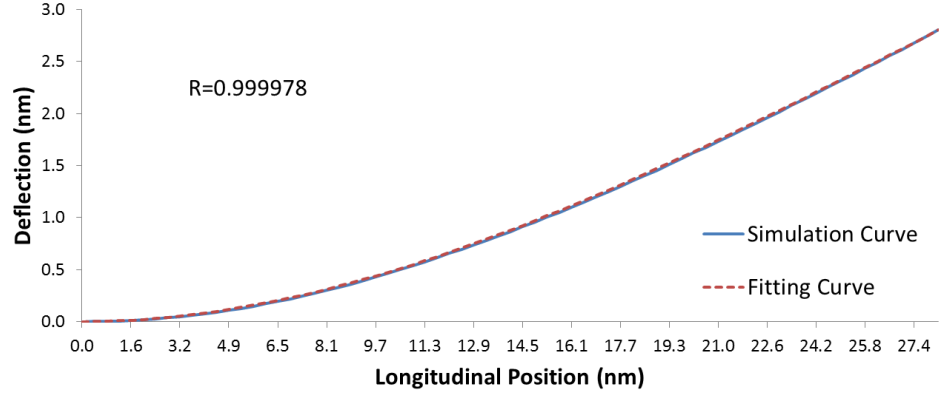
(a)
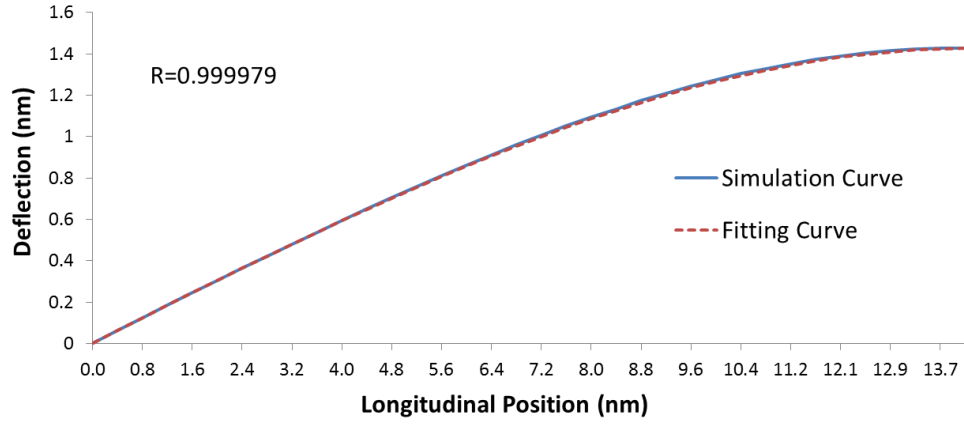
(b)
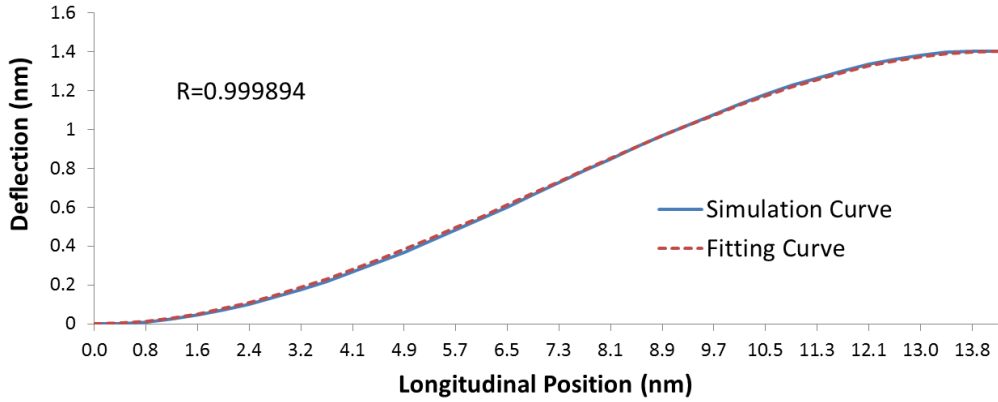
(c)

Figure 5.6. The simulation curves and fitting curves of the central atoms to verify the boundary condition set-up for (a) cantilever, (b) simply-supported and (c) fixed-fixed nanowires.

After validating the boundary conditions, MD simulations were performed on the nanowires using free vibration of the nanowires to obtain the resonant frequencies. The resonance simulations were performed to obtain the resonant frequencies for each combination of lattice orientation, cross-sectional size and boundary condition as shown in Table 5.I. The flexural vibration of the nanowire after the initial relaxation (as introduced in the first paragraph of section 5.2) was achieved by the following steps, as shown in Figure 5.4. First, an incremental displacement was applied to the midplane of simply-supported and fixed-fixed nanowires and the free-end of cantilever nanowires, as indicated by the arrows in Figure 5.4 (a-c). At each loading step, the NVT thermostat was applied to adjust the average temperature of the atoms so that the positions and velocities of atoms can be determined. The incremental displacement was applied until the angular displacement reached 0.5% ($2\delta/L$ for fixed-fixed and simply-supported nanowires, and δ/L for cantilever nanowires). This small deformation was chosen to ensure that the nanowires' vibration was within the purely elastic region. After the 0.5% initial deflection was reached, the deflection was held for a sufficient time (three times as long as the loading time in our simulations) with a NVT thermostat to ensure that the average temperature for the atoms of the nanowires were at 1K. Then, the applied deformation and NVT thermostat was removed to obtain the free vibration of the nanowire. During the free vibration period, the NVE thermostat was applied for enforce energy conservation. Similar procedures can be found in Reference [53] to obtain the resonant frequencies of FCC metals.

Table 5.I. The lattice orientations, sizes and boundary conditions in the resonance MD simulations

Two different lattice orientations		Ag(100)		Ag(110)
Three different sizes (lattice length η=4.09Å) for each orientations	For Ag(100)	5x5x50η	7x7x70η	10x10x100η
	For Ag(110)	3.5x5x35η	5x7x50η	7x10x70η
Three different boundary conditions		Cantilever	Simply-supported	Fixed-fixed

The transverse displacement of the central atoms at the free end for cantilevers and middle plane for simply-supported and fixed-fixed nanowires were stored to perform the Fast Fourier Transform (FFT) to calculate the resonant frequencies of the nanowires. Figure 5.7 shows the displacement of the central atom and FFT result for a 2.86x2.86x28.63nm nanowire with fixed-fixed boundary conditions. Because the second mode of vibration is sometimes not very clear, we use the first (fundamental) resonant frequency to calibrate e_0 in the following analysis. The complete FFT results are presented in Chapter 6 along with the corresponding discussion.
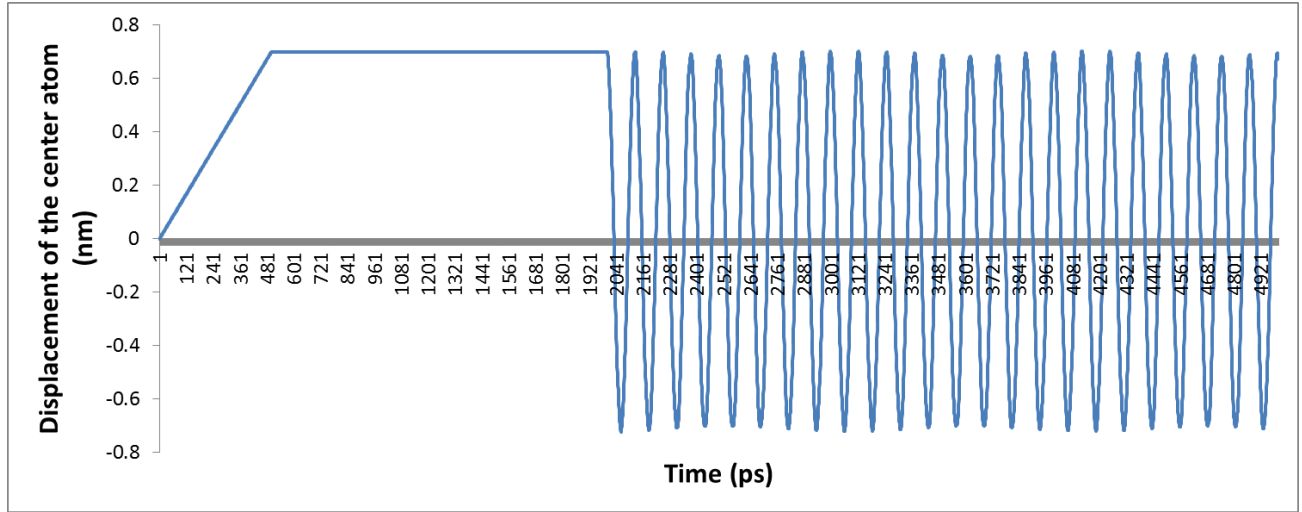
(a)
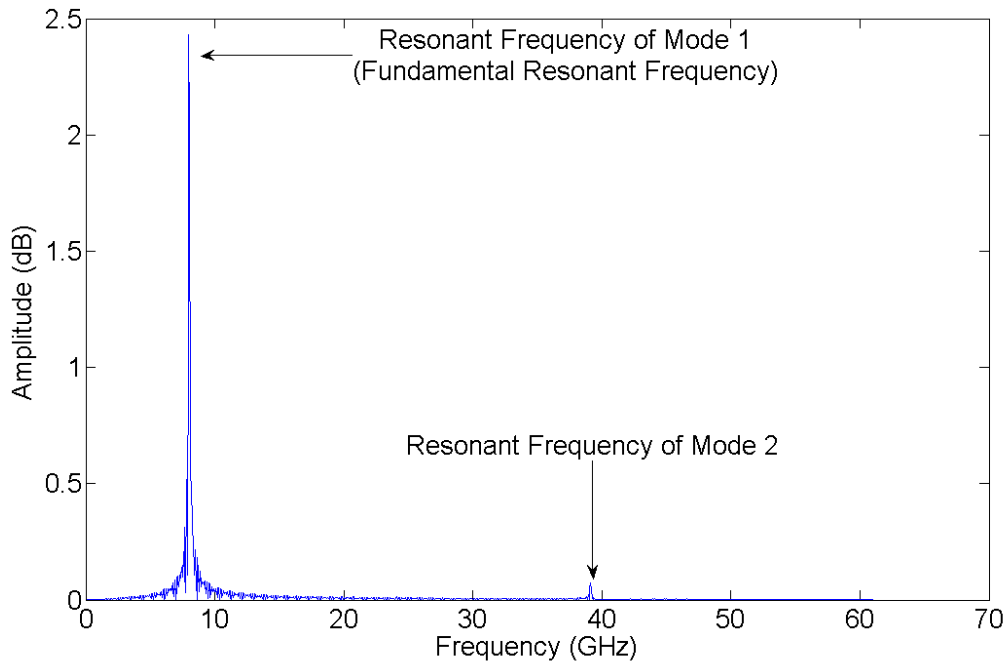
(b)

Figure 5.7. (a) The displacement of the middle atom for the excitement, holding and free vibration stages with the size of 2.86x2.86x28.63nm and fixed-fixed boundary condition. **(b)** The Fast Fourier Transform result of the displacement in the frequency domain for Figure 5.5 (a). Two peaks exist at the resonant frequencies of vibration mode 1 and 2.

93

5.5 <u>Conclusions</u>

This chapter first presents a summary of the MD simulations for the tensile tests and resonant frequencies calculations of the modeled nanowires. A common problem in these publications is that the results from MD simulations for nanoscale materials were not fully compared to mechanics models with size effects. However, size effects are unique for the nanoscale and are important when investigating the mechanical properties of nanomaterials. Therefore, the current analysis of the MD simulations of nanomaterials is lacking fundamental information on the origin of size effects. In the following chapter, a comparison among the MD simulations, Timoshenko beam theory with surface effects, and nonlocal Timoshenko beam theory will be presented.

In addition, the details of the procedures for the tensile tests and resonance tests with MD simulations using LAMMPS are introduced. The size effects will be studied with MD simulation results, obtained with the procedures introduced in section 5.2-5.4. The resonant frequencies of the transverse vibrating nanowires were calculated using FFT, and the results will be discussed in detail in Chapter 6. The fundamental resonant frequencies obtained in the MD simulations will be compared to the theoretical modeling in Chapter 4 to calibrate the nonlocal parameter e_0 of nonlocal elasticity. This comparison will be used to test the hypothesis that MD simulations and nonlocal Timoshenko beam theory include the same surface effects and thus should be consistent.

CHAPTER 6. Calibration of e_0 with Nonlocal Timoshenko Beam Theory, Timoshenko Beam Theory with Surface Effects, and MD Simulations

6.1 <u>Introduction</u>

A fundamental problem of nonlocal elasticity is that e_0 is not well defined.[39] Nonlocal elasticity was originally developed from the atomic scale lattice dynamics model without the nearest neighbor assumption[51], but not directly for nanoscale materials. Researchers to-date commonly assume arbitrary values for e_0 to derive specific nonlocal mechanical theories at the nanoscacle. For example nonlocal beam theory has been derived to investigate the nonlocal effect of the static deflection and resonant frequencies of beams.[40-42] However, the significance of the nonlocal effect is ambiguous because the physical material parameters that affect e_0 are unknown.

Some researchers have tried to calibrate e_0 specifically for the nanoscale. Challamel [60] and Wang [62] derived e_0 from the higher order lattice dynamic models, but they still included the nearest neighbor assumption in their derivation. Thus, their results do not contain the true nonlocal effect, but a higher order finite difference approximation. An alternative method is to calibrate e_0 by comparing the results between molecular dynamics simulations and nonlocal theoretical calculation. Ref. [65] proposed a method which calibrates e_0 of carbon nanotubes from the comparison between nonlocal elasticity and molecular dynamics simulations with the vibrating beam model. However, this calibration is incomplete, because for some combinations of sizes and boundary conditions, the solution of e_0 was not determined. They considered that e_0 for these cases "does not exist" without giving an explanation of the mechanics that result in an

undetermined e_0. In addition, to the best of our knowledge, there is no existing literature on the calibration of e_0 for FCC metal nanowires with different types of lattice orientations and boundary conditions. However, in practice, FCC metal nanowires are commonly used in NEMS for those mass/force sensors with well-developed fabrication technologies.[9, 151, 152] Therefore, finding e_0 for FCC metals is obligatory for contemporary nanotechnology, with the wide applications of metallic nanowires.

As shown in Figure 6.1, the hypothesis of this thesis is that Timoshenko beam theory with surface effects, nonlocal elasticity and the corresponding nonlocal beam theories, and MD simulations results model the same size scale effects for nanoscale beams with dimensions between 1 and100nm. With this hypothesis, e_0 has been calibrated in two different ways. First, the analytical solutions of the resonant frequencies from Timoshenko beam theory with surface effects and nonlocal Timoshenko beam theory are compared for the simply-supported boundary condition. The analytical solution of e_0 for simply-supported nanoscale beams will be discussed in section 6.2. Thereafter, e_0 for all the three boundary conditions, i.e. cantilever, simply-supported and fixed-fixed, is calculated by calibrating the value to achieve the same resonant frequency as calculated with MD simulations to that predicted with nonlocal Timoshenko beam theory. The corresponding discussion is presented in section 6.3. Finally, by comparing the resonant frequencies from MD simulation results, the surface stress for Ag(100) and Ag(110) along the axial direction was calculated. The value of surface stress was found to have a slight difference from the value found in literature. The possible reasons for this difference will also be discussed.
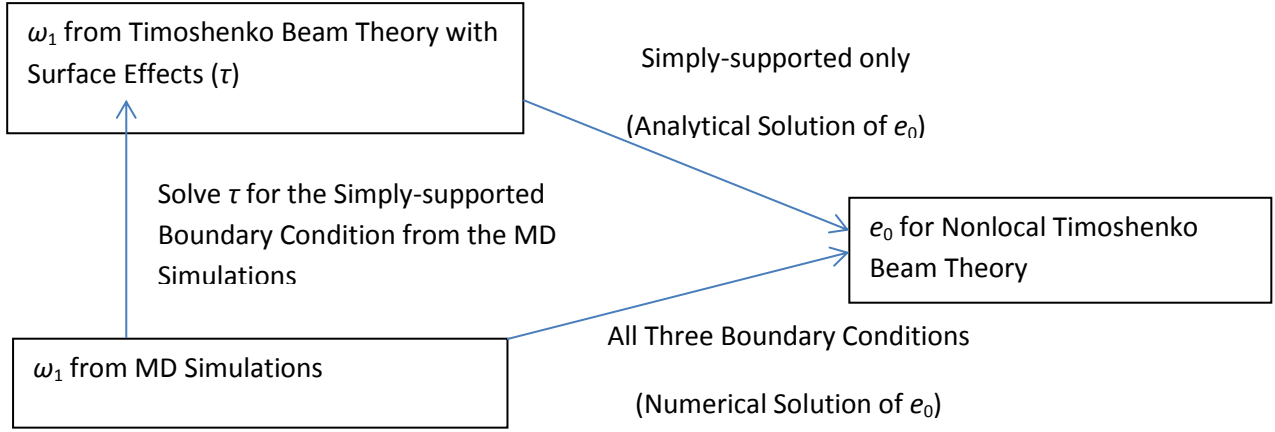
Figure 6.1. The two different approaches used in this research to calibrate the nonlocal parameter e_0 from nonlocal elasticity with beam vibration modeling.

In addition, the hypothesis that, for some combinations of lattice orientation and boundary conditions, e_0 is an imaginary number will also be tested. Duan *et al.* states that a real e_0 exists only when the maximum kinetic energy is larger than the maximum strain energy with the resonant frequencies obtained from the MD simulations for the fixed-fixed boundary condition.[65] Yet, in some instances, they found that the maximum kinetic energy was smaller than the maximum strain energy with the resonant frequencies obtained from MD simulations and they simply concluded that e_0 does not exist in these cases. We believe that for these situations, e_0 is imaginary. Furthermore, many papers indicated that a real e_0 always reduces the stiffness of simply supported beams or plates [37, 39, 43, 80]. Yet, if one considers surface properties of metallic crystals, their surface stress can be either positive or negative and the mechanical stiffness of a beam or plate can decrease or increase depending on both the sign of

the bending curvature and the boundary conditions. Thus, restricting e_0 to a real value that always results in a lower stiffness contradicts mechanical beam theories with surface stress. MD simulations for Ag(100) and Ag(110), as shown in Figure 5.1, will be used to illustrate to the possible range in values for e_0. It will be shown that both real and imaginary e_0 values may be obtained from MD simulations for the simply-supported case.

The boundary condition has significant effect on the stiffness of the beam structures for the beam modeling with surface stress. For instance, a positive surface stress increases the stiffness of a simply-supported beam/plate but decreases the stiffness of cantilevers. [45-50] The boundary condition effect of beam with surface stress is the result of the bending curvature associated with the end boundaries. [31, 79] Similarly, the curvature for different boundary conditions also affects the nonlocal effect in the nonlocal beam theory. To our best knowledge, few researchers have applied the nonlocal beam theory with different boundary conditions. Most of the research on nonlocal beam theory only considered simply-supported nanowires/plates due to the convenience in calculations. [37, 39, 43, 44] However, a cantilever is a more common beam structure in NEMS.[11-16] Additionally, the cantilever and fixed-fixed boundary conditions are typical models in realistic experiments and molecular dynamics simulations [53, 111, 112]. However, analytical solutions for the cantilever and fixed-fixed resonant frequency cases have not yet been found. Therefore, MD simulations for all the three boundary conditions are introduced, and e_0 will be calibrated for each condition. Since the resonant frequencies of the cantilever and fixed-fixed boundary conditions do not have existing analytical solutions, the analytical comparison between surface effects and nonlocal effects is restricted only to the simply supported case.

6.2 Analysis of the Material Parameter e_0 Using Nonlocal Elasticity and Timoshenko Beam Theory with Surface Stress

The analytical solution of the resonant frequencies of simply-supported nanowires from nonlocal Timoshenko beam theory is expressed in Eq. (4.65), and rewritten for convenience below as Eq. (6.1).

$$\omega_{n(\text{Analytical})} = \sqrt{\frac{EI\left(\frac{n\pi}{L}\right)^4}{\left[\frac{EI\rho}{kG}(e_0a)^2+(e_0a)^2\rho I\right]\left(\frac{n\pi}{L}\right)^4+\left[\rho I+\frac{EI\rho}{kG}+(e_0a)^2 A\rho\right]\left(\frac{n\pi}{L}\right)^2+A\rho}}. \qquad (6.1)$$

Recall that in Eq. (4.7), the term $\rho A(e_0a)^2\dfrac{d^4u}{dx^2dt^2}$ is associated to the curvature of the beams and describes the surface stress effect. Also, the resonant frequency for simply-supported Timoshenko beam with surfaces stress, after ignoring the 4th order term in Eq. (3.13) [26], is

$$\omega_n = \sqrt{\left[(1+\frac{H}{AkG})EI\left(\frac{n\pi}{L}\right)^4+H\left(\frac{n\pi}{L}\right)^2\right]\Bigg/\left[\rho A+\rho(\frac{EI}{kG}+I+\frac{HI}{AkG})\left(\frac{n\pi}{L}\right)^2\right]}. \qquad (6.2)$$

The resonant frequency from the two theories should be equal to each other when applying the hypothesis that surface effects and nonlocal effects can be used to model the same effect (i.e. surface properties), and, thus, they should be consistent, as shown in Eq. (6.3).

$$\sqrt{\frac{EI\left(\frac{n\pi}{L}\right)^4}{\left[\frac{EI\rho}{kG}(e_0a)^2+(e_0a)^2\rho I\right]\left(\frac{n\pi}{L}\right)^4+\left[\rho I+\frac{EI\rho}{kG}+(e_0a)^2 A\rho\right]\left(\frac{n\pi}{L}\right)^2+A\rho}} = \sqrt{\frac{(1+\frac{H}{AkG})EI\left(\frac{n\pi}{L}\right)^4+H\left(\frac{n\pi}{L}\right)^2}{\rho A+(\frac{\rho EI}{kG}+\rho I+\frac{\rho HI}{AkG})\left(\frac{n\pi}{L}\right)^2}} \qquad (6.3)$$

Therefore, a solution for $(e_0a)^2$ can be obtained and is as follows:

$$(e_0 a)^2 = \frac{EI\left(\frac{n\pi}{L}\right)^2\left[\rho A + (\frac{\rho EI}{kG} + \rho I + \frac{\rho HI}{AkG})\left(\frac{n\pi}{L}\right)^2\right] - \left[\left(1 + \frac{H}{AkG}\right)EI\left(\frac{n\pi}{L}\right)^2 + H\right]\left[\left(\frac{n\pi}{L}\right)^2\left(\rho I + \frac{EI\rho}{kG}\right) + A\rho\right]}{\left[\left(\frac{n\pi}{L}\right)^2\left(\frac{EI\rho}{kG} + \rho I\right) + A\rho\right]\left[\left(1 + \frac{H}{AkG}\right)EI\left(\frac{n\pi}{L}\right)^4 + H\left(\frac{n\pi}{L}\right)^2\right]} \quad (6.4)$$

.

If one considers that the shear effect is negligible when modeling a slender nanowire with an aspect ratio larger than 5, Eq. (6.4) leads to the expression for the relation between the nonlocal parameter e_0 and surface stress,

$$(e_0 a)^2 = \frac{-1}{\left[\frac{EI}{H}\left(\frac{n\pi}{L}\right)^4 + \left(\frac{n\pi}{L}\right)^2\right]} \quad (6.5)$$

.

The calculated values for e_0 for Ag(111)and Ag(100) using Eqs. (6.4) and (6.5), will be presented in Table 6.I-II and 6.III-IV, respectively. The solution for e_0 from Eq. (6.5) is therefore

$$e_0 = \sqrt{\frac{-1}{\left[\frac{EI}{H}\left(\frac{n\pi}{L}\right)^4 + \left(\frac{n\pi}{L}\right)^2\right]}} \Big/ a \quad (6.6)$$

.

It can be observed from Eq. (6.6) that e_0 is a dimensionless quantity.

The Euler-Bernoulli and Timoshenko beam theories have been widely used and accepted in modeling the surface stress effect on the vibration of nanowires.[45-50] Therefore, the material parameter, e_0, derived with the method introduced in this chapter is calibrated by including surface stress effects. From Eqs. (6.5) and (6.6), it can be seen that e_0 for a simply-supported nanowire in flexural vibration is not a fixed number, but depends on the following parameters: the lattice length a, the elastic modulus E, the surface stress τ, the cross-section size w and shape (included in I and H), the length of the beam L and the vibration modes n. Duan *et al.* obtained values for e_0 of carbon nanotubes by calibrating the molecular dynamics simulation and nonlocal beam theory in Ref. [65]. Similar to their findings, Eq. (6.6) also show that when the vibration mode, n, increases, then e_0 decreases.

In order to test the numerical value of e_0, Ag(111) and Ag(100) with the following parameters will be used as examples and are shown in Figure 6.2 (a) and (b) respectively. The parameter values are: a lattice constant a=0.409nm[131], an elastic modulus, E=63GPa, for Ag(111) [132] and 89GPa for Ag(100) [26], n=1 for the first vibration mode, a surface stress of τ_{111}=-0.2768N/m (-0.0173eVÅ^2) for a Ag(111) surface, and τ_{100}=0.1856N/m (0.0116 eVÅ^2) for a Ag(100) surface [64].

(a)

(b)
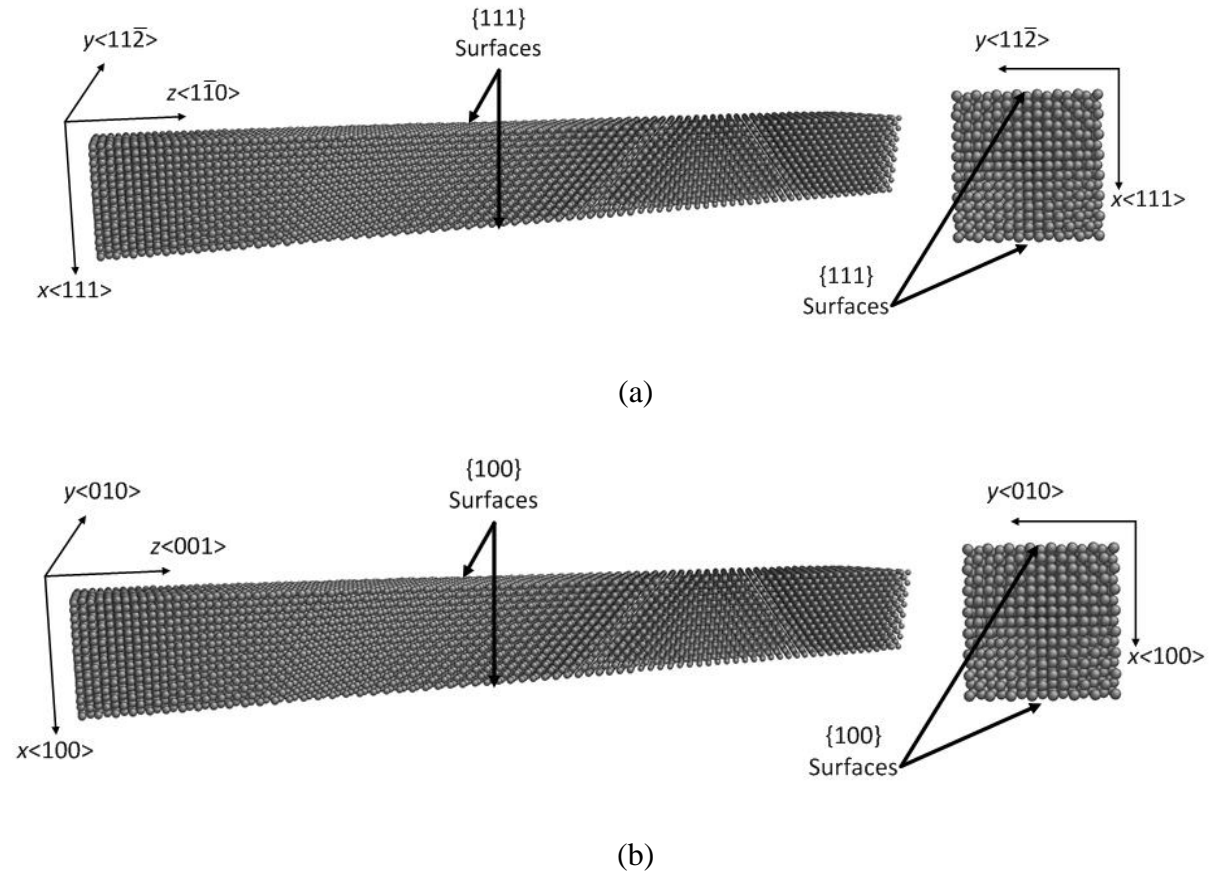
Figure. 6.2. Illustrations of (a) τ_{111}=-0.2768N/m (-0.0173eVÅ^2) for a Ag(111) surface, and (b) τ_{100}=0.1856N/m (0.0116 eVÅ^2) for a Ag(100) surface with left side views.

The cross-section of the beam is a w by w square and I is defined as $w^4/12$. The values for w were chosen to be 5, 50, and 100 nm and the aspect ratios were chosen to be 3, 5, 10, and 20 to study size and aspect ratio effects. With size scales above 5nm, the surface stress effect is demonstrated to have much more significant than the surface elasticity effect.[24] Therefore, the surface elasticity is neglected and the calibrated e_0 only contains the surface stress information for this discussion. The normalized differences (ND) are defined as $(e_{0,\text{w/ surface stress}} - e_{0,\text{w/o surface stress}})/e_{0,\text{w/o surface stress}} \times 100\%$.

Table 6.I. e_0 for Ag(111) calculated from Eq. (6.4) with shear effect.

Aspect ratio	Cross section size (w)		
	5nm	50nm	100nm
3	1.84	5.74	8.12
5	4.85	14.93	21.08
10	20.60	58.22	81.87
20	192.89	238.73	329.94

Table 6.II. e_0 for Ag(111) calculated from Eq. (6.5) without shear effect and the normalized difference (ND).

Aspect ratio	Cross section size (w)					
	5nm		50nm		100nm	
	e_0	ND	e_0	ND	e_0	ND
3	1.63	-11.005%	5.12	-10.79%	7.24	-10.776%
5	4.62	-4.739%	14.26	-4.498%	20.14	-4.485%
10	20.29	-1.534%	57.50	-1.228%	80.88	-1.215%
20	188.78	-2.132%	237.93	-0.335%	328.88	-0.320%

Table 6.III. e_0 for Ag(100) calculated from Eq. (6.4) with shear effect, where i is the imaginary unit.

Aspect ratio	Cross section size (w)		
	5nm	50nm	100nm
3	1.24i	3.95i	5.59i
5	3.20i	10.24i	14.49i
10	11.94i	39.46i	55.95i
20	41.90i	154.12i	220.13i

Table 6.IV. e_0 for Ag(100) calculated from Eq. (6.5) without shear effect and the normalized difference with respect to the calculated values found in Table 6.III, i is the imaginary unit.

Aspect ratio	Cross section size (w)					
	5nm		50nm		100nm	
	e_0	ND	e_0	ND	e_0	ND
3	1.11i	-10.654%	3.53i	-10.753%	4.99i	-10.759%
5	3.06i	-4.356%	9.78i	-4.460%	13.85i	-4.466%
10	11.81i	-1.090%	38.99i	-1.190%	55.28i	-1.196%
20	41.81i	-0.218%	153.67i	-0.294%	219.47i	-0.300%

The difference in values for e_0 between Eq. (6.4) and (6.5) is presented to examine the shear effect in Tables 6.II and 6.IV. The shear effect mainly depends on the aspect ratio of the beam. As the aspect ratio increases, the shear effect is less significant and Eq. (6.4) converges to Eq. (6.5). For small aspect ratios, the shear effect increases the absolute value of e_0 significantly and Eq. (6.4) should be used to calculate e_0.

As can been seen from Tables 6.I-6.IV, for the analytical solutions of Eqs. (6.4) and (6.5), the negative surface stress of Ag(111) results in real values for e_0 and the positive surface stress

for Ag(100) results in imaginary values for e_0. As the cross-section size and aspect ratio grows, the magnitude of e_0 also increases to match the surface stress for both positive and negative surface stress. The fact that the absolute value of e_0 is an increasing function with respect to the cross-sectional size can also be demonstrated by taking the derivate of e_0 with respect to w. From Eq. (6.6), the derivate of e_0 with respect to w is

$$\frac{de_0}{dw} = \begin{cases} \dfrac{-2\tau w\left[\dfrac{Ew}{24}\left(\dfrac{n\pi}{AR}\right)^4 + 2\tau\left(\dfrac{n\pi}{AR}\right)^2\right]}{a\left[\dfrac{Ew}{12}\left(\dfrac{n\pi}{AR}\right)^4 + 2\tau\left(\dfrac{n\pi}{AR}\right)^2\right]^2 \sqrt{\dfrac{-2\tau w^2}{\dfrac{Ew}{12}\left(\dfrac{n\pi}{AR}\right)^4 + 2\tau\left(\dfrac{n\pi}{AR}\right)^2}}} & \text{for } w > \dfrac{-24\tau}{E}\left(\dfrac{AR}{n\pi}\right)^2 \\[2em] \dfrac{2\tau w\left[\dfrac{Ew}{24}\left(\dfrac{n\pi}{AR}\right)^4 + 2\tau\left(\dfrac{n\pi}{AR}\right)^2\right]}{a\left[\dfrac{Ew}{12}\left(\dfrac{n\pi}{AR}\right)^4 + 2\tau\left(\dfrac{n\pi}{AR}\right)^2\right]^2 \sqrt{\dfrac{2\tau w^2}{\dfrac{Ew}{12}\left(\dfrac{n\pi}{AR}\right)^4 + 2\tau\left(\dfrac{n\pi}{AR}\right)^2}}} i & \text{for } w < \dfrac{-24\tau}{E}\left(\dfrac{AR}{n\pi}\right)^2 \end{cases} \qquad (6.7)$$

It was found that only when τ is negative and the cross-section size w at the range of

$\dfrac{-24\tau}{E}\left(\dfrac{AR}{n\pi}\right)^2 < w < \dfrac{-48\tau}{E}\left(\dfrac{AR}{n\pi}\right)^2$, or $-\dfrac{Ew\left(\dfrac{\pi}{AR}\right)^2}{24} < \tau < -\dfrac{Ew\left(\dfrac{\pi}{AR}\right)^2}{48}$, the value of $\dfrac{d\left|e_0\right|}{dw}$ is negative and the

absolute value of e_0 is a decreasing function with respect to w. For the remaining intervals of w, the absolute value of e_0 is an increasing function with respect to w, and also includes the cases where e_0 is an imaginary number. This analysis demonstrates that e_0 increases with an increasing cross-section. The same trend was found in Tables 6.I.-6.IV. Additionally, it can be seen in the MD simulations that e_0 is an increasing function with respect to the cross-sectional size for the three chosen boundary conditions. The discussion of e_0 from MD simulations will be presented in section 6.3.

Finally, e_0 can be a real number only when H is negative and larger than $-EI(n\pi/L)^2$ for a simply-supported beam. This conclusion indicates that a positive surface stress, or negative surface stress with a large absolute value cannot be described by nonlocal elasticity if we prescribe that e_0 must be real. This may explain why for some combinations of aspect ratios and boundary conditions found in Ref. [65], the authors stated that e_0 did not exist. They indicated that by substituting the resonant frequencies from the molecular dynamics simulation, when the maximum kinetic energy is larger than the maximum strain energy, only real values of e_0 can be found. However, they did not discuss the situation when maximum kinetic energy is smaller than the maximum strain energy in detail. They just simply pointed out that e_0 did not exist for these cases. However, we propose that an imaginary e_0 is possible and necessary to describe the above cases. As shown in Eq. (6.8), the limitation of a real e_0 is caused by the minus sign and the square of e_0a.

$$-(e_0a)^2\nabla^2 t_{ij} = \Delta\sigma_{ij} \tag{6.8}$$

This is from the corresponding differential operator of Eq. (4.2) according to Green's function. For a positive Laplacian, $\nabla^2 t_{ij}$, the additional stress $\Delta\sigma_{ij}$, is always negative as shown in Eq. (6.8). Therefore, if e_0 is real, the elastic tensor C_{ijkl} in Eq. (4.2) is always smaller than the bulk value and the stiffness of the nonlocal structure is always decreased by the nonlocal effect. However, this is contrary to beam theory with surface stress. Eq. (6.9) shows that the relation between the additional distributed load, $\Delta p(x)$, and a surface stress.[47] Here, H, defined by Eq. (3.6), can be either negative or positive depending on the sign of the surface stress. The variable u is the deflection of the beam and d^2u/dx^2 is the approximation of the bending curvature.

$$H\,d^2u/dx^2 = \Delta p(x). \tag{6.9}$$

For a simply-supported beam, a positive surface stress increases the stiffness of the beam and a negative surface stress decreases the stiffness due to the bending curvature.[26, 29, 30, 47] The nonlocal strain-stress relation in Eq. (4.2) and the nonlocal beam theory in Eqs. (4.3) and (4.4) are commonly used in today's nanoscale mechanics for the convenience and the advantage of differential (not integral) equations. Hence, we suggest that in order to make nonlocal beam theory describe a broader category of nanomaterials with surface effects, e_0 should be expanded to include an imaginary value to account for positive surface stresses and negative surface stresses with a large absolute value.

6.3 Analysis of the Nonlocal Parameter e_0 Using Nonlocal Elasticity and MD Simulations

6.3.1 The Elastic Moduli from MD Simulations

Table 6.V. lists the elastic moduli and the fundamental resonant frequencies for each combination of lattice orientation, cross-section size and boundary condition of nanowires. The elastic moduli were solved with the energy method using the data from the MD simulations of nanowire tensile tests. The fundamental resonant frequencies were calculated by performing FFT of the beam vibration obtained with MD resonance tests. The equation to fit the elastic modulus E is Eq. (5.2) and rewritten below as Eq. 6.10 for convenience.

$$\frac{\Delta U}{V_0} = E\left(\frac{1}{2}\varepsilon^2 + \frac{1}{3}\varsigma\varepsilon^3\right)$$ (6.10)

Here, ΔU is the change in potential energy in the nanowires during the loading and is obtained from the MD simulations' output file. E, the variable to be solved for, is the elastic modulus at the strain $\varepsilon=0$. V_0 is the initial volume of the nanowire, and ς is a constant from the third order polynomial fitting.

It can be seen in Table 6.V that the elastic modulus of Ag(100) along the <001> direction decreases as the cross-sectional size decreases. However, the elastic modulus of Ag(110) along the <110> direction behave as the opposite, i.e., the elastic modulus increases as the cross-sectional sizes increase. At the size range of 2nm-4nm, Ag nanowires for both lattice orientations

Table 6.V. The fundamental resonant frequency of the vibration of Ag nanowires from MD simulations for different cross-sectional size and lattice orientation.

Ag(100)	f_1 for cantilever (GHz)	f_1 for simply-supported (GHz)	f_1 for fixed-fixed (GHz)	Elastic Modulus (GPa)
4.09x4.09x40.9nm	0.854	2.441	5.676	52.96
2.86x2.86x28.63nm	1.181	3.418	7.996	50.77
2.045x2.045x20.45nm	1.587	4.639	10.986	47.80
Ag(110)				
4.05x4.09x40.49nm	1.343	3.562	7.264	107.21
2.83x2.86x28.34nm	1.831	5.127	10.254	111.08
2.002x2.045x20.02nm	2.583	7.206	13.916	114.07

behave stiffer than the bulk material. The bulk elastic moduli are 44GPa for Ag(100) in the <001> direction and 84.1GPa for Ag(110) in the <110> direction.[111] A similar tendency for the relation between the elastic moduli and cross-sectional sizes was also found by Matthew *et al.* in Ref. [111] and shown in Figure 6.3. Matthew *et al.* focused on the elastic modulus for both lattice orientations with cross-section sizes of 2nm-8nm. The energy method with Eq. (6.10) was applied to calculate the elastic modulus from the tensile test with 2% strain. They found that for Ag(110), 4 nm was the cross-sectional size with the largest elastic modulus of about 46 GPa (see

Figure 6.3) along the <001> direction, i.e., the elastic modulus decreases as the cross-sectional size deceases when it is smaller than 4 nm. However, for Ag(110), the <110> direction does not have a peak value for the elastic modulus. The elastic modulus always increases as the cross-sectional size decreases at the range of 2nm-8nm.
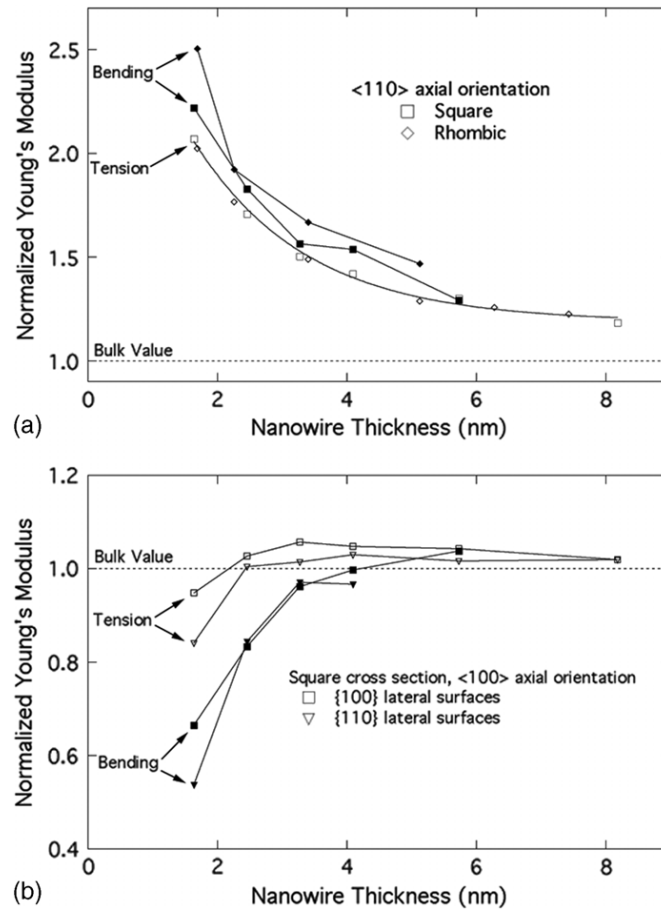
Figure 6.3. The elastic modulus from tensile and bending tests with MD simulations from Ref. [111]. The "tension" curves are used to compare to our values of elastic modulus from the MD tensile test as shown in Table 6.V.

6.3.2 *The Fundamental Resonant Frequencies from MD Simulations and the Corresponding Values of e_0 with Comparisons to the Analytical Solution for Simply-supported Boundary Conditions*

Table 6.V shows the fundamental frequencies of each nanowire with an aspect ratio of 10 and different cross-sectional sizes, lattice orientations, and boundary conditions. Table 6.VI lists the value of e_0 with respect to the fundamental resonant frequency for each combination. The values for e_0 are solved by the bisection numerical method [153] with the determinants introduced from Eq. (4.50-4.63), where $n=1$ and ω_1 ($=2\pi f_1$) as obtained from the FFT values shown in Table 6.V. The simply-supported case was also solved with the numerical method for higher accuracy by neglecting the assumptions used in the analytical solution. It can be clearly seen that e0 is not a constant and depends on the three parameters we choose to study here, namely the boundary conditions, cross-sectional size, and lattice orientation.

Table 6.VI. The nonlocal parameter e_0 of Ag nanowires for different cross-sectional size and lattice orientation.

Ag(100)	e_0 for cantilever	e_0 for simply-supported	e_0 for fixed-fixed
4.09x4.09x40.9nm	27.898i	2.496	10.484i
2.86x2.86x28.63nm	23.65i	1.437	7.675i
2.045x2.045x20.45nm	19.094i	1.250	5.840i
Ag(110)			
4.05x4.09x40.49nm	33.175	6.622i	7.781
2.83x2.86x28.34nm	8.221	3.413i	7.497
2.002x2.045x20.02nm	1.102	1.127i	7.096

Similar to the conclusion found from the analytical analysis, e_0 has to be imaginary for some of the MD simulations cases. Wang *et al.* modeled the resonance of plates and found that a real e_0 always reduces the stiffness of the plates, which has the same effect of negative surface stresses.[22] The conclusion that the real e_0 reduces the stiffness of simply-supported plates and beams is also supported by numerous other researchers. [37, 39, 43, 44] Moreover, Duan *et al.* calibrated e_0 by comparing the nonlocal Timoshenko beam theory and molecular dynamics simulation on the transverse resonance of carbon nanotubes. They did not find the solutions of e_0 for some combination of sizes and boundary conditions.[65] However, we believe that the imaginary solution of e_0 does exist for these cases.

The MD simulations support the previous conclusions from the analytical analysis that e_0 has to be imaginary for some combinations of sizes, boundary conditions and materials. In our simulations, the simply-supported Ag(100) has real e_0 and Ag(110) has imaginary e_0 for all the sizes in our simulations. The MD simulations also support the trend that the absolute value of e_0 increases when the cross-sectional size increases. This matches the analytical relation between e_0 and surface stress τ. It should also be noted that surface elasticity is typically negligible in most studies of surface effects when the cross-sectional size is over 5 nm [24, 26, 29, 30, 32, 59, 78]. However, the size scales in the MD simulations presented here are smaller due to computational restrictions (i.e. 2nm-4nm). Therefore, it is proposed that the surface elasticity must also be considered in our analysis of the resonant frequency properties. Therefore, using Timoshenko beam theory with surface stress and surface elasticity, the calculated resonant frequencies are shown in Eq. (6.12). The method to incorporate surface elasticity is achieved by replacing *EI* in Eq. 6.2 with the term *(EI)** found in equation (6.11) below: [47]

$$\left(EI \right)^{*} = EI + \frac{2}{3} E_{s} w^{3}$$

(6.11)

.

Where, E is the elastic modulus from the tensile test MD simulations, E_s is the surface elasticity of the corresponding material, and w is the cross-sectional size of a square.

Therefore, the resonant frequencies from Timoshenko beam theory with surface stress and surface elasticity is

$$\omega_n(\text{surface-stress and surface-elasticity}) = \sqrt{\left[(1+\frac{H}{AkG})(EI)^*\left(\frac{n\pi}{L}\right)^4 + H\left(\frac{n\pi}{L}\right)^2\right] \Bigg/ \left\{\rho A + \rho\left[\frac{(EI)^*}{kG} + I + \frac{HI}{AkG}\right]\left(\frac{n\pi}{L}\right)^2\right\}} \quad (6.12)$$

From Timoshenko beam theory with the nonlocal effect, the resonant frequencies are

$$\omega_n(\text{nonlocal}) = \sqrt{\frac{EI\left(\frac{n\pi}{L}\right)^4}{\left[\frac{EI\rho}{kG}(e_0a)^2 + (e_0a)^2\rho I\right]\left(\frac{n\pi}{L}\right)^4 + \left[\rho I + \frac{EI\rho}{kG} + (e_0a)^2 A\rho\right]\left(\frac{n\pi}{L}\right)^2 + A\rho}} \quad (6.13)$$

If $\omega_n(\text{surface-stress and surface-elasticity}) = \omega_n(\text{nonlocal})$, the relationship between the nonlocal parameter, e_0, and the surface stress, τ, can be obtained. The difference between Eqs. (6.4) and (6.12) is that Eq. (6.12) contains the additional surface elasticity information for e_0 and should be used for the smaller size scale, such as 2nm-4nm, used in the simulations found in this thesis.

$$(e_0a)^2 = \frac{EI\left(\frac{n\pi}{L}\right)^2\left[\rho A + (\frac{\rho(EI)^*}{kG} + \rho I + \frac{\rho HI}{AkG})\left(\frac{n\pi}{L}\right)^2\right] - \left[\left(1+\frac{H}{AkG}\right)(EI)^*\left(\frac{n\pi}{L}\right)^2 + H\right]\left[\left(\frac{n\pi}{L}\right)^2\left(\rho I + \frac{EI\rho}{kG}\right) + A\rho\right]}{\left[\left(\frac{n\pi}{L}\right)^2\left(\frac{EI\rho}{kG} + \rho I\right) + A\rho\right]\left[\left(1+\frac{H}{AkG}\right)(EI)^*\left(\frac{n\pi}{L}\right)^4 + H\left(\frac{n\pi}{L}\right)^2\right]} \quad (6.14)$$

If the aspect ratio is over 5 and the shear effect is negligible, Eq. (6.13) can be simplified to

$$(e_0a)^2 = \frac{EI\left(\frac{n\pi}{L}\right)^2 - (EI)^*\left(\frac{n\pi}{L}\right)^2 - H}{\left[(EI)^*\left(\frac{n\pi}{L}\right)^4 + H\left(\frac{n\pi}{L}\right)^2\right]} \quad . \quad (6.15)$$

Or equivalently,

$$e_0 = \sqrt{\left. \frac{-\frac{2}{3}E_s w^2 \left(\frac{n\pi}{AR}\right)^2 - 2\tau w^2}{\frac{Ew}{12}\left(\frac{n\pi}{AR}\right)^4 + \frac{2E_s}{3}\left(\frac{n\pi}{AR}\right)^4 + 2\tau\left(\frac{n\pi}{AR}\right)^2} \middle/ a \right.} \qquad (6.16)$$

To study the properties of e_0 with respect to w, we also take the derivative of e_0 with respect to w and to obtain the following equations shown in Eq. (6.17). If the derivative is positive, the e_0 function is an increasing function with respect to w.

$$\frac{de_0}{dw} = \begin{cases} \dfrac{-\left[\frac{2}{3}E_s w\left(\frac{n\pi}{AR}\right)^2 + 2\tau w\right]\left[\frac{Ew}{24}\left(\frac{n\pi}{AR}\right)^4 + \frac{2E_s}{3}\left(\frac{n\pi}{AR}\right)^4 + 2\tau\left(\frac{n\pi}{AR}\right)^2\right]}{a\left[\frac{Ew}{12}\left(\frac{n\pi}{AR}\right)^4 + \frac{2E_s}{3}\left(\frac{n\pi}{AR}\right)^4 + 2\tau\left(\frac{n\pi}{AR}\right)^2\right]^2 \sqrt{\dfrac{-\frac{2}{3}E_s w^2\left(\frac{n\pi}{AR}\right)^2 - 2\tau w^2}{\frac{Ew}{12}\left(\frac{n\pi}{AR}\right)^4 + \frac{2E_s}{3}\left(\frac{n\pi}{AR}\right)^4 + 2\tau\left(\frac{n\pi}{AR}\right)^2}}} & \begin{array}{l} w > \frac{-24\tau}{E}\left(\frac{AR}{n\pi}\right)^2 - \frac{8E_s}{E} \ \text{ when } \tau \le -\frac{1}{3}E_s\left(\frac{n\pi}{AR}\right)^2 \\[2ex] w < \frac{-24\tau}{E}\left(\frac{AR}{n\pi}\right)^2 - \frac{8E_s}{E} \ \text{ when } \tau > -\frac{1}{3}E_s\left(\frac{n\pi}{AR}\right)^2 \end{array} \\[6ex] \dfrac{\left[\frac{2}{3}E_s w\left(\frac{n\pi}{AR}\right)^2 + 2\tau w\right]\left[\frac{Ew}{24}\left(\frac{n\pi}{AR}\right)^4 + \frac{2E_s}{3}\left(\frac{n\pi}{AR}\right)^4 + 2\tau\left(\frac{n\pi}{AR}\right)^2\right]}{a\left[\frac{Ew}{12}\left(\frac{n\pi}{AR}\right)^4 + \frac{2E_s}{3}\left(\frac{n\pi}{AR}\right)^4 + 2\tau\left(\frac{n\pi}{AR}\right)^2\right]^2 \sqrt{\dfrac{\frac{2}{3}E_s w^2\left(\frac{n\pi}{AR}\right)^2 + 2\tau w^2}{\frac{Ew}{12}\left(\frac{n\pi}{AR}\right)^4 + \frac{2E_s}{3}\left(\frac{n\pi}{AR}\right)^4 + 2\tau\left(\frac{n\pi}{AR}\right)^2}}} i & \begin{array}{l} w < \frac{-24\tau}{E}\left(\frac{AR}{n\pi}\right)^2 - \frac{8E_s}{E} \ \text{ when } \tau \le -\frac{1}{3}E_s\left(\frac{n\pi}{AR}\right)^2 \\[2ex] w > \frac{-24\tau}{E}\left(\frac{AR}{n\pi}\right)^2 - \frac{8E_s}{E} \ \text{ when } \tau > -\frac{1}{3}E_s\left(\frac{n\pi}{AR}\right)^2 \end{array} \end{cases}$$

$$(6.17)$$

It is found that only within the region of τ defined by

$$-\frac{Ew\left(\frac{\pi}{AR}\right)^2}{24} - \frac{E_s}{3}\left(\frac{n\pi}{AR}\right)^2 < \tau < -\frac{Ew\left(\frac{\pi}{AR}\right)^2}{48} - \frac{E_s}{3}\left(\frac{n\pi}{AR}\right)^2 \ , \ \frac{d|e_0|}{dw}$$ is a decreasing function. For the

remaining range of values for τ, the absolute value of e_0 is an increasing function with respect to w, including the case when e_0 is an imaginary number. The simulation results found in Table 6.VI for a simply-supported Ag nanowire is consistent with the results found with Eq. (6.17), where e_0 increases when the cross-sectional size w of the nanowires increases. Therefore, e_0 is an increasing function with respect to the cross-section size for both of the lattice orientations tested.

6.3.3 *The Boundary Condition Effect on e_0*

Boundary conditions also have significant influence on the value of e_0, as shown in Table 6.VI. One significant finding is that the real/imaginary property of e_0 is closely associated with the boundary condition. For example, for Ag(100), e_0 is an imaginary number for a cantilever and fixed-fixed nanowire, but real for the simply-supported case. For Ag(110), the opposite trend occurs for e_0. This phenomenon can be explained using Eq. (6.8) as follows. In Chapter 3, it has been found that the changed stiffness of bending nanowires due to the surface stress depends on the boundary condition. The analysis of surface stress effects on bending nanowires found in Refs. [6, 8, 46] demonstrate that the surface stress effect has the opposite influence on the cantilever and simply-supported beams because of the different directions in the bending curvatures. For example, a positive surface stress reduces the stiffness of a cantilever but enhances the stiffness of a simply-supported nanowire. For the nonlocal effect, an imaginary e_0 in Eq. (6.8) increases the stiffness and a real e_0 decreases the stiffness of the material, regardless of the boundary conditions. The elastic tensor C_{ijkl} in Eq. (4.2) is always smaller than the bulk value and the stiffness of the nonlocal structure is always decreased by the nonlocal effect, if $\nabla^2 t_{ij}$ is positive in Eq. (6.8). Therefore, in order to match the result from the beam theory with surface stress modeling, the real/imaginary property (which means the value of e_0 is real or imaginary) of e_0 for cantilever and simply-supported nanowires must be the opposite. The MD simulations support the above analysis. As seen in Table VI, the e_0 values from the MD simulations clearly have opposite real/imaginary values for cantilever and simply-supported boundary conditions.

As discussed in Refs. [26, 29] and as seen in Figure 3.4 (c) and 5.4 (c), the bending curvature for a fixed-fixed nanowire in flexure is different from the uniform bending curvatures

found in cantilever or simply-supported nanowire. A fixed-fixed nanowire has a combination of directions of bending curvatures. The changing stiffness due to the surface stress depends on the overall effect of these curvatures.[26, 29] The changing stiffness can be similar to a cantilever or simply-supported nanowire because of this overall curvature effect. For the selected materials and nanowire dimensions in the MD simulations performed for this research, the resonant frequencies indicate that the value of e_0 for fixed-fixed nanowires have the same real/imaginary property as cantilever nanowires.

6.3.4 *The Conservation of Energy Verification for Real and Imaginary Values of e_0*

To the best of our knowledge, no researchers have proposed the existence of an imaginary value for the nonlocal parameter e_0. Thus, we need to verify whether an imaginary e_0 violates any fundamental rules of physics. It should be emphasized that the MD simulations for free vibration of the nanowires was performed with the NVE constraint. Thus, conservation of energy was enforced for these simulations. The energy of a nanowire with undamped free vibration is the summation of the kinetic energy and the potential energy, and at any time during the vibration should be a constant. The equation of the kinetic energy of the beam is the following [126],

$$T = \frac{1}{2}\int_0^L \rho A \left[\frac{\partial u(x,t)}{\partial t}\right]^2 dx + \frac{1}{2}\int_0^L \rho I \left[\frac{\partial \phi(x,t)}{\partial t}\right]^2 dx \qquad (6.18)$$

The potential energy due to the bending moment (*M*) is

$$U_{\text{bending moment}} = \frac{1}{2EI}\int_0^L M^2 dx \qquad (6.19)$$

Additionally, the shear force (V) also provides a small portion of potential energy as defined in the following equation:

$$U_{shear} = \int_0^L \frac{f_s V^2}{2GA} dx \,. \tag{6.20}$$

Here, $f_s=6/5$ for a rectangular cross-section. The formulas for the bending moment M and shear force V were defined using Eqs. (4.9) and (4.10) in Chapter 4.

Using separation of variables, the kinetic energy is in the form of Eq. (6.21),

$$T = \frac{1}{2} \sin^2(\omega_n t) \left[\int_0^L \rho A X^2 dx + \frac{1}{2} \int_0^L \rho I \Phi^2 dx \right] \tag{6.21}$$

Since the temporal portion of the kinetic energy is the first derivative of the temporal part of the deflection (Eq. 4.11) and angular displacement (Eq. 4.12) with respect to time t, $\sin^2 \omega_n t$ is the temporal term in the potential energy. According to Eqs. (4.9) and (4.10), the temporal potion of the potential energy is $\cos^2 \omega_n t$, and is shown in Eqs. (6.22) and (6.23).

$$\begin{aligned}
U_{bending\ moment} &= \frac{1}{2EI} \int_0^L \left[EI \frac{\partial \phi}{\partial x} + (e_0 a)^2 \left(\rho A \frac{\partial^2 u}{\partial t^2} + \rho I \frac{\partial^3 \phi}{\partial x \partial t^2} \right) \right]^2 dx \\
&= \frac{\cos^2(\omega_n t)}{2EI} \int_0^L \left[EI \frac{\partial \Phi}{\partial x} - (e_0 a)^2 \omega_n^2 \left(\rho A X + \rho I \frac{\partial \Phi}{\partial x} \right) \right]^2 dx
\end{aligned} \tag{6.22}$$

$$\begin{aligned}
U_{shear} &= \int_0^L \frac{f_s \left[AkG(\frac{\partial u}{\partial x} + \phi) + (e_0 a)^2 \rho A \frac{\partial^3 u}{\partial x \partial t^2} \right]^2}{2GA} dx \\
&= \cos^2(\omega_n t) \int_0^L \frac{f_s \left[AkG(\frac{\partial X}{\partial x} + \Phi) - (e_0 a)^2 \omega_n^2 \rho A \frac{\partial^3 u}{\partial x \partial t^2} \right]^2}{2GA} dx
\end{aligned} \tag{6.23}$$

As a result, if the maximum kinetic energy (the amplitude of $\sin^2 \omega_n t$) of the beam is equal to the maximum potential energy (the amplitude of $\cos^2 \omega_n t$), conservation of energy

conservation can be proven with $\cos^2 \omega_n t + \sin^2 \omega_n t = 1$. Therefore, in the following discussion, we will focus on the comparison between the maximum kinetic energy and potential energy for the cases of real and imaginary e_0.

The maximum kinetic energy in the vibrating nanowires is:

$$T_{max} = \frac{1}{2}\omega_n^2 \int_0^L \rho A X^2 dx + \frac{1}{2}\omega_n^2 \int_0^L \rho I \Phi^2 dx. \tag{6.24}$$

The equations for the maximum potential energy of the bending moment and shear force are

$$U_{\text{bending moment max}} = \frac{EI}{2}\int_0^L \left(\frac{\partial\Phi}{\partial x}\right)^2 dx - (e_0a)^2 \omega_n^2 \int_0^L \frac{\partial\phi}{\partial x}\left(\rho A X + \rho I \frac{d\Phi}{dx}\right)dx + \frac{(e_0a)^4}{2EI}\omega_n^4 \int_0^L \left(\rho A X + \rho I \frac{d\Phi}{dx}\right)^2 dx \tag{6.25}$$

And at the same time,

$$U_{\text{shear force max}} = \frac{f_s}{2GA}\int_0^L \left\{\left[AkG\left(\frac{dX}{dx}+\Phi\right)\right]^2 - 2AkG\left(\frac{dX}{dx}+\Phi\right)\omega_n^2 (e_0a)^2 \rho A \frac{dX}{dx} + \left[\omega_n^2 (e_0a)^2 \rho A \frac{dX}{dx}\right]^2\right\}dx$$

$$\tag{6.26}$$

Simply put, $U_{max} = U_{\text{bending moment max}} + U_{\text{shear force max}}$ $\tag{6.27}$

As a first step, the energy conservation of the macroscale beam theory is tested. The resonant frequency from Euler-Bernoulli beam theory is

$$\omega_n = (n\pi)^2 \sqrt{\frac{EI}{\rho A L^4}} \tag{6.28}$$

Therefore the spatial solution of the vertical displacement is

$$X = C_n \sin(n\pi x/L) \tag{6.29}$$

And the spatial solution of the angular displacement is

$$\Phi = \frac{n\pi C_n}{L}\cos(n\pi x/L) \tag{6.30}$$

116

Therefore,

$$\frac{1}{2}\omega_n^2 \int_0^L \rho A X^2 dx = (n\pi)^4 \frac{EIC_n}{2L^4} \int_0^L \sin^2\left(n\pi x/L\right) dx = \frac{EI}{2}\int_0^L \left(\frac{\partial \Phi}{\partial x}\right)^2 dx$$

(6.31)

It can be seen from Eq. (6.31) that the first term of Eq. (6.24) is equal to the first term of Eq. (6.25) for Euler-Bernoulli beam theory. However, it was found that the resonant frequencies from the MD simulations for nanowires have a shift from the bulk value and are not equal to those calculated with Eq. (6.28). The additional terms describe other effects which are not considered in the Euler Bernoulli beam theories. The term $\frac{1}{2}\omega_n^2 \int_0^L \rho I \Phi^2 dx$ is the kinetic energy from the rotational inertia. The term

$$-(e_0 a)^2 \omega_n^2 \int_0^L \frac{\partial \phi}{\partial x}\left(\rho A X + \rho I \frac{d\Phi}{dx}\right) dx + \frac{(e_0 a)^4}{2EI}\omega_n^4 \int_0^L \left(\rho A X + \rho I \frac{d\Phi}{dx}\right)^2 dx$$ is the potential energy due to

the nonlocal effect. Finally, the term $U_{\text{shear force max}}$ is the potential energy due to the shear force with the nonlocal effect. The resonant frequencies from the MD simulations with corresponding values of the nonlocal parameter e_0 are used in the calculation for kinetic energy and potential energy to check whether energy conservation is met.

The shear effect, rotational inertia and the nonlocal effect are all naturally included in the MD simulations. Two materials, Ag(100) and Ag(110), were used to calculate the energies. It should be noted that the unknown constant C_1 (C_n) in eq. (4.64) is determined with the initial conditions of the vibrating beams. However, this constant does not affect the comparison between the kinetic and potential energy, because it is found in both energy calculations. For convenience, C_1 is assumed to have a value of 1 in the presented calculations below. The kinetic energy and potential energy calculations obtained with the fundamental resonant frequency from

117

the MD simulations are shown in Table 6.VII. The maximum kinetic energy from Eq. (6.24), maximum potential energy with $e_0=0$ and with e_0 in Table 6.VI are compared.

Table 6.VII. The calculation for the kinetic energy and potential energy with respect to the fundamental resonant frequencies from the MD simulation and e_0 from the previously introduced calibration. The percentage is from $\dfrac{U_{max}-T_{max}}{T_{max}}\times100\%$ $(U_{max}-T_{max})/T_{max}\times100\%$.

Ag(100)	f_1 for simply-supported (GHz)	Max Kinetic Energy (J with $C_1=1$)	Max Potential Energy (J with $C_1=1$)when $e_0=0$	Max Potential Energy (J with $C_1=1$) using e_0 listed in Table 6.VI
4.09x4.09x40.9nm	2.441	0.42247	0.42901 (1.5475%)	0.42378 (0.31048%)
2.86x2.86x28.63nm	3.418	0.28412	0.28789 (1.3267%)	0.28551 (0. 48909%)
2.045x2.045x20.45nm	4.639	0.19073	0.19360 (1.5070%)	1.9124 (0.26602%)
Ag(110)				
4.05x4.09x40.49nm	3.562	0.89959	0.86846 (-3.4607%)	0.89213 (-0.83016%)
2.83x2.86x28.34nm	5.127	0.63926	0.62987 (-1.4697%)	0.63507 (-0.65647%)
2.002x2.045x20.02nm	7.206	4.6202	4.6021 (0.3921%)	4.6211 (-0.02063%)

The following conclusions can be made from table 6.VII. When the maximum kinetic energy is smaller than the maximum potential energy with the resonant frequencies obtained from the MD simulations, as found in Ref. [65] for fixed-fixed boundary condition, real values of e_0 exist. However, conservation of energy implies that the maximum kinetic and potential

energies are equal when there is not energy loss or external loads acting on the system. It should be noted that during the vibration MD simulations, the NVE thermostat was applied; thus, the positions and velocities of the atoms were adjusted based on the assumption that the energy of the system was constant. In addition, there are no external loads acting on the system during vibration. Thus, conditions for the MD simulations ideally satisfy energy conservation. As seen in Table 6.VII, an imaginary e_0 is required to ensure that the maximum potential energy and maximum kinetic energy are equal for the cases discussed. Finally, it can be seen that the imaginary e_0 does not violate the energy conservation rule. In fact, it adjusts the maximum potential energy so that is approximately equal to the maximum kinetic energy with an error of less than 0.5%. We have already discussed that the imaginary e_0 should exist to describe the positive surface stress for the simply-supported case. The energy analysis also supports that an imaginary e_0 does not violate the conservation of energy.

6.3.5 *Calibrating the Surface Stress τ with e_0 or Resonant Frequencies from MD Simulations*

The surface stress was calculated from the calibrated e_0 with Eq. (6.32) as an additional analysis.

$$2\tau w = \frac{EI\left(\frac{n\pi}{L}\right)^2\left\{\rho A + \left[\frac{\rho(EI)^*}{kG}+\rho I\right]\left(\frac{n\pi}{L}\right)^2\right\}-(EI)^*\left(\frac{n\pi}{L}\right)^2\left[\left(\frac{n\pi}{L}\right)^2\left(\rho I+\frac{EI\rho}{kG}\right)+A\rho\right]-(e_0a)^2\left[\left(\frac{n\pi}{L}\right)^2\left(\frac{EI\rho}{kG}+\rho I\right)+A\rho\right](EI)^*\left(\frac{n\pi}{L}\right)^4}{(e_0a)^2\left[\left(\frac{n\pi}{L}\right)^2\left(\frac{EI\rho}{kG}+\rho I\right)+A\rho\right]\left[\left(\frac{n\pi}{L}\right)^2+(EI)^*\left(\frac{n\pi}{L}\right)^4\frac{1}{AkG}\right]-\left\{EI\left(\frac{n\pi}{L}\right)^2\frac{\rho I}{AkG}\left(\frac{n\pi}{L}\right)^2-\left[\left(\frac{n\pi}{L}\right)^2\left(\rho I+\frac{EI\rho}{kG}\right)+A\rho\right]\left[(EI)^*\left(\frac{n\pi}{L}\right)^2\left(\frac{1}{AkG}\right)+1\right]\right\}}$$

(6.32)

If the shear effect is negligible (i.e. AR >5), then Eq. 6.32 reduces to Eq. 6.33.

$$2\tau w = \frac{-\frac{2}{3}E_s w^3 \left(\frac{n\pi}{L}\right)^2 - (e_0 a)^2 \left(EI + \frac{2}{3}E_s w^3\right)\left(\frac{n\pi}{L}\right)^4}{(e_0 a)^2 \left(\frac{n\pi}{L}\right)^2 + 1} \tag{6.33}$$

The surface stress value can therefore be solved from a known e_0 and the results are listed in Table 6.VIII. The surface stress can also be calculated with Eq. (6.34) from Eq. (3.13) with the resonant frequencies obtained from MD simulations. Eqs. (6.32) and (6.34) are equivalent and have the same results.

$$2\tau w = \frac{\omega_1^2 \rho A + \left(\frac{\pi}{L}\right)^2 \rho \omega_n^2 \left[\frac{(EI)^*}{kG} + I\right] - (EI)^* \left(\frac{\pi}{L}\right)^4}{\frac{(EI)^*}{AkG}\left(\frac{\pi}{L}\right)^4 + \left(\frac{\pi}{L}\right)^2 - \left(\frac{\pi}{L}\right)^2 \frac{\rho I \omega_1^2}{AkG}} \tag{6.34}$$

Table 6.VIII. The surface stress of simply-supported Ag nanowires for different cross-section size and lattice orientation with surface elasticity, -0.216eV/Å^2 for Ag(100) and -0.571eV/ Å^2 for Ag(110).

Ag(100)	e_0 for simply-supported	τ (N/m) from Eq. (6.18) and (6.20)	τ from Ref. [64]
4.09x4.09x40.9nm	2.496	0.1083	0.1856N/m (0.0116 eV/Å^2)
2.86x2.86x28.63nm	1.437	0.1112	
2.045x2.045x20.45nm	1.250	0.1112	
Ag(110)			
4.05x4.09x40.49nm	6.622i	0.3821	0.4336N/m (0.0271 eV/Å^2)
2.83x2.86x28.34nm	3.413i	0.3320	
2.002x2.045x20.02nm	1.127i	0.3054	

Table 6.VIII. lists the surface stress values from Eq. (6.32) for each cross-section size for Ag(100) and Ag(110) with surface elasticity values of -0.216eV/$Å^2$ and -0.571eV/ $Å^2$, respectively [66]. It was found that the surface stress for Ag(100) in the axial direction is approximately a constant with variation of 2% (0.1083N/m as compared to 0.1112N/m). However, the difference in surface stress for Ag(110) is larger, with a maximum difference of 20% (0.3821N/m as compared to 0.3054N/m). The calculation of the surface stress from the surface energy using the modified embedded atom method (MEAM) [64] is referred here as reference data listed in Table 6.VII. There is a shift between the calculated surface stress from the beam modeling method discussed above and the surface stress from the MEAM calculation.

There are several possible reasons for the differences in the surface stresses. The first reason is that the shift of the surface stress might be caused by the difference between the EAM and MEAM method. The electron density of the EAM is spherically symmetric, but the MEAM assumes that the electron density is a function of angles between atoms with additional angular forces.[154] However, it may not be necessary to consider angular forces for FCC metals.[155] To our best knowledge, we cannot find the surface stress value for Ag(110) with EAM. However, in order to present both real and imaginary e_0, Ag(110) as modeled as a comparison to Ag(100).

Another reason of the difference for the surface stress shift is that the current modeling methods of the surface stress and surface elasticity on bending nanowires may not be sufficient for sizes below 4nm, i.e., the nonlocal effect is not completely equal to the summation of surface stress and surface elasticity effect as there may be other effects that have not been considered. The surface stress and surface elasticity modeling has been shown to be appropriate for the size scale over 15nm.[90] However, validation of surface stress and surface elasticity modeling for cross-sectional size of 2-4 nm has not been verified numerically or experimentally. Therefore,

the hypothesis that the beam theories with surface effect and nonlocal effect may still be limited within the sizes tested since the nonlocal modeling is a more general method that also includes other size effects, such as van der Waals interaction [22, 23] and phonon dispersion [156-158]. Thus, it may be necessary to include these effects for dimensions from 1-5 nm. However, due to the limitation of computational resources, MD simulations for structures larger than 4 nm x 4 nm were time prohibitive.

A third reason for the difference in surface stress values may be due to the results being highly sensitive to the elastic moduli values used in the calculations. In this research, the elastic moduli were obtained by applying a fitting calculation to the MD simulations of a tensile test for the different sizes and lattice orientations using Eq. (6.10). However, as can be seen clearly in Table 6.IX, nanowires do not necessarily behave linearly elastic for the size scales used in the MD simulations. Therefore, the elastic modulus E is not a constant as found for linearly elastic materials. For MD simulations, different strains, ε, give different values of elastic modulus E, therefore, E is a function of ε and can be described as $E(\varepsilon)$. To-date, it is still a challenge to determine which elastic modulus to use in the beam equation associated with a specific strain value, even for strain values less than 5%. However, in the linear modeling presented in this thesis, the elastic modulus E must be a constant. To the best of this author's knowledge, most of the literature on MD simulations of tensile test for the elastic modulus, arbitrarily assume a strain range for linear fitting or polynomial fitting [111, 112, 134, 135, 149, 150]. In this paper, the elastic modulus with respect to strain $\varepsilon=0.01$ is chosen. However, other researchers use ranges of 0.01-0.12 which result in different values of the moduli [111, 112, 134, 135, 149, 150]. More work is needed to investigate which elastic modulus value is the best for the linear beam modeling. Otherwise, the Hooke's law assumption in linear elasticity may not be accurate

enough for the materials of this size scale. Thus, nonlinear mechanics may be needed for greater accuracy in modeling nanowires below 5nm.

Table 6. IX. The elastic moduli values, E, with for different strain ε in Eq. (6.10).

Ag(100)	$\varepsilon=0.01$	$\varepsilon=0.02$	$\varepsilon=0.05$
4.09x4.09x40.9nm	52.96 GPa	57.2 GPa	51.983 GPa
2.86x2.86x28.63nm	50.77 GPa	55.75 GPa	53.217 GPa
2.045x2.045x20.45nm	47.80 GPa	55.84 GPa	53.607 GPa
Ag(110)			
4.05x4.09x40.49nm	107.21 GPa	95.4 GPa	broken
2.83x2.86x28.34nm	111.08 GPa	92.57 GPa	107.16 GPa
2.002x2.045x20.02nm	114.07 GPa	88.73 GPa	103.56 GPa

6.4 <u>Conclusions</u>

The relation between the nonlocal material parameter, e_0, and surface stress, τ, is derived by solving the resonant frequencies of a simply-supported nonlocal Timoshenko beam and comparing to the solution from the Timoshenko beam theory with surface stress. The analytical analysis found that e_0 is determined not only by the material constants (elastic modulus E and surface stress τ), but also by the dimensions (cross-section size and length) and the vibration modes of the beam. Furthermore, Eq. (6.8) indicates that an imaginary e_0 is needed in order to describe a positive surface stresses or negative surface stresses with large absolute values, when

the surface elasticity is negligible. Otherwise, the application of nonlocal elasticity is limited to negative surface stresses and smaller problem definitions of nanoscale materials.

The resonant frequencies from molecular dynamics are also compared to the theoretical solution of nonlocal Timoshenko beam theory to calibrate the nonlocal parameter e_0 of the nonlocal beam modeling. Similar to the analytical analysis with surface effects, the analysis with MD simulations also supports that e_0 can be either an imaginary or real number with different combination of lattice orientation and boundary conditions. If e_0 is real for a cantilever, it is real for fixed-fixed but imaginary for simply supported due to the curvature effects, as found for Ag(110). Conversely, Ag(100) has an imaginary e_0 for the cantilever and fixed-fixed cases, but a real e_0 for the simply-supported case. The reason for this inconsistency between the cantilever and simply-supported cases can be explained by applying beam theory with surface stress. For example, a positive surface stress decreases the stiffness of cantilever but increases the stiffness of simply-supported nanowires due to the opposite curvature and resulting transverse load as obtained with the Young-Laplace equation. The real/imaginary property of e_0 agrees with the surface stress effect on bending beams. Therefore, the nonlocal stress-strain relation of Eq. (6.8) should be modified to allow imaginary values of e_0 in order to describe materials with arbitrary surface stress and different boundary conditions. In addition, the absolute value of e_0 increases with the cross-sectional size when the surface stress is ***not*** in the range of

$$-\frac{Ew\left(\dfrac{\pi}{AR}\right)^2}{24}-\frac{E_s}{3}\left(\frac{n\pi}{AR}\right)^2 < \tau < -\frac{Ew\left(\dfrac{\pi}{AR}\right)^2}{48}-\frac{E_s}{3}\left(\frac{n\pi}{AR}\right)^2.$$

Finally, the surface stress, τ for the materials used in the MD simulations presented in this research were also calculated. The surface stress can either be solved directly from the resonant frequencies of the nanowires (Eq. 6.29), or from the nonlocal parameter e_0 (Eqs. 6.31). It was

found that there is a difference between the surface stress of the beam modeling developed in this thesis and the direct MEAM calculation found from Ref. [64]. The possible reasons for these differences were discussed.

CHAPTER 7. Conclusions and Future Work

7.1 <u>Conclusions</u>

This thesis focuses on the modeling and analysis of size effects for nanoscale materials. The research goal was to develop mechanical modeling theories for nanoscale structures with critical dimensions of 1-100nm. To achieve this goal, the research aim was to test the hypothesis that Timoshenko beam theory with surface effects, Eringen's nonlocal elasticity and the corresponding nonlocal beam theories, and MD simulations results should all be consistent for nanoscale structures with critical dimensions of 1-100nm.

There are three research objectives to test the hypothesis. The first research objective is to obtain and verify a more general solution of continuum beam theories with surface effect to investigate the surface effect on bending nanowires with the "core-shell" approach. Timoshenko beam theory with surface effects has been applied with consideration of shear effect and rotational inertia effect. Consequently, the limitation of aspect ratio of Euler-Bernoulli beam theory was eliminated. The modeling for the resonant frequencies of the first three vibration modes of nanowires with three boundary conditions was detailed. The fixed-fixed case was compared to published results from MD simulations of Au(100) to verify the validation of this method. The aspect ratio was studied with this theoretical modeling.

The second objective of this research was to develop a bridging theory by incorporating surface properties with the nonlocal elasticity theory parameter e_0 to bridge the classical beam theories with nonlocal beam theory at the nanoscale. Two different modeling methods for the resonant frequencies of simply-supported nanowires were introduced in Chapters 3 and 4. The

two methods are Timoshenko beam theory with surface effects and nonlocal Timoshenko beam theory. With the hypothesis that the solutions from the two methods are consistent, the relation between the surface stress τ and the nonlocal parameter e_0 has been derived and shown in Eq. (6.4). It was found that e_0 for a simply-supported nanowire in flexural vibration is not a fixed number, but depends on the following parameters: the lattice length a, the elastic modulus E, the surface stress τ, the cross-section size w and shape (included in I and H), the length of the beam L and the vibration modes n. Therefore, the physical meaning of the nonlocal parameter e_0 has been explained for the first time to the best of this researcher's knowledge. The nonlocal parameter e_0 is based on eliminating the nearest neighbor assumption from classical elasticity theory and describes surface effects when the critical length (cross-section size for the nanowires) is comparable to the atomic structure (defined as a lattice unit length in this thesis). Additionally, by studying the analytical solution for e_0, it was found to be an imaginary number when the surface effects increase the stiffness of the nanowires. This case corresponds to a positive surface stress effect on the simply-supported nanowires in the surface stress modeling. Hence, if the surface elasticity is negligible, the nonlocal parameter e_0 has to be imaginary to match the modeling result of positive surface stress for nanowires with simply-supported boundary conditions.

The third objective of the research was to validate the hypothesis that Timoshenko beam theory with surface effects, Eringen's nonlocal elasticity and the corresponding nonlocal beam theories, and MD simulations results should be consistent at the nanoscale range of 1-100nm. The hypothesis was tested by comparing beam theory with surface effects and beam theory with nonlocal effect with MD simulations. The MD simulations also had the same trends found with the nonlocal beam modeling using surface stress τ and the nonlocal parameter e_0. For example, e_0

was found to increase with increasing cross-sectional sizes. An imaginary e_0 was also found by calibrating e_0 with the resonant frequencies obtained from the MD simulations. Additionally, the surface stress was solved by the Timoshenko beam theory with surface effects by assuming that the resonant frequency and surface elasticity were known and the surface stress is unknown. The surface stress from the resonance MD simulations is almost a constant, which is more obvious for Ag(100) with 2% variation as compared to Ag(110) with a 20% variation. However, there is a difference between the calculated surface stress in our research and the values from the values found in in Ref. [64].

There are several possible causes to these differences. One reason may be that Timoshenko beam theory with surface effect have more sources of error for the size scale of 2nm-4nm used in the simulations presented in this thesis. Other effects, such as van der Waals interaction [22, 23] and phonon dispersion [156-158] from quantum mechanics theory may be necessary to be considered at this smaller nanoscale range. The nonlocal parameter e_0 should contain not only the surface effects at the quasi-continuum level, but also the atomic level effects which are considered in the embedded atom models in MD simulations, such as the effects of electrons. Therefore, quantum mechanics may be needed to further develop the nonlocal elasticity theory and calibrate the nonlocal parameter e_0 more accurately for sub 5nm dimensions. A second error when calibrating the nonlocal parameter e_0 is that the constant elastic modulus from the tensile test is difficult to obtain because the material at the chosen size scale does not behave linearly. It was found that the elastic modulus E depends on the strain ε. As a result, nonlinear beam theories with changing elastic modulus E with respect to the strain ε might be better to model the nanowires with cross-section size of 2-4nm or lower.

7.2 <u>Recommendations for Future Work</u>

In this thesis, the basic concept of nanoscale mechanics and the methods to develop the nanoscale mechanics are introduced. However, there are still several unanswered questions that need to be addressed. The size-scale gap between the MD simulations and the modified continuum mechanics for nanoscale materials should be better bridged. On one hand, the MD simulations should describe larger structures. Nanowires with cross-sectional sizes over 15nm by 15nm have been shown to be accurate with the "core-shell" approach to describe surface effects.[90] Additionally, nanowires with >15nm cross-sectional sizes may also behave more linearly than the sizes in this thesis. Thus, the difficulty to obtain the best elastic modulus for the beam modeling can be eliminated by using sizes larger than 15 nm. Ideally, experiments that measure the resonant frequencies of nanowires on real systems are also needed to verify the theoretical modeling and computational simulations. In addition to surface effects, other size effects may also need to be modeled to further improve the continuum mechanics at the nanoscale. For example, Van der Waals interaction[22, 23] and phonon dispersion [156-158] may result in the differences or errors observed when calibrating the values of e_0. Therefore, quantum mechanics might be necessary to model some nanoscale materials with sub 5nm dimensions. The elastic modulus used in the beam modeling also needs to be further studied with nonlinear mechanics, due to the nonlinear mechanical deformation of the nanowires in tension for the sizes studied in this thesis.

Some other analysis and comparisons can be developed to more deeply understand nanoscale mechanics. Metals with different crystalline structures, for example Body-Centered Cubic (BCC) and Hexagonal Close Packed (HCP), should be modeled and compared to the

current Face Centered Cubic (FCC) structure to study the nonlocal parameter e_0 on different crystalline structures. BCC and HCP metals are also common materials in practical NEMS for their unique properties. The fabrication of Fe (BCC metals) nanowires has been studied in order to study the size effects on the magnetic property[159]. Electrochemical synthesis of vertically aligned Zn (HCP metals) nanowires has been developed due to the superconducting magneto-resistance and thermo-power properties of Zn.[160] Therefore, only focusing on the FCC metals have some limitation and cannot satisfy the widely application of different nanomaterial metals.

Different aspect ratios may also need to be tested in the MD simulations for e_0. Researchers found from both the surface stress modeling and surface energy modeling that the aspect ratio is a significant parameter to determine the surface effects. The theoretical calibration (Eq. 6.4) also shows that e_0 is a function of the aspect ratio (i.e., length) of the nanowires. Therefore, different aspect ratios may also need to be tested in the MD simulations to verify the theoretical modeling. However, it requires the MD simulations to model larger structures in the axial direction, and is not achievable with the current research conditions.

In this thesis, only the analytical relation between the surface stress τ and the nonlocal effect e_0 for the simply-supported boundary condition was presented. The relation between nonlocal parameter e_0 and surface stress τ for cantilever and fixed-fixed boundary conditions should also be derived, possibly numerically, to encompass all of the most common boundary conditions. For example, the cantilever boundary condition is a more widely used boundary condition in NEMS (examples can be seen in Chapter 1) and fixed-fixed boundary condition is common in the research modeling and MD simulations.

REFERENCES

[1]   X. L. Feng, R. He, P. Yang, and M. L. Roukes, "Very High Frequency Silicon Nanowire Electromechanical Resonators," Nano Letters, vol. 7, pp. 1953-1959, 2007/07/01 2007.

[2]   A. Choudhury, R. Vujanic, P. J. Hesketh, T. Thundar, and Z. Hu, "Evaluation of chemical reaction kinetics using a thermally active piezoresistive microcantilever array," in Micro Electro Mechanical Systems, 2008. MEMS 2008. IEEE 21st International Conference on, 2008, pp. 228-231.

[3]   D. E. R. M. A. CHANGIZI, I. STIHARU, "Detection of bio-chemical reactions through micro structural interactions," Journal of Optoelectronics and Advanced Materials, vol. 13, 2011.

[4]   H. Jerman, "Electrically-activated, micromachined diaphragm valves," in 1990 IEEE Solid-State Sensor and Actuator Workshop, June 4, 1990 - June 7, 1990, Hilton Head Island, SC, USA, 1990, pp. 65-69.

[5]   A. Pralle, E.-L. Florin, E. H. K. Stelzer, and J. K. H. Hörber, "Photonic Force Microscopy: A New Tool Providing New Methods to Study Membranes at the Molecular Level," Single Molecules, vol. 1, pp. 129-133, 2000.

[6]   E. T. Carlen, M. S. Weinberg, A. M. Zapata, and J. T. Borenstein, A micromachined surface stress sensor with electronic readout vol. 79: AIP, 2008.

[7]   J. Wan, S.-R. Deng, R. Yang, Z. Shu, B.-R. Lu, S.-Q. Xie, et al., "Silicon nanowire sensor for gas detection fabricated by nanoimprint on SU8/SiO2/PMMA trilayer," Microelectronic Engineering, vol. 86, pp. 1238-1242.

[8]   B. Sanii and P. D. Ashby, "High Sensitivity Deflection Detection of Nanowires," Physical Review Letters, vol. 104, p. 147203, 2010.

[9]   A. Chakraborty and C. Luo, "Fabrication and application of metallic nano-cantilevers," Microelectronics Journal, vol. 37, pp. 1306-1312, 2006.

[10]   B. B. Laura and et al., "Characterization of silver–gallium nanowires for force and mass sensing applications," Nanotechnology, vol. 21, p. 305701, 2010.

[11]   G. A. J. Hool, Nathan C, Handbook of building construction; data for architects, designing and construction engineers, and contractors, 1929.

[12]   M. Su, S. Li, and V. P. Dravid, "Microcantilever resonance-based DNA detection with nanoparticle probes," Applied Physics Letters, vol. 82, pp. 3562-3564, 2003.

[13]   R. Mukhopadhyay, M. Lorentzen, J. Kjems, and F. Besenbacher, "Nanomechanical Sensing of DNA Sequences Using Piezoresistive Cantilevers," Langmuir, vol. 21, pp. 8400-8408, 2005/08/01 2005.

[14]   K. M. Klein, Z. Jiantao, A. Gewirtz, D. S. Sarma, S. Rajalakshmi, and K. Sitaraman, "Array of Nano-Cantilevers as a Bio-Assay for Cancer Diagnosis," in Electronic Components and Technology Conference, 2005. Proceedings. 55th, 2005, pp. 583-587.

[15]   K. Gruber, T. Horlacher, R. Castelli, A. Mader, P. H. Seeberger, and B. A. Hermann, "Cantilever Array Sensors Detect Specific Carbohydrate−Protein Interactions with Picomolar Sensitivity," ACS Nano, vol. 5, pp. 3670-3678, 2011/05/24 2011.

[16]   D. Vita and et al., "Antibody-based protein detection using piezoresistive cantilever arrays," Nanotechnology, vol. 18, p. 125503, 2007.

[17]   G. Wu, H. Ji, K. Hansen, T. Thundat, R. Datar, R. Cote, et al., "Origin of nanomechanical cantilever motion generated from biomolecular interactions," Proceedings of the National Academy of Sciences, vol. 98, pp. 1560-1564, February 13, 2001 2001.

[18]   S. V. Pham, M. Dijkstra, H. A. G. M. van Wolferen, M. Pollnau, G. J. M. Krijnen, and H. J. W. M. Hoekstra, "Integrated mechano-optical hydrogen gas sensor using cantilever bending readout with a Si3N4 grated waveguide," Opt. Lett., vol. 36, pp. 3003-3005, 2011.

[19]   C. Emrah and et al., "Mechanical characterization of nickel nanowires by using a customized atomic force microscope," Nanotechnology, vol. 22, p. 155702, 2011.

[20]   T. Chang and H. Gao, "Size-dependent elastic properties of a single-walled carbon nanotube via a molecular mechanics model," Journal of the Mechanics and Physics of Solids, vol. 51, pp. 1059-1074, 2003.

[21]   C. Liu, Foundations of MEMS. Upper Saddle River, NJ: Prentice Hall; US ed edition, 2005.

[22]   T. Hertel, R. E. Walkup, and P. Avouris, "Deformation of carbon nanotubes by surface van der Waals forces," Physical Review B, vol. 58, pp. 13870-13873, 1998.

[23]   A. M. Rao, J. Chen, E. Richter, U. Schlecht, P. C. Eklund, R. C. Haddon, et al., "Effect of van der Waals Interactions on the Raman Modes in Single Walled Carbon Nanotubes," Physical Review Letters, vol. 86, pp. 3895-3898, 2001.

[24]   M. E. Gurtin, X. Markenscoff, and R. N. Thurston, "Effect of surface stress on the natural frequency of thin crystals," Applied Physics Letters, vol. 29, pp. 529-530, 1976.

[25]   Z. Yin, Q. Ren, and Y.-p. Zhao, "Modelling analysis of surface stress on a rectangular cantilever beam," Journal of Physics D: Applied Physics, vol. 37, p. 2140, 2004.

[26]   Q. He and C. M. Lilley, "Resonant frequency analysis of Timoshenko nanowires with surface stress for different boundary conditions," Journal of Applied Physics, vol. 112, pp. 074322-074322-7, 2012.

[27]   H. S. Park, P. A. Klein, and G. J. Wagner, "A surface Cauchy–Born model for nanoscale materials," International Journal for Numerical Methods in Engineering, vol. 68, pp. 1072-1095, 2006.

[28]   J. Diao, K. Gall, and M. L. Dunn, "Surface stress driven reorientation of gold nanowires," Physical Review B, vol. 70, p. 075413, 2004.

[29]   J. He and C. M. Lilley, "Surface stress effect on bending resonance of nanowires with different boundary conditions," Applied Physics Letters, vol. 93, pp. 263108-3, 2008.

[30]   Q. He and C. M. Lilley, "The vibration model and quality factor analysis of Timoshenko nanowires with surface stress," in Nanotechnology (IEEE-NANO), 2012 12th IEEE Conference on, 2012, pp. 1-6.

[31]   G. Wang and X. Feng, "Effects of surface elasticity and residual surface tension on the natural frequency of microbeams," Applied Physics Letters, vol. 90, p. 231904, 2007.

[32]   W. Gang-Feng and F. Xi-Qiao, "Effect of surface stresses on the vibration and buckling of piezoelectric nanowires," EPL (Europhysics Letters), vol. 91, p. 56007, 2010.

[33]   J. Reddy, "Nonlocal theories for bending, buckling and vibration of beams," International Journal of Engineering Science, vol. 45, pp. 288-307, 2007.

[34]   S. Papargyri-Beskou, K. Tsepoura, D. Polyzos, and D. Beskos, "Bending and stability analysis of gradient elastic beams," International Journal of Solids and Structures, vol. 40, pp. 385-400, 2003.

[35]   B. Gheshlaghi and S. M. Hasheminejad, "Vibration analysis of piezoelectric nanowires with surface and small scale effects," Current Applied Physics, vol. 12, pp. 1096-1099, 2012.

[36]   X. Zhu and H. Dai, "Solution for a nonlocal elastic bar in tension," Science China Physics, Mechanics and Astronomy, vol. 55, pp. 1059-1065, 2012.

[37]   T. Murmu and S. Pradhan, "Vibration analysis of nanoplates under uniaxial prestressed conditions via nonlocal elasticity," Journal of Applied Physics, vol. 106, pp. 104301-104301-9, 2009.

[38]   S. Papargyri-Beskou, A. Giannakopoulos, and D. Beskos, "Variational analysis of gradient elastic flexural plates under static loading," International Journal of Solids and Structures, vol. 47, pp. 2755-2766, 2010.

[39]   C. Y. Wang, T. Murmu, and S. Adhikari, "Mechanisms of nonlocal effect on the vibration of nanoplates," Applied Physics Letters, vol. 98, pp. 153101-3, 2011.

[40]   S. Papargyri-Beskou and D. Beskos, "Static analysis of gradient elastic bars, beams, plates and shells," Open Mechanics Journal, vol. 4, pp. 65-73, 2010.

[41]   K. G. Tsepoura, S. Papargyri-Beskou, D. Polyzos, and D. E. Beskos, "Static and dynamic analysis of a gradient-elastic bar in tension," Archive of Applied Mechanics, vol. 72, pp. 483-497, 2002.

[42]   C. Lim, "Equilibrium and static deflection for bending of a nonlocal nanobeam," Advances in Vibration Engineering, vol. 8, pp. 277-300, 2009.

[43]   H.-T. Thai, "A nonlocal beam theory for bending, buckling, and vibration of nanobeams," International Journal of Engineering Science, vol. 52, pp. 56-64, 2012.

[44]   P. Lu, P. Zhang, H. Lee, C. Wang, and J. Reddy, "Non-local elastic plate theories," Proceedings of the Royal Society A: Mathematical, Physical and Engineering Science, vol. 463, pp. 3225-3240, 2007.

[45]   F. Song, G. L. Huang, H. S. Park, and X. N. Liu, "A continuum model for the mechanical behavior of nanowires including surface and surface-induced initial stresses," International Journal of Solids and Structures, vol. 48, pp. 2154-2163, 2011.

[46]   L. H. He, C. W. Lim, and B. S. Wu, "A continuum model for size-dependent deformation of elastic films of nano-scale thickness," International Journal of Solids and Structures, vol. 41, pp. 847-857, 2004.

[47]   J. He and C. M. Lilley, "Surface Effect on the Elastic Behavior of Static Bending Nanowires," Nano Letters, vol. 8, pp. 1798-1802, 2008.

[48]   B. Gheshlaghi and S. M. Hasheminejad, "Adsorption-induced resonance frequency shift in Timoshenko microbeams," Current Applied Physics, vol. 11, pp. 1035-1041, 2011.

[49]   W. Gang-Feng and F. Xi-Qiao, "Timoshenko beam model for buckling and vibration of nanowires with surface effects," Journal of Physics D: Applied Physics, vol. 42, p. 155411, 2009.

[50]   H. Li and et al., "Deflections of Nanowires with Consideration of Surface Effects," Chinese Physics Letters, vol. 27, p. 126201, 2010.

[51]   A. C. Eringen and B. S. Kim, "RELATION BETWEEN NONLOCAL ELASTICITY AND LATTICE-DYNAMICS," Crystal Lattice Defects, vol. 7, pp. 51-57, 1977.

[52]   P. A. T. Olsson, "Transverse resonant properties of strained gold nanowires," Journal of Applied Physics, vol. 108, p. 034318, 2010.

[53]   P. A. T. Olsson, H. S. Park, and P. C. Lidstrom, "The Influence of shearing and rotary inertia on the resonant properties of gold nanowires," Journal of Applied Physics, vol. 108, p. 104312, 2010.

[54]   B. J. Alder and T. E. Wainwright, "Studies in Molecular Dynamics. I. General Method," The Journal of Chemical Physics, vol. 31, pp. 459-466, 1959.

[55]   D. Thompson, M. Sikora, P. Szymczak, and M. Cieplak, "A multi-scale molecular dynamics study of the assembly of micron-size supraparticles from 30 nm alkyl-coated nanoparticles," Physical Chemistry Chemical Physics, vol. 15, pp. 8132-8143, 2013.

[56]   J. Diemand, R. Angélil, K. K. Tanaka, and H. Tanaka, "Large scale molecular dynamics simulations of homogeneous nucleation," The Journal of Chemical Physics, vol. 139, pp. -, 2013.

[57]   K. Mylvaganam and L. C. Zhang, "Important issues in a molecular dynamics simulation for characterising the mechanical properties of carbon nanotubes," Carbon, vol. 42, pp. 2025-2032, 2004.

[58]   J. A. Morrone, R. Zhou, and B. J. Berne, "Molecular Dynamics with Multiple Time Scales: How to Avoid Pitfalls," Journal of Chemical Theory and Computation, vol. 6, pp. 1798-1804, 2010/06/08 2010.

[59]   H. S. Park, Surface stress effects on the resonant properties of silicon nanowires vol. 103: AIP, 2008.

[60]   N. Challamel, J. Lerbet, C. M. Wang, and Z. Zhang, "Analytical length scale calibration of nonlocal continuum from a microstructured buckling model," ZAMM - Journal of Applied Mathematics and Mechanics / Zeitschrift für Angewandte Mathematik und Mechanik, pp. n/a-n/a, 2013.

[61]   N. Challamel, Z. Zhang, and C. Wang, "Nonlocal Equivalent Continua for Buckling and Vibration Analyses of Microstructured Beams," Journal of Nanomechanics and Micromechanics, vol. 0, p. A4014004.

[62]   C. M. Wang, Z. Zhang, N. Challamel, and W. H. Duan, "Calibration of Eringen's small length scale coefficient for initially stressed vibrating nonlocal Euler beams based on microstructured beam model," Journal of Physics D: Applied Physics, vol. 46, p. 345501, 2013.

[63]   A. C. Eringen, "On differential equations of nonlocal elasticity and solutions of screw dislocation and surface waves," Journal of Applied Physics, vol. 54, pp. 4703-4710, 1983.

[64]   W. Jun, Y. L. Fan, D. W. Gong, S. G. Shen, and X. Q. Fan, "Surface relaxation and stress of fcc metals: Cu, Ag, Au, Ni, Pd, Pt, Al and Pb," Modelling and Simulation in Materials Science and Engineering, vol. 7, p. 189, 1999.

[65]   W. H. Duan, C. M. Wang, and Y. Y. Zhang, "Calibration of nonlocal scaling effect parameter for free vibration of carbon nanotubes by molecular dynamics," Journal of Applied Physics, vol. 101, pp. 024305-7, 2007.

[66]   V. B. Shenoy, "Atomistic calculations of elastic properties of metallic fcc crystal surfaces," Physical Review B, vol. 71, p. 094104, 2005.

[67]   B. Medasani, Y. H. Park, and I. Vasiliev, "Theoretical study of the surface energy, stress, and lattice contraction of silver nanoparticles," Physical Review B, vol. 75, p. 235436, 2007.

[68]   R. C. Cammarata and K. Sieradzki, "Surface and Interface Stresses," Annual Review of Materials Science, vol. 24, pp. 215-234, 1994.

[69]   J. K. Diao, K. Gall, and M. L. Dunn, J. Mech. Phys. Solids, vol. 52, p. 1935, 2004.

[70]   H. S. Park and P. A. Klein, "A Surface Cauchy-Born model for silicon nanostructures," Computer Methods in Applied Mechanics and Engineering, vol. 197, pp. 3249-3260, 2008.

[71]   E. M. Ronald and B. S. Vijay, "Size-dependent elastic properties of nanosized structural elements," Nanotechnology, vol. 11, p. 139, 2000.

[72]   Y. Zhang, L. J. Zhuo, and H. S. Zhao, "Determining the effects of surface elasticity and surface stress by measuring the shifts of resonant frequencies," Proceedings of the Royal Society A: Mathematical, Physical and Engineering Science, vol. 469, November 8, 2013 2013.

[73]   J. Ericksen, "On the Cauchy—Born Rule," Mathematics and mechanics of solids, vol. 13, pp. 199-220, 2008.

[74] J. Liu, J. Song, and Y. Wei, "Size effects of elastic modulus of fcc metals based on the Cauchy-Born rule and nanoplate models," Acta Mechanica Solida Sinica, vol. 27, pp. 111-121, 2014.

[75] S. Cuenot, eacute, phane, Fr, C. tigny, S. Demoustier-Champagne, et al., "Surface tension effect on the mechanical properties of nanomaterials measured by atomic force microscopy," Physical Review B, vol. 69, p. 165410, 2004.

[76] P. Lu, L. H. He, H. P. Lee, and C. Lu, "Thin plate theory including surface effects," International Journal of Solids and Structures, vol. 43, pp. 4631-4647, 2006.

[77] A. Assadi, B. Farshi, and A. Alinia-Ziazi, Size dependent dynamic analysis of nanoplates vol. 107: AIP, 2010.

[78] R. Ansari and S. Sahmani, "Surface stress effects on the free vibration behavior of nanoplates," International Journal of Engineering Science, vol. 49, pp. 1204-1215, 11// 2011.

[79] J. M. G. S. P. Timoshenko, Mechanics of material: Brooks/Cole engineering Division, 1984.

[80] P. Lu, P. Q. Zhang, H. P. Lee, C. M. Wang, and J. N. Reddy, "Non-local elastic plate theories," Proceedings of the Royal Society A: Mathematical, Physical and Engineering Science, vol. 463, pp. 3225-3240, December 8, 2007 2007.

[81] R. Haberman, Applied partial differential equations: with Fourier series and boundary value problems: Pearson, 2013.

[82] E. Inan and A. C. Eringen, "Nonlocal theory of wave propagation in thermoelastic plates," International Journal of Engineering Science, vol. 29, pp. 831-843, 1991.

[83] Q. Wang, "Wave propagation in carbon nanotubes via nonlocal continuum mechanics," Journal of Applied Physics, vol. 98, pp. 124301-6, 2005.

[84] J. N. Reddy and C. M. Wang, "Deflection relationships between classical and third-order plate theories," Acta Mechanica, vol. 130, pp. 199-208, 1998.

[85] P. Lu, H. P. Lee, C. Lu, and P. Q. Zhang, "Dynamic properties of flexural beams using a nonlocal elasticity model," Journal of Applied Physics, vol. 99, pp. 073510-9, 2006.

[86] Q. Wang and V. K. Varadan, "Vibration of carbon nanotubes studied using nonlocal continuum mechanics," Smart Materials and Structures, vol. 15, p. 659, 2006.

[87] M. Xu, "Free transverse vibrations of nano-to-micron scale beams," Proceedings of the Royal Society A: Mathematical, Physical and Engineering Science, vol. 462, pp. 2977-2995, October 8, 2006 2006.

[88] L. J. Sudak, "Column buckling of multiwalled carbon nanotubes using nonlocal continuum mechanics," Journal of Applied Physics, vol. 94, pp. 7281-7287, 2003.

[89] L. Wang and H. Hu, "Flexural wave propagation in single-walled carbon nanotubes," Physical Review B, vol. 71, p. 195412, 2005.

[90] S. Govindjee and J. L. Sackman, "On the use of continuum mechanics to estimate the properties of nanotubes," Solid State Communications, vol. 110, pp. 227-230, 3/31/ 1999.

[91] L. Y. Jiang and Z. Yan, "Timoshenko beam model for static bending of nanowires with surface effects," Physica E: Low-dimensional Systems and Nanostructures, vol. 42, pp. 2274-2279, 7// 2010.

[92] B. Farshi, A. Assadi, and A. Alinia-ziazi, "Frequency analysis of nanotubes with consideration of surface effects," Applied Physics Letters, vol. 96, pp. -, 2010.

[93] H.-L. Lee and W.-J. Chang, "Surface effects on frequency analysis of nanotubes using nonlocal Timoshenko beam theory," Journal of Applied Physics, vol. 108, pp. -, 2010.

[94] X.-w. Lei, T. Natsuki, J.-x. Shi, and Q.-q. Ni, "Surface effects on the vibrational frequency of double-walled carbon nanotubes using the nonlocal Timoshenko beam model," Composites Part B: Engineering, vol. 43, pp. 64-69, 1// 2012.

[95] Z. Jin, W. Chengyuan, and A. Sondipon, "Surface effect on the buckling of piezoelectric nanofilms," Journal of Physics D: Applied Physics, vol. 45, p. 285301, 2012.

[96] H. S. Park, "Surface stress effects on the critical buckling strains of silicon nanowires," Computational Materials Science, vol. 51, pp. 396-401, 1// 2012.

[97] G.-F. Wang and X.-Q. Feng, "Surface effects on buckling of nanowires under uniaxial compression," Applied Physics Letters, vol. 94, pp. -, 2009.

[98] Z. Yan and L. Y. Jiang, "The vibrational and buckling behaviors of piezoelectric nanobeams with surface effects," Nanotechnology, vol. 22, p. 245703, 2011.

[99] L. Yuhang, S. Jizhou, F. Bo, and Z. Jiazhong, "Surface effects on the postbuckling of nanowires," Journal of Physics D: Applied Physics, vol. 44, p. 425304, 2011.

[100] R. Finn, "Capillary surface interfaces," Notices of the AMS, vol. 46, pp. 770-781, 1999.

[101] G. Y. Jing, H. L. Duan, X. M. Sun, Z. S. Zhang, J. Xu, Y. D. Li, et al., "Surface effects on elastic properties of silver nanowires: Contact atomic-force microscopy," Physical Review B, vol. 73, p. 235409, 06/13/ 2006.

[102] S. Cuenot, C. Frétigny, S. Demoustier-Champagne, and B. Nysten, "Surface tension effect on the mechanical properties of nanomaterials measured by atomic force microscopy," Physical Review B, vol. 69, p. 165410, 04/20/ 2004.

[103] J. Thijssen, Computational Physics: Cambridge University Press, 2007.

[104] J. Lao, M. Naghdi Tam, D. Pinisetty, and N. Gupta, "Molecular Dynamics Simulation of FCC Metallic Nanowires: A Review," JOM, vol. 65, pp. 175-184, 2013/02/01 2013.

[105] D. C. Rapaport, The art of molecular dynamics simulation: Cambridge University Press, 1995.

[106] J.-F. Dufrêche, B. Rotenberg, V. Marry, and P. Turq, "Bridging molecular and continuous descriptions: the case of dynamics in clays," Anais da Academia Brasileira de Ciências, vol. 82, pp. 61-68, 2010.

[107] L. Yuan, D. Shan, and B. Guo, "Molecular dynamics simulation of tensile deformation of nano-single crystal aluminum," Journal of Materials Processing Technology, vol. 184, pp. 1-5, 2007.

[108] J. Diao, K. Gall, and M. L. Dunn, "Atomistic simulation of the structure and elastic properties of gold nanowires," Journal of the Mechanics and Physics of Solids, vol. 52, pp. 1935-1962, 2004.

[109] W. Wang, C. Yi, and B. Ma, "Molecular dynamics simulation on the tensile behavior of gold nanowires with diameters between 3 and 6 nm," Proceedings of the Institution of Mechanical Engineers, Part N: Journal of Nanoengineering and Nanosystems, vol. 227, pp. 135-141, September 1, 2013 2013.

[110] M. F. Horstemeyer, M. I. Baskes, and S. J. Plimpton, "Length scale and time scale effects on the plastic flow of fcc metals," Acta Materialia, vol. 49, pp. 4363-4374, 12/3/ 2001.

[111] T. M. Matthew, M. L. Austin, and G. Ken, "Bending and tensile deformation of metallic nanowires," Modelling and Simulation in Materials Science and Engineering, vol. 16, p. 045003, 2008.

[112] R. Mohan and Y. Liang, "Tensile and Flexural Deformation of Nickel Nanowires via Molecular Dynamics Simulations."

[113] J. E. Jones, "On the Determination of Molecular Fields. II. From the Equation of State of a Gas," Proceedings of the Royal Society of London. Series A, vol. 106, pp. 463-477, October 1, 1924 1924.

[114] J. E. Lennard-Jones, "Cohesion," Proceedings of the Physical Society, vol. 43, p. 461, 1931.

[115] M. S. Daw and M. I. Baskes, "Embedded-atom method: Derivation and application to impurities, surfaces, and other defects in metals," Physical Review B, vol. 29, pp. 6443-6453, 06/15/ 1984.

[116] M. S. Daw, S. M. Foiles, and M. I. Baskes, "The embedded-atom method: a review of theory and applications," Materials Science Reports, vol. 9, pp. 251-310, 1993.

[117] S. M. Foiles, M. I. Baskes, and M. S. Daw, "Embedded-atom-method functions for the fcc metals Cu, Ag, Au, Ni, Pd, Pt, and their alloys," Physical Review B, vol. 33, pp. 7983-7991, 1986.

[118] M. Baskes, S. Foiles, and M. Daw, "Application of the embedded atom method to the fracture of interfaces," Le Journal de Physique Colloques, vol. 49, pp. C5-483-C5-495, 1988.

[119] A. M. Leach, "Atomistic simulations of the mechanical deformation and energetics of metal nanowires," Georgia Institute of Technology, 2007.

[120] E. V. Zarochentsev, S. M. Orel, and V. N. Varyukhin, "Elastic constants of a stressed crystal. II. Cubic crystal," physica status solidi (a), vol. 53, pp. 75-85, 1979.

[121] H. A. Wu, "Molecular dynamics study of the mechanics of metal nanowires at finite temperature," European Journal of Mechanics - A/Solids, vol. 25, pp. 370-377, 3// 2006.

[122] G. Na, L. Yingchun, and L. Bingguo, "Static Analysis of Nano Fixed-Fixed Beam Based on Molecular Dynamics Simulation," in Mechatronics and Automation, 2007. ICMA 2007. International Conference on, 2007, pp. 879-883.

[123] C. Peng, Y. Zhong, Y. Lu, S. Narayanan, T. Zhu, and J. Lou, "Strain rate dependent mechanical properties in single crystal nickel nanowires," Applied Physics Letters, vol. 102, p. 083102, 2013.

[124] G. Julien, G. Julien, and B. Sandrine, "Deformation of silicon nanowires studied by molecular dynamics simulations," Modelling and Simulation in Materials Science and Engineering, vol. 19, p. 074003, 2011.

[125] S. Hoffmann, I. Utke, B. Moser, J. Michler, S. H. Christiansen, V. Schmidt, et al., "Measurement of the Bending Strength of Vapor−Liquid−Solid Grown Silicon Nanowires," Nano Letters, vol. 6, pp. 622-625, 2006/04/01 2006.

[126] S. Timoshenko, Vibration Problems in Engineering. New York: John Wiley & Sons, 1937.

[127] J. S. Wu and D. W. Chen, "Free vibration analysis of a Timoshenko beam carrying multiple spring–mass systems by using the numerical assembly technique," International Journal for Numerical Methods in Engineering, vol. 50, pp. 1039-1058, 2001.

[128] J. Diao, K. Gall, and M. L. Dunn, "Surface-stress-induced phase transformation in metal nanowires," Nat Mater, vol. 2, pp. 656-660, 2003.

[129] S. Timoshenko, "Vibration problems in engineering," 1974.

[130] C. M. Wang, Y. Y. Zhang, and X. Q. He, "Vibration of nonlocal Timoshenko beams," Nanotechnology, vol. 18, p. 105401, 2007.

[131] J. B. Adams, S. M. Foiles, and W. G. Wolfer, "Self-diffusion and impurity diffusion of fee metals using the five-frequency model and the Embedded Atom Method," Journal of Materials Research, vol. 4, pp. 102-112, 1989.

[132] H. Huang and F. Spaepen, "Tensile testing of free-standing Cu, Ag and Al thin films and Ag/Cu multilayers," Acta Materialia, vol. 48, pp. 3261-3269, 2000.

[133] M. P. Allen, "Introduction to molecular dynamics simulation," Computational Soft Matter: From Synthetic Polymers to Proteins, vol. 23, pp. 1-28, 2004.

[134] R. Komanduri, N. Chandrasekaran, and L. M. Raff, "Molecular dynamics (MD) simulation of uniaxial tension of some single-crystal cubic metals at nanolevel," International Journal of Mechanical Sciences, vol. 43, pp. 2237-2260, 2001.

[135] W.-J. Chang and T.-H. Fang, "Influence of temperature on tensile and fatigue behavior of nanoscale copper using molecular dynamics simulation," Journal of Physics and Chemistry of Solids, vol. 64, pp. 1279-1283, 2003.

[136]   W. Jiang and R. C. Batra, "Molecular statics simulations of buckling and yielding of gold nanowires deformed in axial compression," Acta Materialia, vol. 57, pp. 4921-4932, 2009.

[137]   F. Jensen, Introduction to computational chemistry: John Wiley & Sons, 2007.

[138]   I. Navon and D. M. Legler, "Conjugate-gradient methods for large-scale minimization in meteorology," Monthly Weather Review, vol. 115, pp. 1479-1502, 1987.

[139]   V. Rühle, "Berendsen and nose-hoover thermostats," Am. J. Phys, 2007.

[140]   W. G. Hoover, Computational statistical mechanics: Elsevier, 1991.

[141]   T. Schlick, Molecular Modeling and Simulation: An Interdisciplinary Guide: An Interdisciplinary Guide vol. 21: Springer, 2010.

[142]   D. Frenkel and B. Smit, Understanding molecular simulation: from algorithms to applications vol. 1: Academic press, 2001.

[143]   W. G. Hoover, "Canonical dynamics: Equilibrium phase-space distributions," Physical Review A, vol. 31, pp. 1695-1697, 1985.

[144]   J. O. Hirschfelder, C. F. Curtiss, and R. B. Bird, Molecular theory of gases and liquids vol. 26: Wiley New York, 1954.

[145]   P. H. Hünenberger, "Thermostat algorithms for molecular dynamics simulations," in Advanced Computer Simulation, ed: Springer, 2005, pp. 105-149.

[146]   J. R. Ray and H. Zhang, "Correct microcanonical ensemble in molecular dynamics," Physical Review E, vol. 59, pp. 4781-4785, 1999.

[147]   J. W. Gibbs, Elementary principles in statistical mechanics: developed with especial reference to the rational foundation of thermodynamics: Cambridge University Press, 2010.

[148]   W. Liang and M. Zhou, "Response of copper nanowires in dynamic tensile deformation," Proceedings of the Institution of Mechanical Engineers, Part C: Journal of Mechanical Engineering Science, vol. 218, pp. 599-606, June 1, 2004 2004.

[149]   H. A. Wu, "Molecular dynamics study on mechanics of metal nanowire," Mechanics Research Communications, vol. 33, pp. 9-16, 2006.

[150]   S. J. A. Koh and H. P. Lee, "Molecular dynamics simulation of size and strain rate dependent mechanical response of FCC metallic nanowires," Nanotechnology, vol. 17, p. 3451, 2006.

[151]   S.-E. Park, S. Kim, D.-Y. Lee, E. Kim, and J. Hwang, "Fabrication of silver nanowire transparent electrodes using electrohydrodynamic spray deposition for flexible organic solar cells," Journal of Materials Chemistry A, vol. 1, pp. 14286-14293, 2013.

[152]   Y. Tao, Y. Tao, L. Wang, B. Wang, Z. Yang, and Y. Tai, "High-reproducibility, flexible conductive patterns fabricated with silver nanowire by drop or fit-to-flow method," Nanoscale research letters, vol. 8, pp. 1-5, 2013.

[153] W. H. Press, Numerical recipes 3rd edition: The art of scientific computing: Cambridge university press, 2007.

[154] F. J. Cherne, M. I. Baskes, and P. A. Deymier, "Properties of liquid nickel: A critical comparison of EAM and MEAM calculations," Physical Review B, vol. 65, p. 024209, 2001.

[155] M. I. Baskes, "Modified embedded-atom potentials for cubic materials and impurities," Physical Review B, vol. 46, pp. 2727-2742, 1992.

[156] P. J. Koppinen and I. J. Maasilta, "Phonon Cooling of Nanomechanical Beams with Tunnel Junctions," Physical Review Letters, vol. 102, p. 165502, 2009.

[157] K. Andreas, E. Artur, and H. B. Robert, "Nanomechanical vibrating wire resonator for phonon spectroscopy in liquid helium," Nanotechnology, vol. 11, p. 165, 2000.

[158] W. Cheng, N. Gomopoulos, G. Fytas, T. Gorishnyy, J. Walish, E. L. Thomas, et al., "Phonon Dispersion and Nanomechanical Properties of Periodic 1D Multilayer Polymer Films," Nano Letters, vol. 8, pp. 1423-1428, 2008/05/01 2008.

[159] S. Yang, H. Zhu, D. Yu, Z. Jin, S. Tang, and Y. Du, "Preparation and magnetic property of Fe nanowire array," Journal of magnetism and magnetic materials, vol. 222, pp. 97-100, 2000.

[160] S. Z. EláAbedin, "Electrochemical synthesis of vertically aligned zinc nanowires using track-etched polycarbonate membranes as templates," Physical Chemistry Chemical Physics, vol. 15, pp. 11362-11367, 2013.

NAME: Qilu He

EDUCATION: Ph.D. Candidate, Mechanical Engineering University of Illinois at

                                Chicago (UIC), Chicago, Illinois   2015

                                B.S., Mechanical Engineering, Shanghai University, Shanghai,

                                China,   2006

EXPERIENCE: Teaching Assistant, UIC, Fall and Spring 2009-2014

                                Research Assistant, UIC, Summer 2010-2013

JOURNAL PAPERS: He, Qilu, and Carmen M. Lilley. "Resonant frequency analysis of

                                Timoshenko nanowires with surface stress for different boundary

                                conditions." Journal of Applied Physics (2012)

                                He, Qilu, and Carmen M. Lilley. "Analysis of the Material

                                Parameter e_0 using Nonlocal Elasticity and Timoshenko Beam

                                Theory with Surface Stress when Modeling Resonance of

                                Nanowires." Journal of Physics D, In Review

                                He, Qilu, and Carmen M. Lilley. "Modeling a static bending

                                nanoplate with surface stress and different boundary conditions."

                                Journal of Applied Mechanics, In Preparation

He, Qilu, and Carmen M. Lilley. "Calibration of the Nonlocal

Parameter e_0 in the Nonlocal Timoshenko Beam Theory with

Molecular Dynamic Simulation" In Preparation

CONFERENCE PAPERS: He, Qilu, and Carmen M. Lilley. "The vibration model and quality

factor analysis of Timoshenko nanowires with surface stress."

Nanotechnology (IEEE-NANO), 2012 12th IEEE Conference.

PRESENTATION: He, Qilu and Lilley, Carmen. "Resonance Frequency Analysis on

Nanowires with Surface and Shear Effects". ASME Applied

Mechanics and Materials Conference, June 2011, Chicago, IL

MEMBERSHIP: ASME Student Member